

The Structural Characterization of a Novel Influenza Vaccine by Transmission Electron Microscopy

By

Brianne Lindsay

Department Of Anatomy and Cell Biology
McGill University, Montréal
October, 2016

A thesis submitted to McGill in partial fulfillment of requirements for a Master's degree in
Science

© Brianne Lindsay, 2016

Table of contents

List of figures	v
List of tables	vi
List of abbreviations	vii
Abstract	ix
Résumé	x
Acknowledgments	xii
Preface and contributions to authors	xiii
Contributions to original knowledge	xv
Chapter 1: Literature review and research aims	1
1-1. Influenza	2
1-1.1. Seasonal influenza (commonly known as the “flu”)	2
1-1.2. Pandemic influenza	2
1-2. The Virus	4
1-2.1. Viral organization	4
1-2.2. Viral structure	4
1-2.3. Viral replication within cells	7
1-3. Vaccination	9
1-3.1. The first vaccine	9
1-3.2. Global impact of vaccination	10
1-3.3. Discovery of the influenza virus	10
1-3.4. Vaccination against influenza	11
1-3.5. Limitations of influenza vaccines	13
1-4. Novel Strategies for influenza vaccines	15
1-4.1.a. Recombinant based vaccines	15
1-4.1.b. Anti-HA stalk vaccines	16
1-4.2. Virus-like particles (VLP)	17
1-5. Introduction to electron microscopy techniques	21
1-5.1. Resin embedding transmission electron microscopy	21
1-5.2. Cryo-electron microscopy	21
1-5.3. Tomography	22
1-5.4. Subtomogram averaging	23
1-6. Rationale and research aims	24
Chapter 2: Morphological Characterization of a Plant Made Virus-Like Particle Vaccine Bearing Influenza Virus Hemagglutinins by Electron Microscopy	27
2-1. Preface	28
2-2. Abstract	29
2-3. Introduction	30

2-4. Methods	31
2-4.1. Virus-like particles (VLP)	31
2-4.2. Negative stain preparation	32
2-4.3. Observation of VLPs by cryo-TEM	32
2-4.4. Cryo-TEM tomography image processing	33
2-4.5. Resin-embedded cell monolayer interactions with VLP	34
2-4.6. Ultrastructural analysis of cell features	35
2-5. Results	35
2-5.1. Majority of VLPs are discus-shaped with HA trimers inserted at the disc-circumference	35
2-5.2. Plant-made influenza VLPs stored at 4°C does not change shape or size over time	37
2-5.3. Interaction of H1- and H5-VLPs with antigen presenting cells	41
2-6. Discussion	44
2.7. Acknowledgements	48
Chapter 3: Establishment of a correlative light and electron microscopy method to visualize virus-like particles interacting with immune cells	49
3-1. Preface	50
3-2. Abstract	51
3-3. Introduction	52
3-4. Methods	53
3-4.1 Virus-like particles (VLP)	53
3-4.2. Observation of VLPs by cryo-EM	54
3-4.3. U-937 cell preparation	54
3-4.4. Human peripheral blood mononuclear cell (PBMC) preparation	54
3-4.5. Fluorescence microscopy imaging	55
3-4.6. Resin-embedded cell monolayer interactions with VLP	56
3-5. Results	57
3-5.1. DiD lipophilic dye does not interfere with VLP morphology	57
3-5.2. Fluorescence LM studies of the interaction of H1- and H5-VLP with U-937 lymphocytes	58
3-5.3. Fluorescence LM studies of the interaction of H1- and H5-VLP with peripheral blood mononuclear cells	60
3-5.4. TEM observations of the interaction of H1- and H5-VLP with human U-937 lymphocytes	62
3-5.5. TEM observations of the interaction of H1- and H5-VLP with peripheral blood mononuclear cells	63
3-5.6. Methods towards correlative light and electron microscopy (CLEM) with influenza VLP vaccine sample	64
3-6. Discussion	66
3-7. Acknowledgements	71
Chapter 4: Progress toward determining the 3D structure of HA on the surface of plant-generated virus-like particles	72
4-1. Preface	73

4-2.	Abstract	74
4-3.	Introduction	75
4-4.	Methods	77
	4-4.1. Observation of VLPs by cryo-EM	77
	4-4.2. Cryo-TEM tomography image processing	77
	4-4.3. Manual model point selection	78
	4-4.4. Preliminary 3D reconstruction of manually selected HA using Imod	78
	4-4.5. Semi-automatic particle selection using EMAN2	79
4-5.	Results	80
	4-5.1. Image contrast improvement using the VPP for cryo-EM tomography	80
	4-5.2. Manual model selection of HA protein from VPP cryo-tomograms	82
	4-5.3. Preliminary 3D reconstruction of H1 attached to the membrane of VLPs by subtomogram averaging	83
	4-5.4. Semi-automatic approach to HA protein selection	84
4-6.	Discussion	85
4-7.	Acknowledgements	90
Chapter 5: Conclusion and future perspectives		91
5-1.	Major findings	92
	5-1.1. Morphological Characterization of a Plant Made Virus-Like Particle Vaccine Bearing Influenza Virus Hemagglutinins by Electron Microscopy	92
	5-1.2. Establishment of a correlative light and electron microscopy method to visualize virus-like particles interacting with immune cells	93
	5-1.3. Establishing the experimental conditions to determine the 3D structure of HA on the surface of virus-like particles	94
5-2.	Future perspectives	94
	5-2.1. Correlative LM and EM experimental improvements	95
	5-2.2. Higher resolution of H1 and H5 subtomogram structures	97
5-3.	Concluding remarks	98
5-4.	References	99
Appendix A: Quantification of VLP clustering over time visualized by cryo-EM		109
Appendix B: Quantification of cluster bound VLPs versus free VLPs by cryo-EM		110

List of Figures

Chapter 1

Figure 1-1: Schematic of the influenza A virus	6
Figure 1-2: 3D structure of H1 HA trimer.....	7
Figure 1-3: Stages of influenza virus infection to target host immune cells.....	8
Figure 1-4: Schematic of the HA conformational change.....	9
Figure 1-5: TEM micrograph of H5 VLPs budding from plant plasma membrane	19
Figure 1-6: Schematic of the iterative subtomogram averaging process.....	24

Chapter 2

Figure 2-1: 3D-morphological characterization of VLPs found in the H1 and H5 formulations.....	37
Figure 2-2: Distribution and size of the particles found in the H1 and H5 formulations during storage at 4°C for one year.....	39
Figure 2-3: Observation by cryo-EM of VLP clustering in the H1 and H5 formulations.....	40
Figure 2-4: Interaction of the discus-shape H1 and H5 VLPs with murine dendritic cells (DC) and U-937 cells examined by TEM of ultrathin epon resin sections	42
Figure 2-5: Murine DCs activated from incubation with H1-VLP.....	43
Figure 2-6. Ultrastructural quantification of murine dendritic cells activated from incubation with H1-VLP	44

Chapter 3

Figure 3-1: Schematic of CLEM experiments with U-937 blood lymphocytes and human PBMCs	57
Figure 3-2: Comparison of DiD lipophilically dyed H5 VLP to non-dyed VLP by cryo-EM	58
Figure 3-3: U-937 blood lymphocytes treated with DiD-labelled VLP by confocal microscopy.....	59
Figure 3-4. Human peripheral blood mononuclear cells (PBMC) treated with DiD-labelled VLP.....	61
Figure 3-5: TEM micrographs of human U-937 blood lymphocytes treated with DiD-labelled VLP.....	63
Figure 3-6: TEM micrographs of PBMCs treated with DiD-labelled VLP.....	64
Figure 3-7: CLEM approach to find cells of interest	66

Chapter 4

Figure 4-1: Schematic of semi-automatic particle selection.....	80
Figure 4-2: Comparison of 3D slices from cryo-EM tomograms of Volta-phase plate applied data to non-phase plate tomograms of H1 HA virus-like particles (VLP) produced in plants.....	82
Figure 4-3: Volta phase plate cryo-EM tomogram displaying manual selection of model points.....	83
Figure 4-4: Low resolution structure of H1 protein acquired through manual particle selection and subtomogram averaging approaches.....	84
Figure 4-5: Semi-automatic particle selections of the H1 attached to the VLPs.....	85

List of Tables

Chapter 1

Table 1-1: Influenza vaccines currently available in the United States, 2016-2017.....	13
--	----

List of Abbreviations

2D	Two-Dimensional
3D	Three-Dimensional
Alum	Aluminum salt adjuvant
APC	Antigen presenting cell
CCD	Charged coupled device
CLEM	Correlative light and electron microscopy
Cryo-EM	Cryo-electron microscopy
Cryo-STEM	Cryo-scanning transmission electron microscope
DC	Dendritic cell
DDD	Direct detector device
DiD	1,1'-Dioctyladecyl-3,3,3',3'-tetramethylindodicarocyanine iodide
DLS	Dynamic light scattering
FEI	Field Electron and Ion Co
FIB	Focused ion beam
GIF	Quantum energy filter
GM-CSF	Granulocyte macrophage colony stimulating factor
HA	Hemagglutinin
HEPES	4-(2-hydroxyethyl)-1-piperazineethanesulfonic acid
HIV	Human immunodeficiency virus
HPV	Human papillomavirus
H1	Hemagglutinin 1
H5	Hemagglutinin 5
H1N1	Hemagglutinin 1 Neuraminidase 1
H2N3	Hemagglutinin 2 Neuraminidase 3

IgE	Immunoglobulin E protein
IgG	Immunoglobulin G protein
M1	Influenza matrix 1 protein
M2	Influenza matrix 2 protein
MHC I/II	Major histocompatibility complex I/II
NA	Neuraminidase
NMR	Nuclear magnetic resonance
NP	Nucleoprotein
NS1/ NS2	Viral non-structural protein I/ II
PA	Polymerase acidic protein
PB1	Polymerase basic protein I
PB2	Polymerase basic protein II
PB1-F2	Polymerase basic protein I-full length
PBS	Phosphate buffered saline
PBMC	Peripheral blood mononuclear cell
PFA	Paraformaldehyde
Poly-L	Poly-Lysine
RNA	Ribonucleic acid
RPMI	Roswell Park Memorial Institute
SDS-PAGE	Sodium dodecyl sulfate polyacrylamide gel electrophoresis
SIRT	Simultaneous iterative reconstruction technique
SIV	Simian immunodeficiency virus
TEM	Transmission electron microscopy
VLP	Virus-like particle
WHO	World Health Organization

Abstract

Current influenza vaccine production strategies are based on methods developed 60 years ago and have serious limitations that leave vulnerable individuals at risk. Many approaches have been pursued to improve influenza vaccine effectiveness. A method has been developed by Medicago Inc, where virus-like particles (VLP) are generated using the plant expression platform of *Nicotiana benthamiana* with transient *Agrobacterium* transfection. The plant-generated vaccine candidate is promising as it offers numerous advantages compared to the current egg-based vaccine. In particular, this vaccine alternative can be produced in large quantities within a mere two weeks, it is safe and it promotes strong immune response and protection as currently being analyzed through animal and human preclinical and clinical trials, respectively. The clinical grade vaccine formulation has not yet been characterized at the morphological and structural level. In this thesis, we conducted an in-depth morphological analysis of the VLP formulation using advanced electron microscopy techniques. We have imaged the VLP in the most native state possible using cryo-EM and have determined the 3-dimensional shape of the different particles present in the formulation using cryo-electron tomography and the stability of the product upon one year storage at 4°C has been analyzed. We have imaged the VLP interacting with mouse dendritic cells, human U-937 lymphocytes and human peripheral blood mononuclear cells, and have made progress toward the establishment of correlative light and electron microscopy approaches (CLEM) to better characterize the interaction of immune cells with the VLP. Lastly, we have developed subtomographic averaging methods in order to determine the 3D structure of influenza hemagglutinin (HA) embedded in the VLP membrane. These results in their entirety will help to understand the structure of Medicago's influenza VLPs as this is a novel influenza vaccine approach.

Résumé

Les stratégies actuelles de production de vaccins contre la grippe sont basés sur des méthodes développées il y a 60 ans et ont des limitations sérieuses qui exposent les personnes vulnérables. De nombreuses études ont été menées pour améliorer l'efficacité du vaccin contre la grippe. Par exemple, Medicago Inc, a développé une méthode pour générer, des particules pseudo-virales (VLPs) dans la plate-forme d'expression utilisant la plante *Nicotiana benthamiana* transfectée par *Agrobacterium*. Ces VLPs sont un candidat de vaccin prometteur qui offre de nombreux avantages par rapport au vaccin courant produit dans les d'œufs. En particulier, ce vaccin alternatif peut être produit en grandes quantités en deux semaines seulement, il est sécuritaire et il induit une réponse immunitaire forte et protectrice (tel que démontré lors d'études menées en essais cliniques et précliniques chez l'humain et les animaux respectivement). La formulation du vaccin de grade clinique n'a pas encore été caractérisée au niveau morphologique et structural. Dans cette thèse, nous avons mené une analyse morphologique détaillée de deux formulations de VLPs en utilisant des techniques de microscopie électronique de pointe. On a imagé les VLPs dans l'état le plus natif possible en utilisant la cryo-EM et nous avons déterminé la forme tridimensionnelle des différentes particules présentes dans la formulation en utilisant la cryo tomographie électronique et analysé la stabilité du produit lors d'un stockage pendant une-année à 4°C. Nous avons imagé l'interaction des -VLPs avec des cellules dendritiques de souris, des lymphocytes humains (U-937) et des cellules mononucléaires de sang périphérique humain. Nous avons, fait des progrès vers la mise en place d'approches corrélatives microscopie optique et électronique (CLEM) afin de mieux caractériser l'interaction des cellules immunitaires avec les VLPs. Enfin, nous avons développé des méthodes de calcul des moyennes subtomographiques afin de déterminer la

structure 3D des molécules d'hémagglutinine (HA) intégrées dans la membrane des VLPs. Ces résultats dans leur intégralité aideront à comprendre la structure des VLPs présentes dans les formulations des nouveaux vaccins contre la grippe développés par Medicago Inc.

Acknowledgements

I wish to first thank my supervisor Dr. Isabelle Rouiller, for your guidance, approachable nature, and contagious passion for scientific discovery. Thank you for your continuous enthusiasm and for the opportunities you encouraged and provided during my time in your laboratory. I am very grateful for the opportunity to have worked with you.

To my parents David and Maureen Lindsay, thank you for your unwavering belief in me; for your support, and for instilling the importance of hard work and dedication. To my older brother and sister, Nicholas and Fallon, thank you for being the best role models a person can have.

To Benjamin Hughes, this journey would not have been as enjoyable without you. Thank you for your passion to learn, your desire to explore new places, and for continuing to bring out my best self. You inspire me each and every day.

To the people who have made this project possible, I next wish to thank Medicago Inc, for the privilege to work on the vaccine product. This project has been of substantial importance to me as it one day will be aiding in influenza protection worldwide. Thank you for the opportunity to be involved in such a positive global influence.

I would like to thank the FEMR facility at McGill University, in particular, Dr. Kelly Sears and Dr. Kaustuv Basu. You both work very hard to keep the facility running at its top capacity and that has been greatly appreciated. To Jeannie Mui and Lee-Ann Monaghan, thank you for your extensive microscopy knowledge and kindness.

I would like to thank the people I have had the pleasure of collaborating with, Kristin Hunt, Dr. Alexander Makarkov, Dr. Sabrina Chierzi, as well as all of the undergraduate students who were eager to learn and help with the project: Carson Wong, Joe Di Paolo, Jakub Qazi, Annaelle Gauvin, and Zoe Zhiyi. I would also like to thank Dr. Driss Mountassif a previous Rouiller lab member, for his patience while training and availability to help whenever I required assistance.

To Dr. Patrick Nahirney, thank you for the extensive training I received in your laboratory, and for your continued support through my academic career. My experience there gave me a lift in my academic confidence when I required it the most.

I lastly would like to thank my committee members Dr. Huy Bui, Dr. Brian Ward, and Dr. Christian Rocheleau. Your scientific expertise and feedback have been a great contribution to this work, thank you.

Preface

The manuscript based thesis by Brianne Lindsay has been prepared in accordance with the guidelines of McGill University, Quebec Canada “thesis research may be presented as a collection of scholarly papers of which the student is the authors or co-author; that is it can include the text of one or more manuscripts, submitted or to be submitted for publications, and/or published articles reformatted according to thesis requirements” (<http://www.mcgill.ca/gps/thesis/guidelines/preparation>).

Contributions of Authors

Chapter 1:

Brianne Lindsay, Isabelle Rouiller.

Literature review and thesis objectives

This chapter has no contributions.

Chapter 2:

Brianne Lindsay, Kristin Hunt, Alexander Makarkov, Sabrina Chierzi, Connie Krawzyk, Brian Ward, Nathalie Landry, and Isabelle Rouiller.

Morphological Characterization of a Plant Made Virus-Like Particle Vaccine Bearing Influenza Virus Hemagglutinins by Electron Microscopy

Brianne Lindsay: Performed cryo-EM preparation and imaging analysis of influenza VLPs, as well as resin embedding procedures and TEM imaging analysis of cells interacting with VLPs. Wrote and edited manuscript

Kristin Hunt: Performed and collected mouse bone marrow derived dendritic cells for TEM analysis.

Alexander Makarkov & Sabrina Chierzi: Performed and collected U-937 cells for TEM analysis.

Nathalie Landry: The monovalent VLPs used in the study were clinical-grade material and were produced by Medicago Inc. (Quebec, QC).

Chapter 3:

Brianne Lindsay, Alexander Makarkov, Sabrina Chierzi, Brian Ward, Nathalie Landry, and Isabelle Rouiller.

Establishment of a correlative light and electron microscopy method to visualize virus-like particles interacting with immune cells

Brianne Lindsay: Performed TEM resin embedding and CLEM methodology of immune cells interacting with VLPs. Wrote and edited manuscript.

Alexander Makarkov & Sabrina Chierzi: Performed and collected U-937 cells, fluorescently labelled VLP, and performed confocal microscopy of immune cells with labelled VLP.

Nathalie Landry: The monovalent VLPs used in the study were clinical-grade material and were produced by Medicago Inc. (Quebec, QC).

Chapter 4:

Brianne Lindsay, Nathalie Landry, Isabelle Rouiller.

Progress toward determining the 3D structure of HA on the surface of plant-generated virus-like particles

Brianne Lindsay: Performed cryo-EM tomography analysis, and subtomogram averaging reconstruction. Wrote and edited manuscript.

Zoe Hu: Developed python script for semi-automatic particle selection

Nathalie Landry: The monovalent VLPs used in the study were clinical-grade material and were produced by Medicago Inc. (Quebec, QC)

Contributions to Original Knowledge

The work completed in this thesis contributes original findings toward the morphological characterization of a clinical-grade influenza vaccine generated in plants. Cryo-electron tomography was used to determine the 3D structure of the virus-like particles (VLPs) found in the preparation. Cryo-electron microscopy was utilized to assess the stability of the preparation upon one year storage at 4°C. Interactions of the VLPs with immune cells were visualized using classical resin-embedding electron microscopy. Methods for correlative light and electron microscopy (CLEM) were developed as well as methods to determine the structure of the HA trimer found on the surface of the VLPs at high resolution.

Chapter 1:

- This chapter is provided as a literature review on influenza, vaccines targeted for influenza as well as offers the reader background information as to the microscopy experimental techniques used.

Chapter 2:

- Direct visualization of the clinical grade plant-generated influenza vaccine by cryo-electron microscopy and cryo-electron tomography: the majority (~95%) of particles were disc-shaped VLPs with either loosely or densely packed HA trimers inserted along the membrane, accounting for ~99.9% of the HA trimers.
- Year-long investigation as to structural stability of plant-generated VLP.
- Images of VLPs interacting with antigen presenting cells (dendritic and U-937 cells).

Chapter 3:

- Labelling of the VLPs with DiD: incorporation of DiD in the membrane of VLPs does not modify the general morphology.

- Plant-made VLPs were imaged by fluorescence and electron microscopy and found to bind at the surface of human macrophages and in the endosomes.
- Development of the methodology to perform CLEM in order to characterize at high magnification the differential binding properties of the VLPs observed by light microscopy (that is diffused and clustered binding).

Chapter 4:

- Comparison of electron tomography data collected with and without the phase-plate technology, gain of image contrast using phase-plate technology.
- Description of the methods to manually select protein from phase plate tomograms of VLP with varied spacing between neighbouring proteins.
- Preliminary 3D subtomogram average of H1 HA located at the surface of the plant-made VLPs.
- Development of a method to semi-automatically select protein from tomograms. To incorporate larger data set to subtomogram averaging procedure.

Chapter 1. Literature review and thesis objectives

1-1. Influenza

1-1.1. Seasonal influenza (commonly known as the “flu”)

Influenza commonly called the flu is caused by the influenza virus. Serious secondary medical complications occur in individuals with weakened or naïve immune systems (Patriarca *et al.*, 1984) such as bacterial pneumonia (Morens *et al.*, 2008). Pregnant women, young and elderly populations are typically most vulnerable to such problems, causatively due to low innate immunities and immunosenescence (Haq & McElhaney, 2014; Carrat & Flahault, 2007).

The infection is spread by close contact with an infected individual, either from mucous droplets from the nose and throat when those individuals cough or sneeze. Symptoms of the seasonal influenza respiratory infection include fever, headache, sore throat, muscle soreness, and fatigue. The disease can often be confused and misdiagnosed as the common cold, as so many of the symptoms are similar.

This virus undergoes continuous mutations resulting in seasonal outbreaks each year, most often occurring during the winter months. Influenza infections typically cause minor symptoms for healthy adults whom have already built immunity for protection against similar strains. Even though the influenza virus has been studied for decades it remains a global health threat (Carrat & Flahault, 2007). The World Health Organization (WHO) is responsible for tracing mutations within the viral strains; there are hundreds of laboratories stationed around the world to monitor these mutations (WHO, 2016).

1-1.2. Pandemic influenza

Pandemic influenza occurs when influenza viruses typically infecting different species (birds, pigs and human) re-assort. Over the last century there have been three major influenza pandemics, 1918, 1957, and 1968 (reviewed in Moren & Fauci, 2007). These pandemic

outbreaks spread easily due to low innate immunity within populations (Cummings *et al.*, 2014; Carrat & Flahault, 2007; Lazzari & Stohr, 2004). Devastating consequences have occurred upon rapid pandemic outbreaks, such as the infamous avian H1N1 1918 Spanish flu, which killed approximately 50-70 million people worldwide. More individuals died from the influenza pandemic worldwide than the number of casualties killed during the First World War (reviewed in Oxford, 2000). The mortality rate of healthy adults between the ages of 20-50 years was high for the Spanish flu; it is still unknown why so many healthy individuals died from the virus. Patients diagnosed with the virus suffered from dangerously high fevers, sore throats and limbs, bloodshot eyes, and some patients suffered from violent pulmonary hemorrhages and nosebleeds.

In the late 1960s the H3N2 strain circulated in Hong Kong and it quickly travelled to North America. The Hong Kong flu resulted in an estimated 1-4 million deaths worldwide. Multivariant immunity was shown to protect some populations from the pandemic, particularly within Asian populations, while Western populations had low innate immunity toward the specific strain (reviewed in Viboud *et al.*, 2005).

The most recent pandemic scare occurred in 2009, when H1N1 re-emerged after reassortment mutations within swine, and rapidly spread inflicting an estimated range of deaths from between 151,700 and 575,400 people (Dawood *et al.*, 2012). The majority of the patients diagnosed with H1N1 in 2009 were between the ages of 20-60, which correlated with the uniqueness of the Spanish flu back in 1918 (CDC, 2009). Fortunately, the outbreak of 2009 was not as deadly as the 1918 pandemic. However, pandemic influenza remains a very serious health threat in the 21st century.

1-2. The Virus

1-2.1. Viral organization

Influenza is a member of the *Orthomyxoviridae* family. *Orthomyxoviridae* re-groups six genera: Influenza A, Influenza B, Influenza C, Isavirus, Thogotoviruses and Quaranjavirus (Allison *et al.*, 2015; Kibenge *et al.*, 2004; Wright & Webster, 2001; Leahy *et al.*, 1997). Isavirus, Thogotoviruses and Quaranjavirus do not infect humans whereas Influenza A, B and C viruses infect a variety of mammalian (human, pig, horse, seal, dog) and bird species. Serotypes of the same influenza species share sequence similarities within conserved proteins (Palese & Shaw, 2007; Smith & Palese, 1989).

The genome of viruses within this family are composed of 6 to 8 segments of linear negative-sense single stranded RNA. The size of Influenza A and B viral species are between 100-200nm in diameter (Katz *et al.*, 2014; Bouvier & Palese, 2008; Harris *et al.*, 2006). The viruses are pleomorphic with a lipid membrane and can assemble into spherical and filamentous shapes (Bouvier & Palese, 2008; Palese & Shaw, 2007; Harris *et al.*, 2006)

1-2.2. Viral structure

Influenza A is the most virulent human pathogen among influenza viruses (Cox & Subbarao, 2000). Its genome contains 11 genes on eight pieces of RNA, encoding for 11 proteins: hemagglutinin (HA), neuraminidase (NA), nucleoprotein (NP), matrix proteins (M1 and M2), viral non-structural proteins (NS1 and NS2), and polymerase proteins (PA, PB1, PB1-F2 and PB2) and the lipid membrane is derived from the host cell as viewed in red in Fig.1-1. Influenza A is further divided into subtypes based on antibody responses to the viral surface glycoproteins HA and NA located at its surface (Palese & Shaw, 2007). For Influenza A, in total

there are 16 serotypes of HA, and 9 of NA that have been isolated thus far (Palese & Shaw, 2007).

The matrix protein 2 (M2), is an integral ion channel found within the lipid membrane (Zebedee & Lamb, 1988; Lamb *et al.*, 1985). M2 is essential for flow of ions to the interior of the viral particles upon acidification environments within late endosomes, a stage which facilitates viral infection (Mould *et al.*, 2000) (Fig. 1-1). Below the lipid layer, the M1 matrix protein encapsulates the ribonucleic material (Palese & Shaw, 2007). M1 interacts and stabilizes the transmembrane proteins and it is involved in the maintenance of the virion spherical structure (Chen *et al.*, 2007). It is also thought the M1 protein is involved during organization of viral surface proteins before the particles bud from the cell membrane (Lamb, 1983) (Fig. 1-1).

Embedded into the viral membrane are the two surface glycoproteins, HA and NA that are found at a ratio of 4:1 on the viral surface (Bouvier & Palese, 2008; Palese & Shaw, 2007) (Fig. 1-1). NA is a glycoside hydrolase enzyme and is essential for the cleavage and separation of the influenza virions from the host cell surface (Varghese & Colman, 1991). The enzymatic activity is necessary to promote release of the particles, by cleaving glycosidic linkages between the HA protein and sialic acid receptors. This helps to avoid viral aggregation on the host membrane. The structure of NA was first solved by Varghese *et al.*, 1983 to a resolution of 2.9Å by X-ray crystallography. The protein is a homotetramer composed of a stem and head domain and is approximately 240kD in size (Varghese & Coleman, 1991).

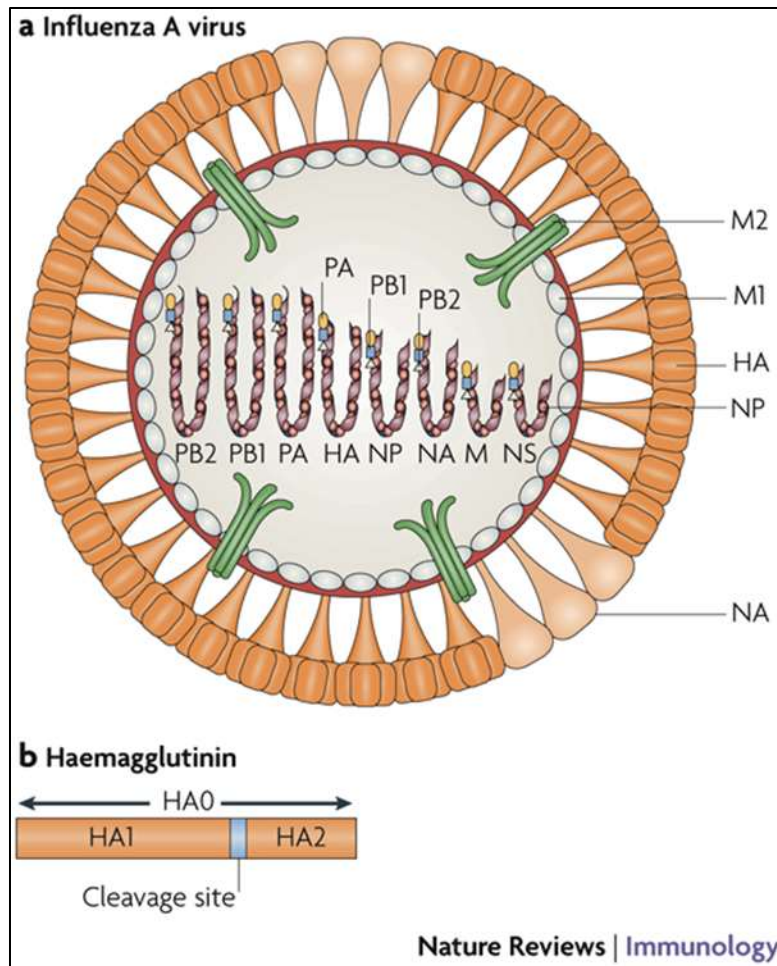


Figure 1-1. Schematic of the influenza A virus

(Reprinted from Subbarao & Joseph, 2007 with permission from the *Nature Reviews Immunology*)

The structure of HA was first solved in 1981 to 3Å resolution by X-ray crystallography (Wilson *et al.*, 1981). HA is a trimeric protein, with each monomer composed of two polypeptides, HA1 and HA2 linked through disulfide bonds. HA have two distinct regions, a stem domain which comprises the fusion machinery and a distal globular head region, which contains the receptor binding region (Wilson *et al.*, 1981; Palese & Shaw, 2007) (Fig 1-2).

Cryo-EM reconstructions of the H1 strain of HA protein have been achieved using cryo-subtomogram averaging approaches. The use of subtomogram averaging renders a 3D *in situ*

visualization of the protein attached to the viral surface, to view stalk and globular head regions of the protein, and identify antibody binding accessibility on the viral surface (Harris *et al.*, 2013) (Fig. 1-2).

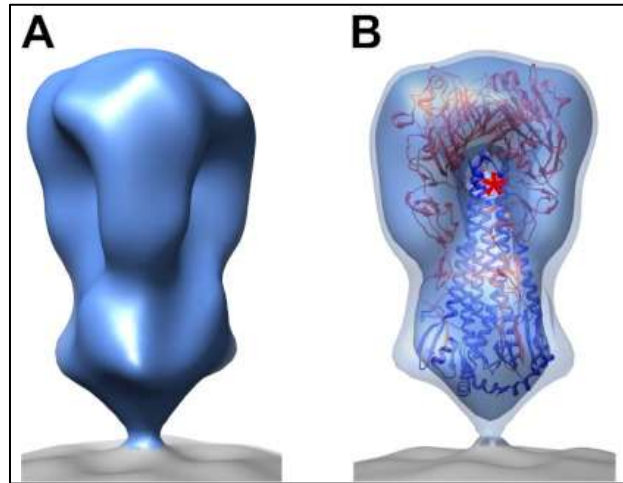


Figure 1-2. 3D Structure of H1 HA trimer. A-B) Side views of the 3D structure of HA embedded in the viral membrane.
(Reprinted from Harris *et al.*, 2013 with permission from the *PNAS Journal USA*)

1-2.3. Viral replication within cells

The influenza viral surface protein hemagglutinin (HA) binds to sialic acid receptors on the target host cell membrane. HA is the key protein to initiate infection to target immune cells (Ruigrok *et al.*, 1986; Skehel *et al.*, 1982). This binding interaction initiates viral uptake by receptor mediated endocytosis, and cooperative activity of host cell dynamin (Roy *et al.*, 2000; Stegmann *et al.*, 1987) (Fig.1-3). The host cell machinery is utilized to transcribe viral proteins using RNA polymerase. New influenza particles bud from the host cell membrane to target other cells (Wilson *et al.*, 1981) (Fig.1-3).

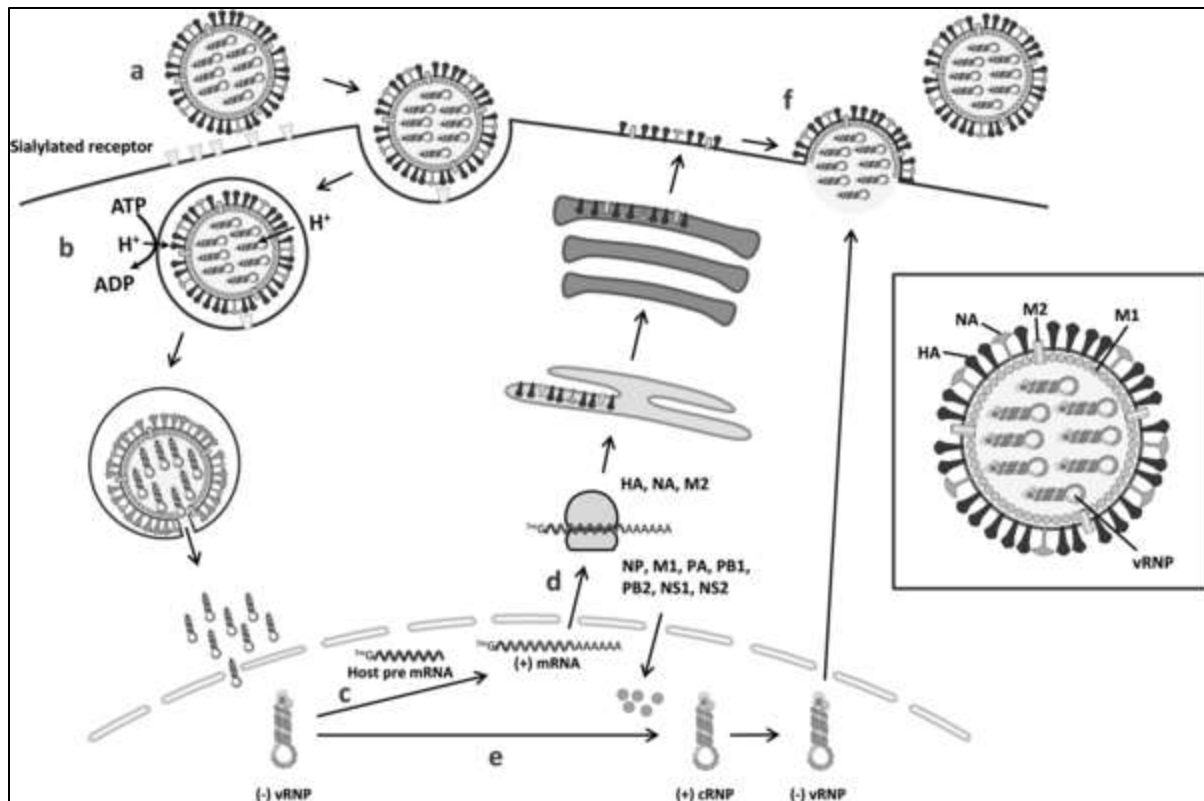


Figure 1-3. Stages of influenza virus infection to target host immune cells.

(Reprinted from Vanderlinden & Naesens, 2013 with permission from *Medicinal Research Reviews*)

HA undergoes a conformation change at low pH conditions (Skehel *et al.*, 1982). An extended intermediate conformation is formed causing the fusion peptide at the N-terminal domain of HA2 to become bound to the endosomal membrane (Harrison, 2015) (Fig. 1-4). The central helix of HA2 breaks and the portion between the break and the membrane is reconfigured; pulling of the fusion peptide, the C-terminal transmembrane anchor, the endosomal membrane and the viral membrane all take place to facilitate the fusion of the viral particle to the cell endosome (Chen *et al.*, 1999) (Fig. 1-2). The endosomal membrane fusion event was structurally verified by Ruigrok *et al.*, 1986, through electron microscopy.

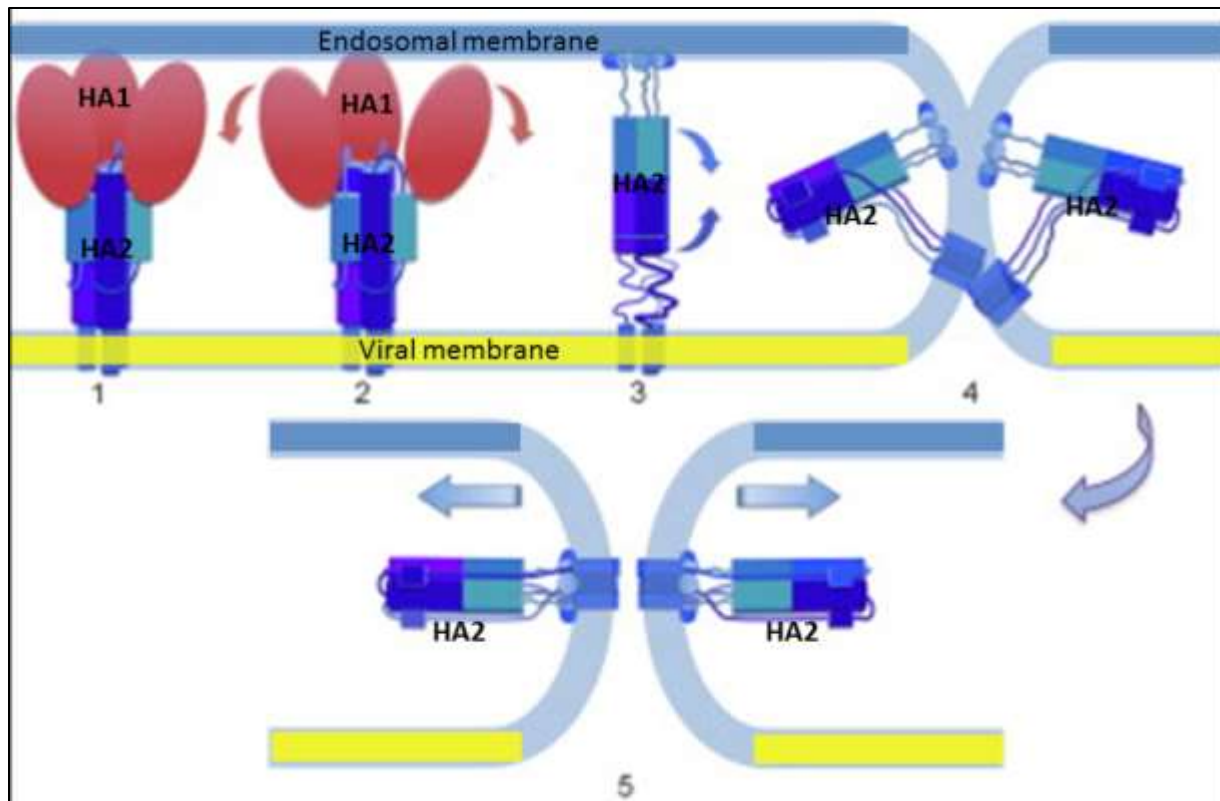


Figure 1-4: Schematic of the HA conformational change. 1) Receptor attachment. 2) Separation of HA1 heads triggered by reduced pH. 3) Extended intermediate, only HA2 shown. 4) Hemifusion induced by refolding of HA2. (5) Final refolding steps stabilize nascent fusion pore. (Modified figure from Harrison, 2015 with permission from the journal *Virology*)

1-3. Vaccination

1-3.1. The first vaccine

Vaccines are the most effective approach to fight and eradicate infectious disease. Edward Jenner considered as one of the founders of vaccinology (Lakhani, 1992). In England, cow-maids and farmers, who suffered from infection of the cowpox virus, were immune to the deadly smallpox virus (reviewed in Riedel, 2005). Jenner was the first to provide scientific evidence that cowpox exposure provided immunity against smallpox; he later termed his inoculation process vaccination (Jenner, 1798).

Jenner demonstrated these finding by taking fluid expelled from an infected cowpox lesion, and scratched it into the arm of an 8 year old boy. The child developed a fever and mild

rash, and a few months later was subjected to smallpox exposure and was completely immune (Jenner, 1978). As of 1980, smallpox has been globally eradicated as a result of worldwide efforts to eliminate the virus (Lakhani, 1992; WHO, 1980).

1-3.2. Global impact of vaccination

Vaccination has improved viral and bacterial incidence rates worldwide. Common preventable diseases include rubella, tetanus, pertussis (whooping cough), diphtheria, poliomyelitis, rabies, measles, mumps, *Haemophilus influenzae* type b, to name a few (Plotkin & Plotkin, 2008). Polio has been eradicated in the western world and is predicted to be the next disease to be globally eliminated as reviewed by Andre *et al.*, 2008 and Ehreth, 2003. Overall vaccination prevents an estimated 6 million deaths worldwide, but greater efforts could save an additional 1.5 million lives each year (reviewed in Ehreth, 2003).

More recently, vaccines have been generated to eradicate infection of viruses that induce particular types of cancer. It is known that cervical, anal, and some forms of throat cancer can develop due to infection of human papilloma virus (HPV). In 2008, the Nobel Prize in Physiology or Medicine was awarded to Harald Zur Hausen, for his discovery that HPV caused cervical cancer. Cervical cancer is the second most common form of cancer in women and the HPV vaccine Gardasil became commercially available in 2006 (Harper *et al.*, 2004).

1-3.3. Discovery of the influenza virus

In 1898, a German bacteriologist, Richard Pfeiffer isolated the influenza virus from patients' nostrils. He assumed the isolated samples to be of a bacterial origin and named it *Bacillus influenzae* (Pfeiffer, 1892). Soon after the notorious 1918 Spanish pandemic flu, many studies were conducted on this mysteriously unusual bacterium.

It wasn't until Robert Shope, in 1928, discovered the disease was caused by a virus. He infected healthy pigs with samples taken from the respiratory tract of the infected animals. He used non-filtered material which allowed the passage of viral particles, compared to previous experiments where a filtration system was utilized inhibiting the viral particles. When the non-filtered material positively transmitted the infection, it became evident the disease was a virus (Shope, 1931). Since then the scientific community, pharmaceutical companies, epidemiologists and health care providers have focused their efforts to try and eradicate influenza through vaccine manufacturing to avoid the consequences of future pandemics.

1-3.4. Vaccination against influenza

There are numerous methods to generate seasonal and pandemic influenza vaccines involving either live-attenuated or inactivated vaccines (Cox *et al.*, 2004). The first vaccines were produced using weaker, attenuated viruses to generate immunity. Live attenuated vaccines are composed of a similar live virus to the native form, but have been modified in the laboratory as to become non-virulent to human hosts. A foreign host (i.e. fertilized egg, tissue culture, or animals) are subjected to the native viral particles and re-assortment mutations occur to the surface glycoprotein to help facilitate the spread of viral growth within the new host. The mutated particles become structurally distinct from the native virus.

The advantage to this approach is the species vulnerable to the native virus, once subjected to the live-attenuated viral particles, will develop immunologic protection against the native virus. Some examples of live attenuated vaccines include the smallpox vaccine, the measles vaccine, the polio vaccine, and the seasonal influenza 'nasal spray'. A major medical advantage to the live attenuated vaccines is that complete inoculation only requires one

treatment. Live vaccines are a highly cost effective medical development (reviewed in Minor, 2015).

The most common influenza vaccine administered today however is an inactivated-type of vaccine, composed of H1N1, H3N2 and Influenza type B (WHO, 2016; Cox *et al.*, 2004). There are three different structural conformations this vaccine can be produced as: whole virus preparation, split-detergent based, or subunit preparation (WHO, 2016; Wong & Webby, 2013). All of these preparations are first grown in fertilized chicken embryos. The virus is injected and allowed to propagate within the allantoic fluid of the egg. The viral particles are isolated, concentrated, then purified and inactivated with a combination of formaldehydes (WHO, 2016).

The whole viral preparation is the simplest of these forms: influenza particles after purification are chemically fixed and there is no disruption to the overall structure. The split made vaccine is generated using detergents to break apart the lipid membrane to expose all viral protein (WHO, 2016; Duxbury *et al.*, 1968). This is an advantageous approach as it exposes the immune system to all viral proteins. Subunit vaccines are composed of only purified HA to stimulate the immune system to generate neutralizing antibodies to specific HA subtypes (WHO, 2016; Bachmayer *et al.*, 1976). Since the 1970s, the split and subunit vaccines are most commonly used (Wong & Webby, 2013).

TABLE 1. Influenza vaccines — United States, 2016–17 influenza season*

Trade name	Manufacturer	Presentation	Age indication	Mercury (from thimerosal), µg/0.5mL	Latex	Route
Inactivated Influenza Vaccine, quadrivalent (IIV4), standard dose[†]						
Fluarix Quadrivalent	GlaxoSmithKline	0.5 mL single-dose prefilled syringe	≥3 yrs	NR	No	IM [§]
Flulaval Quadrivalent	ID Biomedical Corp. of Quebec (distributed by GlaxoSmithKline)	0.5 mL single-dose prefilled syringe	≥3 yrs	NR	No	IM
		5.0 mL multi-dose vial	≥3 yrs	<25	No	IM
Fluzone Quadrivalent	Sanofi Pasteur	0.25 mL single-dose prefilled syringe	6 through 35 mos	NR	No	IM
		0.5 mL single-dose prefilled syringe	≥36 mos	NR	No	IM
		0.5 mL single-dose vial	≥36 mos	NR	No	IM
		5.0 mL multi-dose vial	≥6 mos	25	No	IM
Fluzone Intradermal Quadrivalent [¶]	Sanofi Pasteur	0.1 mL single-dose prefilled microinjection system	18 through 64 yrs	NR	No	ID ^{**}
Inactivated Influenza Vaccine, quadrivalent, cell culture-based (ccIIV4), standard dose[†]						
Flucelvax Quadrivalent	Seqirus	0.5 mL single-dose prefilled syringe	≥4 yrs	NR	No	IM
Inactivated Influenza Vaccine, trivalent (IIV3), standard dose[†]						
Afluria	Seqirus	0.5 mL single-dose prefilled syringe	≥9 yrs ^{††}	NR	No	IM
		5.0 mL multi-dose vial	≥9 yrs ^{††}	24.5	No	IM
Fluzirin	Seqirus	0.5 mL single-dose prefilled syringe	≥4 yrs	≤1	Yes ^{§§}	IM
		5.0 mL multi-dose vial	≥4 yrs	25	No	IM
Adjuvanted Inactivated Influenza Vaccine, trivalent (aIIV3), standard dose[†]						
Fluad	Seqirus	0.5 mL single-dose prefilled syringe	≥65 yrs	NR	Yes ^{§§}	IM
Inactivated Influenza Vaccine, trivalent (IIV3), High Dose^{¶¶}						
Fluzone High-Dose	Sanofi Pasteur	0.5 mL single-dose prefilled syringe	≥65 yrs	NR	No	IM
Recombinant Influenza Vaccine, trivalent (RIV3)^{***}						
Flublok	Protein Sciences	0.5 mL single-dose vial	≥18 yrs	NR	No	IM
Live Attenuated Influenza Vaccine, quadrivalent (LAIV4) ^{†††}						
FluMist Quadrivalent	MedImmune	0.2 mL single-dose prefilled intranasal sprayer	2 through 49 yrs	NR	No	NAS

Abbreviations: ACIP = Advisory Committee on Immunization Practices; ID = intradermal; IM = intramuscular; NAS = intranasal; NR = not relevant (does not contain thimerosal). Immunization providers should check Food and Drug Administration–approved prescribing information for 2016–17 influenza vaccines for the most complete and updated information, including (but not limited to) indications, contraindications, warnings, and precautions. Package inserts for U.S.-licensed vaccines are available at <http://www.fda.gov/BiologicsBloodVaccines/Vaccines/ApprovedProducts/ucm093833.htm>. Availability of specific products and presentations might change and differ from what is described in this table.

- [†] Standard dose intramuscular IIVs contain 15 µg of each vaccine HA antigen (45 µg total for trivalents and 60 µg total for quadrivalents) per 0.5mL dose.
- [‡] For adults and older children, the recommended site for intramuscular influenza vaccination is the deltoid muscle. The preferred site for infants and young children is the anterolateral aspect of the thigh. Specific guidance regarding site and needle length for intramuscular administration may be found in the ACIP General Recommendations on Immunization, available at <http://www.cdc.gov/mmwr/preview/mmwrhtml/r6002a1.htm>.
- [§] Quadrivalent inactivated influenza vaccine, intradermal: a 0.1-mL dose contains 9 µg of each vaccine HA antigen (36 µg total).
- [¶] The preferred injection site is over the deltoid muscle. Fluzone Intradermal Quadrivalent is administered using the delivery system included with the vaccine.
- ^{††} Age indication per package insert is ≥5 years; however, ACIP recommends that Afluria not be used in children aged 6 months through 8 years because of increased risk for febrile reactions noted in this age group with Seqirus' 2010 Southern Hemisphere IIV3. If no other age-appropriate, licensed inactivated seasonal influenza vaccine is available for a child aged 5 through 8 years who has a medical condition that increases the child's risk for influenza complications, Afluria can be used; however, providers should discuss with the parents or caregivers the benefits and risks of influenza vaccination with Afluria before administering this vaccine. Afluria may be used in persons aged ≥9 years. Afluria is licensed for administration by jet injector for persons aged 18 through 64 years only.
- ^{§§} Syringe tip cap might contain natural rubber latex.
- ^{¶¶} High-dose IIV3 contains 60 µg of each vaccine antigen (180 µg total) per 0.5mL dose.
- ^{***} RIV3 contains 45 µg of each vaccine HA antigen (135 µg total) per 0.5mL dose.
- ^{†††} ACIP recommends that FluMist (LAIV4) not be used during the 2016–17 season.

Table 1-1. Influenza vaccines currently available in the United States, 2016-2017. (Reprinted from the US Department of Health and Human Services, Morbidity and Mortality Weekly Report with permission from the Centre of Disease Control and Prevention).

1-3.5. Limitations of influenza vaccines

There are many issues with current influenza vaccines. Common methods such as the whole-inactivated, split-made, and subunit vaccines take months to prepare and are economically expensive. The WHO analyzes fluctuations and strain mutations each year to predict upcoming

mutations (WHO, 2016). This prediction strategy is lacking in specificity and it requires at least 6 months to produce large quantities of the vaccine (reviewed in Stephenson *et al.*, 2004). More recently this vaccine development strategy underwent scrutiny due to the delay with the swine flu pandemic in 2009.

Influenza continuously undergoes amino acid substitutions resulting in seasonal flu epidemics each year (Gabriel *et al.*, 2005). This process has been termed as ‘antigenic drift’ where upon an already circulated strain of the virus undergoes single point mutations, or substitutions (Gabriel *et al.*, 2005). ‘Antigenic shift’ is a result of re-assortment of different viruses, causing the viral surface glycoprotein to develop a new subtype circulating within populations. Re-assortments occur when a host has been infected with two different influenza viruses. The RNA material from both of the viral particles is integrated into the host genome and progeny budding from the cell surface have new RNA segments integrated from the two parent viruses. Antigenic shift mutations result in major pandemic outbreaks, such as in 2009 when H1N1 re-assorted within swine species.

The split and subunit vaccines can be produced within cell cultures which decreases production time, however this approach is costly as reviewed in Wong & Webby, 2013. As well it is not fully effective for elderly populations (Kang *et al.*, 2009). One of the strongest protective mechanisms to aid against influenza infectivity are broadly neutralizing antibodies specific to HA epitopes (Verilizer, 1975). However, majority of neutralizing antibodies bind to the globular head region of the protein which undergoes frequent mutations. Superior approaches to influenza vaccine manufacturing are required for increased specificity and speed of production

1-4. Novel strategies for influenza vaccines

Extensive strategies have been pursued to improve vaccine effectiveness, specificity, and speed of production. Novel techniques recently have been developed utilizing molecular biology approaches to precisely target viral protein specificity using recombinant biotechnology, including reverse genetics and approaches to produce virus-like particles (VLP).

1-4.1.a Recombinant based vaccines

Reverse genetics is a technique to obtain influenza viral strains. Research using these approaches has been ongoing since the 1980s (reviewed in Li *et al.*, 2013). The genes that encode viral proteins are isolated, spliced or mutated (to modify the protein function), and transfected within plasmids to be expressed within stable cell lines. The active viral particles obtained through this approach have slight mutations to the surface glycoprotein, similar to live-attenuated vaccines (reviewed in Plotkin, 2009). Clinical trials using this recombinant form of vaccine development have demonstrated high levels of cross-reactive immunity (Wacheck *et al.*, 2010). There are associated risks with these live viral particles used as vaccines, as there is a potential for reversion to virulent forms of the virus. There are likely events the live recombinant based vaccines may combine and assort with the circulating strains of influenza virus as well. This could be disadvantageous as re-assortment of influenza viral proteins is known to induce pandemic strains.

A recombinant based subunit vaccine approach has been demonstrated to show strong immune responses in mice (Lin *et al.*, 2010). Subunits of surface glycoproteins such as HA and NA are expressed within insect cells and baculoviral expression systems. These subunit vaccines have generated expression of neutralizing antibodies within animal studies (Lin *et al.*, 2010). Recently FDA approval has been granted for use of recombinant subunit vaccine from

baculovirus expression in insect cells (FDA Approves Flublok, 2016). The issues with recombinant subunit based vaccines as of today are the requirement of larger vaccine doses, repeated inoculations and/or adjuvant delivery systems to prime the immune system (Lin *et al.*, 2011).

Other recombinant based vaccines are currently under development for the protection against influenza viruses. A recombinant system fusing the globular head of HA to bacterial flagellin has been developed by Vaccinate, and shown elicitation of strong protective immunities in preclinical studies (Liu *et al.*, 2012). An orally administered adenovirus-based vaccine developed by Vaxart, has also shown protective immunity in ferrets subjected to lethal challenge of H5N1 avian influenza (Scallan *et al.*, 2013). Lastly, some recombinant influenza vaccine developers such as Biondvax, has focused on targeting protection against a broad range of influenza viruses, by selecting highly conserved portions of the influenza A virus through the construction of antibody and T cell inducing peptide-based vaccines (Rosendahl-Huber *et al.*, 2015).

1.4.1. b. Anti-HA stalk vaccines

It has been well known that the receptor binding site and fusion machinery regions of HA would be excellent targets for antibody neutralization. The HA stalk region of the protein is conserved among various HA subtypes. Vaccination most often induces production of antibodies specific to the stalk region of HA and binding of antibodies to the stalk typically block viral fusion and also inhibits antibody-dependent cellular cytotoxicity (Krammer & Palese, 2014). A monoclonal antibody was first isolated from mice immunized with H2N2 virus. The antibody C179 was found to neutralize H1, 2, 5, 6, and 9 subtypes. C179 did not block HA from binding

to sialic acid receptors, however it blocked membrane fusion indicating it bound to the HA2 region of the stem domain (Okuno *et al.*, 1993).

Extensive research over the last 20 years has identified specific antibodies that broadly neutralize epitope binding regions on the native HA stalk for a variety of influenza viruses (Dreyfus *et al.*, 2012; Corti *et al.*, 2011; Okuno *et al.*, 1993). This has been an area of interest as the HA stalk region of the protein is highly conserved among various HA subtypes. CR6261 and F10 antibodies were identified as novel antibodies expressed in humans (Throsby *et al.*, 2008; Sui *et al.*, 2009). The antibodies were able to neutralize a variety of influenza A viruses. Studies demonstrating these antibodies provided protective immunity within mouse models indicated that they may be useful for vaccine production. For vaccine generation the challenge now is eliciting potent immune responses from memory B cells that produce such antibodies to block HA activity.

1-4.2. Virus-like particles (VLPs)

The use of VLPs has been a promising approach to influenza vaccines, as these particles are non-virulent, economically feasible, and are demonstrating to have high immunogenicity within humans. Recombinant baculovirus in insect cell expression has yielded expression of recombinant proteins and has developed large scale manufacturing of VLP vaccines. VLP vaccines for a variety of diseases have been developed through this method, including SIV and HIV, HPV, and rotavirus vaccines. The use of VLPs for protection against influenza has been developed through many different expression systems such as DNA transfection, mammalian, and within insect cells as reviewed in Kang *et al.*, 2009. Novavax influenza VLPs expressed within insect cells have demonstrated broad immune responses in animal studies (Bright *et al.*,

2007). Currently clinical trials for influenza VLPs and Norwalk VLPs are ongoing (Roldao *et al.*, 2010).

Medicago Inc, is a biotechnology company founded in Quebec, Canada. The company has been focused on developing a novel approach to generate VLPs using *Agrobacterium* expression system within plants. These VLPs have been shown to be an advantageous method to generate an influenza vaccine against seasonal and pandemic strains (D'Aoust *et al.*, 2010; D'Aoust *et al.*, 2008). The VLP do not have any of the ribonucleic acids incorporated necessary for viral replication. The only protein expressed in this system is HA, and the protein is inserted into the VLP lipid membrane surface derived from the plant cell plasma membrane (D'Aoust *et al.*, 2008). Large scale vaccine manufacturing can be accomplished with this plant-based method within three weeks, an advantage for protection in case of pandemic influenza outbreaks (Le Mauff *et al.*, 2014).

Medicago's HA-VLP transient expression is achieved by targeting the promoter and terminator sequence of the alfalfa plastocyanin gene (Vézina *et al.*, 2009; D'Aoust *et al.*, 2008). Seed and *Agrobacterium* banks are generated on a yearly basis to avoid mutations induced from the plant or bacteria (D'Aoust *et al.*, 2010). Approximately 1500 plants are infiltrated with the *Agrobacteria* containing the HA gene of interest (D'Aoust *et al.*, 2010). The plants are lowered into a vacuum system and all air is drawn out of the leaves of the plant, consequently this enables the *Agrobacterium* to be drawn into the leaf cells. The *Agrobacterium* function as a vector to insert the HA gene into the plant cells specifically targeting the promoter and terminator sequence of the alfalfa plastocyanin gene (Vézina *et al.*, 2009). This allows constitutive expression of the recombinant HA protein using the plant cell machinery without HA gene insertion in the plant genome. After 6-10 days, the leaves are collected and the VLPs are

extracted and purified. This process is done by homogenizing the leaves and soluble material is extracted through centrifugation. The extract is concentrated before purification, that includes ion exchange and affinity chromatography purification steps (D'Aoust *et al.*, 2010).

The budding of individual VLPs has been imaged by TEM (D'Aoust *et al.*, 2008) (Fig 1-5). VLPs accumulate in between the plasma membrane and the cell wall of the plant cells (D'Aoust *et al.*, 2008). The visualization of VLPs demonstrated that HA is the driving force of VLP budding from the plasma membrane upon absence of sialic acids (D'Aoust *et al.*, 2008) (Fig 1-5). Plants are an advantageous host to produce these influenza VLPs. Plant cells do not express sialyted substrates, therefore HA cannot become bound to the plant cell surface which makes extraction easier (Saint-Jore-Dupas *et al.*, 2007; Seveno *et al.*, 2004; Lerouge *et al.*, 1998).

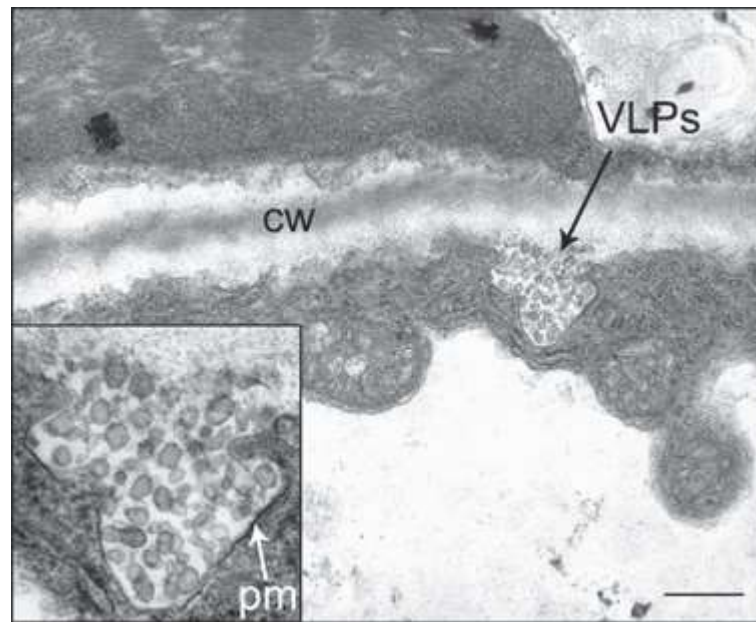


Figure 1-5. TEM micrograph of H5 VLPs budding from plant plasma membrane. The bar represents 500 nm. (Reprinted from D'Aoust *et al.*, 2008 with permission from the *Journal of Plant Biotechnology*)

Numerous studies have characterized and analyzed the immune response to these plant-made VLPs. A study using mass spectroscopy was conducted to analyze the purity of the influenza plant-derived particles. The VLP samples were 98% pure with no plant or *Agrobacterium* proteins found within the samples. However, it was identified that the plant-derived HA had glycans specific to the plant cell (Le Mauff *et al.*, 2014). Within human clinical trials the vaccine did produce IgG and IgE responses not associated with the plant glycans as no allergenic response was observed against the HA glycoproteins (Ward *et al.*, 2014).

Glycans are synthesized via host cell enzymes and influenza viral surface proteins are coated by glycosylation to evade the immune system. Even though plant glycan presence on HA VLP was determined, potent adaptive immune responses have been demonstrated extensively. In animal models, H7 strain of the VLP influenza vaccine protected mice and ferrets against lethal doses of H7N9 influenza (Pillet *et al.*, 2015) and in 2016 Pillet *et al.*, found cross-reactive antibody and T cell responses to a quadrivalent form of the influenza VLPs in healthy adults. VLPs carrying HA subtype 5 were found to be immunogenic in human clinical trials and there were no anaphylactic symptoms within participants (Landry *et al.*, 2010).

This novel approach has shown potential to be an advantageous vaccine, however little is known about the ultrastructure of the VLPs. Upon viral infection, typically HA is folded within mammals, which can then generate potent neutralizing antibody response. The N-glycosylation and folding differences that occur within plant-derived protein needs to be investigated at high resolution. Furthermore, the protein presentation to target immune cells has to be studied to gain a full comprehension of plant-generated VLPs for the protection against influenza.

1-5. Introduction to electron microscopy techniques

To understand Medicago's plant derived VLP for the protection against influenza, we used a variety of microscopy techniques to ascertain high resolution comprehension of the particles structure to correlate to functional studies currently ongoing in other laboratories at McGill University, University of Sherbrooke, and Medicago Inc.

1-5.1. Resin embedding transmission electron microscopy

Resin embedded TEM is a classical approach for viewing cell and tissues samples that are too thick to be observed directly in the TEM. Fixatives such as paraformaldehyde and glutaraldehyde are used to preserve cellular architecture, including proteins and carbohydrates. Post-fixation using osmium tetroxide strongly interacts with lipid membrane material in the samples and creates very dense stains (Wilney *et al.*, 2014). After fixation, samples undergo progressive dehydration with increasing concentrations of alcohol. The majority of biological samples are composed of water, and if the samples were not dehydrated and replaced with resin, quick evaporation would occur upon exposure to the electron beam in the microscope. Once the water has been replaced with plastic resin, the samples are then polymerized and hardened by placing the embedded samples at 57°C for a minimum of 24 hours. After embedding and polymerization has taken place the samples can be cut in thin sections for visualization in the TEM. Post-staining of EM thin sections is optional but does provide enhanced contrast, and observations are conducted at room temperature.

1-5.2. Cryo-electron microscopy

Cryo-electron microscopy (cryo-EM), allows for the visualization of small molecular complexes, cells or organelles (less than 500nm thick) in the most native state possible within vitreous ice. There is no addition of fixatives, stains, or dehydration to induce ultrastructural

changes or interfere with structural interpretation. Cryo-sample preparation allows for the structure of proteins to be preserved due to the rapidity of the freezing process (Takeuchi *et al.*, 2010). To avoid destruction of the frozen biological specimens, images must be acquired using low electron conditions, vitreous samples are also imaged at low temperatures ($\sim -170^{\circ}\text{C}$) to preserve the amorphous ice layer and prevent ice crystal formation (Knapek & Dubochet, 1980; Thach & Thach, 1971).

1-5.3. Tomography

Tomography is an imaging technique that can be used for cryo-samples to obtain 3D-image acquisition of macromolecular shapes. A series of 2D images are acquired at different angles in the positive and negative direction, and are compiled together (*as reviewed by* Wilson & Bacic, 2012; Subramaniam & Milne, 2004). The reconstruction of 3D structures from projection EM images was established in the 70s (Crowther *et al.*, 1970; Hoppe *et al.*, 1974)

Recent advancements within 5 years have revolutionized the field of cryo-EM (Kühlbrandt, 2014). Using cryo-EM methods, researchers have been able to solve the structure of proteins at a resolution 2-3Å, a resolution that was until recently only achievable using X-ray crystallography and NMR. This revolution has occurred after the introduction of direct electron detectors (DDD). DDDs are able to directly detect electrons and avoid the conversion of electrons to photons. In 2011, the first comparison between DDD collected data in comparison to CCD collected data showed higher resolution of GroEL, a bacterial chaperone, as a test specimen through single particle cryo-EM approaches (Milazzo *et al.*, 2011). The speed at which images have been captured while using DDDs has identified that there is beam induced motion upon electron beam exposure to cryo-prepared samples. These findings now have led to

optimization of beam induced motion within particle reconstruction procedures to aid with high resolution protein reconstructions (Li *et al.*, 2013).

The potential for *in-situ* high resolution structural biology is now possible. The implementation of Volta-phase plate (VPP) technology, created by Danev & Baumeister (2016), has revolutionized cryo-EM imaging. Recently using a variety of biological samples the VPP has been proven to improve image contrast and avoid structural deformation that typical tomography approaches could not avoid (Danev & Baumeister, 2016; Mahamid *et al.*, 2016; Asano *et al.*, 2015; Fukuda *et al.*, 2015; Danev *et al.*, 2014).

Utilizing standard approaches to improve image contrast without damaging fragile amorphous ice samples, images are captured with limited electron exposures ($<20\text{e}/\text{\AA}^2$ - $30\text{e}/\text{\AA}^2$). The resulting image has low contrast so microscopists typically defocus images to boost the signal to noise ratio. This has its own limitations as low-resolution information is lost and high-resolution is deformed which are detrimental components for obtaining high resolution protein reconstructions. The VPP combats this defocusing issue by allowing images to be captured at near in-focus levels (Danev *et al.*, 2014). The improved phase contrast is due to a charging of the electron beam inducing electrostatic potential (Danev *et al.*, 2014).

1-5.4. Subtomogram averaging

Obtaining protein reconstructions from cryo-EM tomography data is an advantageous approach to understand protein structure *in situ*. This process has been termed as subtomogram averaging. Complexes such as the HA proteins along the VLP membrane, are selected from tomogram 3D volumes, aligned, classified and averaged similar to single particle approaches (Fig.1-6). The alignment process is iterative, meaning it repeats the alignment procedure with

reference particles until the complex of interest stabilizes and no longer changes as reviewed in Briggs, 2013 (Fig. 1-6).

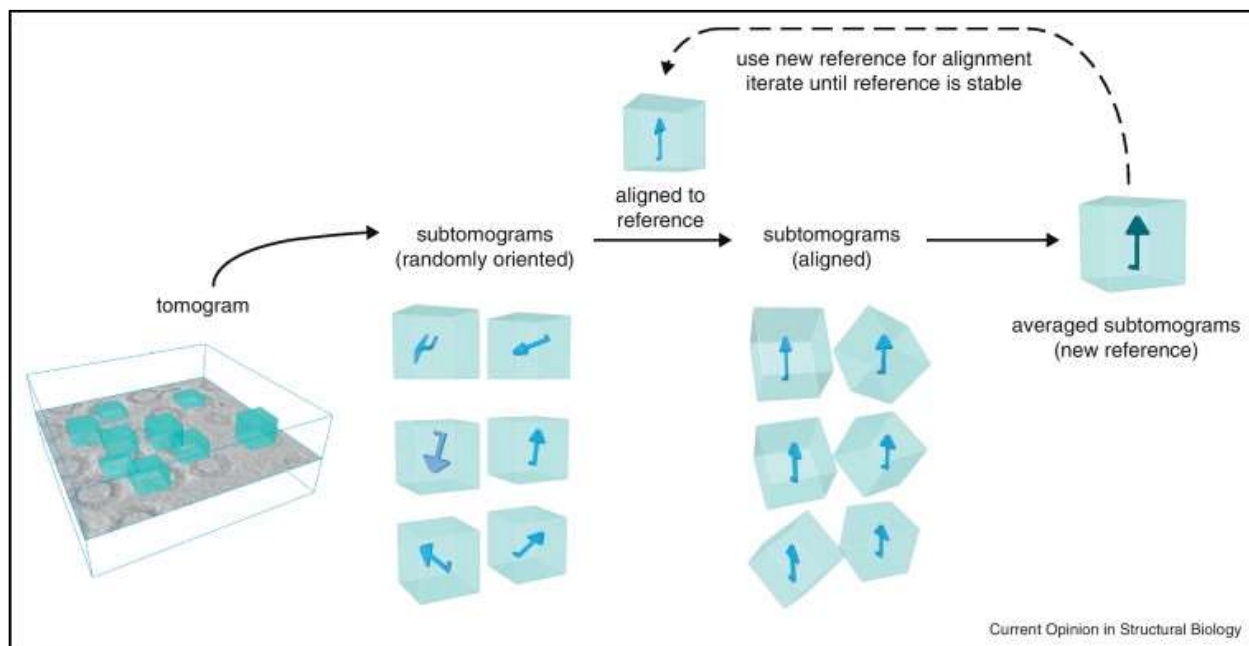


Figure 1-6. Schematic of the iterative subtomogram averaging process. (Reprinted from Briggs, 2013 with permission from the journal *Current Opinion in Structural Biology*)

1-6. Rationale and research aims

Plant-produced VLPs are a promising alternative for influenza vaccine generation compared to traditional egg-based formulations. Medicago Inc. is developing plant-generated influenza VLPs vaccine that is only composed of recombinant HA embedded in lipid vesicles of plant origin (Vézina *et al.*, 2011). There is no genetic material within the VLPs. Production is fast (2-3 weeks after identification of a strain; D'Aoust *et al.*, 2010). Vaccines are safe (Landry *et al.*, 2010) and promote potent cellular and humoral responses in both animals and humans (Pillet *et al.*, 2016; Landry *et al.*, 2014; Ward *et al.*, 2014; Landry *et al.*, 2010; D'Aoust *et al.*, 2008).

A better morphological and structural analysis of the vaccine product will provide essential clues for understanding the nature of the immune response observed and indicate which features of the candidate vaccines should be further developed to improve influenza vaccine and

other plant-generated vaccines. Of particular interest are the particle composition of the formulation, the stability of the product, the distribution of the antigen at the surface of the particles, the exact folding of HA and the interaction of the particles with immune cells. The objectives of this thesis were to incorporate a variety of microscopy methods to provide morphological and structural information on the vaccine formulation.

The native viral structure of influenza and presentation of HA along the membrane surface affect the potency of immune responses (Ruigrok *et al.*, 1986; Ruigrok *et al.*, 1985). For this reason, we investigated if the plant-made VLPs were structurally similar to the native virus. This question was addressed by using cryo-EM tomography approaches to gain 3D comprehension of particle composition and to determine the localization and distribution of HA proteins on the VLPs. To observe the stability of the preparation, we analyzed the particle composition and distribution of two formulations of HA-VLP upon storage at 4°C over one year. From the tomography reconstructions we found that the VLP were structurally distinct from the native virus, with the majority of particles of discus-shape presenting HA at low density. We detected also the presence of spheroid particles with a higher density of HA, HA star-shaped particles with no apparent membrane, and empty vesicles.

We then assessed by resin embedding TEM if the VLPs of vaccine preparations interacted with immune cells as the native virus does. We were able to capture the VLPs at the surface of immune cells, interacting at the plasma membrane and within endosomes of murine dendritic cells and human U-937 lymphocytes. Our images showed that the discus-shaped VLP are amongst the interacting particles even though they contain trimers at a much lower density than the native viruses.

Fluorescence light microscopy studies conducted in parallel in the Ward lab using lipophilic DiD-labelled VLP showed that VLPs interacted differentially at the cell surface of U-937 lymphocytes and human peripheral blood mononuclear cells. Some cells had diffuse binding around the entire membrane of the cell, while others exhibited a concentrated cluster of VLP at one area of the plasma membrane. It is known the processing of antigen stimulates differing immune responses (Chemali *et al.*, 2011; Duclos *et al.*, 2011; Houde *et al.*, 2003). With the objective to determine structural explanations for the different staining patterns seen at the LM level, we worked at establishing methods to achieve correlative light and electron microscopy (CLEM) to gain more understanding as to VLP processing within immune cells.

HA is the main surface glycoprotein of the viral cell surface and therefore a majority of neutralizing antibodies that are produced upon influenza infection are specific to epitope regions on the HA protein. Plant protein glycosylation is different than protein glycosylation in animals (Le Mauff *et al.*, 2014). At higher resolution, we will be able to observe the conformation of HA, which will help to establish the folding outcomes of HA transiently expressed within plants. Additionally, there may be an advantage to the N-glycosylation of the HA protein, as plant specific N-glycans have the capacity to facilitate antigen capture by antigen presenting cells through binding to sugar-specific cell surface receptors (Saint-Jore-Dupas *et al.*, 2007)

To assess if glycosylation impacts the HA structure and determine the conformational state of HA, we have been developing subtomogram averaging approaches using new imaging technology with the objective to determine a 10Å resolution structure of the HA protein attached to the VLP membrane. At this resolution, it will allow for the visualization of secondary structures, such as alpha-helices and beta-pleated sheets. We will be able to visualize the stem region of the HA protein and attempt to identify the epitope binding regions.

Morphological Characterization of a Plant Made Virus-Like Particle Vaccine Bearing Influenza Virus Hemagglutinins by Electron Microscopy

Authors:

Brianne J. Lindsay¹, Michal Bonar¹, Kristin Hunt², Alex Makarkov³, Sabrina Chierzi³, Connie M. Krawczyk², Nathalie Landry⁴, Brian J. Ward³, Isabelle Rouiller¹

Affiliation:

1. Department of Anatomy & Cell Biology; Faculty of Medicine; McGill University; Groupe de Recherche Axe sur la Structure des Proteines (Grasp); Groupe d'Etude de Proteines Membranaires (GEPRM), 3640 University Street, Montréal, QC, H3A 2B2, Canada.
2. Department of Microbiology and Immunology, and Physiology, Goodman Cancer Research Center, McGill University, Montréal, QC, Canada.
3. Research Institute of McGill University Health Centre-Suite EM3-3248, 1001 Decarie Street, Montréal, QC, H4A 3J1, Canada.
4. Medicago Inc. Ste-Foy, QC, Canada

Corresponding author:

Dr. Isabelle Rouiller
Department of Anatomy & Cell Biology
Faculty of Medicine
McGill University
Tel: 514 398-3244
Email: Isabelle.rouiller@mcgill.ca

2-1. Preface

Plant-made virus-like particle (VLPs) vaccines bearing the hemagglutinin (HA) protein of influenza viruses induce strong immune responses in animals and humans. Relatively little is known about the detailed structure of these VLPs, and particle morphology is likely to powerfully influence both immunogenicity and efficacy of these novel vaccines. To assess structural similarities between the plant-made vaccines and native influenza viruses, we used cryo-electron microscopy (cryo-EM) to directly image the VLPs in frozen hydrated conditions. Structural integrity of the VLP vaccines was analyzed over a 12-month period, using both qualitative and quantitative measures. The interaction of VLPs with immune cells was visualized using resin-embedding microscopy methods, a more classical transmission electron microscopy method.

2-2. Abstract

Available influenza vaccines have many limitations including variable effectiveness and over-reliance on egg-based production. New and better vaccines need to be developed. One promising approach is the production of virus-like particles (VLPs) using the *Nicotiana benthamiana* plant-based expression system. Candidate VLP vaccines bearing wild-type influenza hemagglutinins (HA) produced with this platform are currently advancing through clinical trials. Ultrastructural characterization of these novel vaccines is important to understand how the VLPs interact with the immune system. Using cryo-electron tomography, we determined that almost 100% of the HA content is found on discus-shaped particles with 30-50 HA trimers at the outer diameter, or ovoid VLPs with more densely packed trimers (65% and 30% of total particles respectively). The remaining ~5% were either star-shaped (0.1% total HA content) or empty vesicles. The distribution of particles, their size and shape did not change significantly during 12 months of storage at 4°C. Using resin-embedding transmission electron microscopy, we visualized the interaction of VLPs with the plasma membrane and in endosomes of mouse dendritic cells and human monocytoïd cells (U-937). Mouse dendritic cells exposed to VLPs displayed the classic morphological changes associated with activation including the formation of dendrites. Our findings demonstrate that the plant-made VLPs bearing influenza HA trimers are morphologically stable over time and raise the possibility that these VLPs may interact with and activate antigen presenting cells in a manner similar to the intact virus.

2-3. Introduction

Influenza infection is a major global health threat (WHO, 2014; Carrat & Flahault, 2007). Each year 5-15% of the world's population is infected leading to a minimum of 500,000 deaths (WHO, 2014). Currently, vaccine production relies primarily on fertilized chick embryos, with strain choice for southern and northern hemisphere formulations based on the viruses circulating in the opposite hemisphere during the previous influenza season (D'Aoust *et al.*, 2008; Johansson & Brett, 2007). This approach typically requires several months to adapt circulating strains for optimal growth in eggs and to generate large quantities of the vaccine (Gerdil, 2003). Furthermore, this process can introduce mutations that interfere with vaccine efficacy (Parker *et al.*, 2016; Raymond *et al.*, 2016). New approaches for influenza vaccines are needed both to better target wild-type viruses and to increase the speed of production in case of a pandemic.

Using transient *Agrobacterium* transfection of a distant relative of the tobacco plant (*Nicotiana benthamiana*), Medicago Inc., is developing candidate virus-like particle (VLPs) vaccines for influenza (D'Aoust *et al.*, 2010; D'Aoust *et al.*, 2008). The VLPs are composed of recombinant wild-type viral hemagglutinin (HA) incorporated in a lipid envelope derived from the plant cell membrane (D'Aoust *et al.*, 2008). Viral HA accounts for >98% of the VLPs protein content (Le Mauff *et al.*, 2015). VLPs do not contain any detectable nucleic acid of viral, bacterial, or plant origin. The scalability of the plant-based platform and the speed of recombinant vaccine production (weeks rather than months) offer real advantages in epidemic, pre-pandemic, and pandemic situations. These plant-made VLPs have proved to be immunogenic in both animal models and human clinical trials (Landry *et al.*, 2010; D'Aoust *et al.*, 2010; D'Aoust *et al.*, 2008), eliciting durable and cross-reactive antibody production as well as robust poly-functional T cell responses (Pillet *et al.*, 2016; Landry *et al.*, 2014).

The general size and shape of the plant-made VLPs, the form assumed by the HA itself (eg: monomer, dimer, trimer), the number of HA molecules per particle and the distribution of HA at the VLPs surface could all plausibly influence VLPs-immune cell interactions and consequently the immune response (Katz *et al.*, 2014; Harris *et al.*, 2006; Ruigrok *et al.*, 1985). We therefore sought to obtain a better morphological and structural characterization of two VLP vaccines bearing either a seasonal (H1-VLP: A/California/7/2009) or avian strain HA (H5-VLP: A/Indonesia/5/05). Using cryo-electron microscopy (cryo-EM), we performed a detailed analysis of VLP structure and analyzed particle integrity by shape and size during storage at 4°C over a year. We also visualized VLPs interacting with immune cells using transmission electron microscopy (TEM). Overall, we demonstrated that the plant-made VLPs are mostly disc- or ovoid-shaped with HA trimers inserted predominantly at the circumference. Both H1 and H5-VLPs interacted rapidly with the plasma membrane of antigen presenting cells (APC) *in vitro*, were internalized and induced ultrastructural changes consistent with cell activation.

2-4. Methods

2-4.1. Virus-Like particles (VLPs)

The monovalent VLPs used in the current study were clinical-grade material produced by Medicago Inc (Quebec, QC) as previously described (D'Aoust *et al.*, 2010). The native HA sequences targeted were derived from A/California/7/2009 (H1-VLP: 441µg/mL based on HA content) or A/Indonesia/5/05 (H5-VLP: 209µg/mL based on HA content). VLP stock solutions were maintained in aliquots in phosphate-buffered saline (PBS: pH 7.4) at 4°C in the dark.

2-4.2. Negative stain preparation

The VLP samples were diluted with PBS pH 7.4 to 100 μ g/mL based on estimated HA content. 5 μ L of the diluted VLP solution was placed for 30s on 200 Hex grids (Electron Microscopy Sciences, (EMS Inc.)), formerly carbon coated and glow-discharged. The grids were washed twice with 5 μ L of distilled water for 30 s followed by two incubations with a solution of 1.5% uranyl formate (EMS Inc.). Excess fluid was removed and samples were left to air dry.

Several approaches were to facilitate visualization of individual VLPs for the long-term stability analyses including 1) Trituration x 15 by pipette (tip inner-diameter of 0.018in); 2) passages through a Hamilton micro-syringe (5 μ L RN syringe, with a 26s bevel tip, inner diameter 0.005in); 3) Inversion x 10; 4) vortexing 30 sec.

2-4.3. Observation of VLPs by cryo-EM

Cryo-EM was performed on fresh VLPs, and every 3 months on stored aliquots over a 12 month period as follows: 5 μ L of either H1-VLP or H5-VLP were placed for 1 minute on a Quantifoil R2/2 copper grid (EMS Inc.) previously glow-discharged for 30 seconds. Excess fluid was removed and the sample was plunged frozen in liquid ethane at -180 $^{\circ}$ C using a Vitrobot (FEI Inc.) The chamber was set to 100% humidity at 4 $^{\circ}$ C. Grids were stored in liquid nitrogen until imaging. The cryo-prepared VLP samples were visualized on a Tecnai F20 microscope (FEI Inc.) At each time point, 100-150 images from one grid were recorded at 29,000x magnification and a defocus of -9 μ m using a Ultrascan 4k x 4k CCD Camera (Gatan Inc.)

The micrographs were analyzed using Image J software (Schneider *et al.*, 2012). Overall, 4,666 H1-VLPs and 3,424 H5-VLPs (~1000 particles at each time point) were classified according to shape and size. The average diameters and standard deviations were calculated and

the statistical significance was determined with One-way ANOVA. Both H1- and H5-VLPs tended to settle/cluster over time, a process that was quantified prior to re-suspension according to the number, and the size of clusters per field of view.

2-4.4. Cryo-TEM tomography image processing

The frozen hydrated VLP samples were imaged in a Titan Krios 300kV Cryo-STEM (FEI Inc.) equipped with a Volta Phase Plate (FEI Inc.) Images were recorded on a Falcon 2 Direct Detection Device (DDD) (FEI Inc.) at a pixel size at the specimen level of 3.6Å. Tilt series were collected with the FEI tomography software at +/-60° in 2° increments at the nominal magnification of 22,500x (pixel size at the specimen level of 3.7Å) and a defocus level of -0.5µm. The images were binned by a factor of two for processing. 3D reconstructions were calculated using the Imod Etomo package suite (Mastronarde, 1997) and a simultaneous iterative reconstruction technique (SIRT) procedure with 15 iterations.

The distance between HA trimers was measured by recording the coordinates in the tomogram of points located at the center of the tail and head regions of adjacent trimers. A total of 162 trimers were included in this analysis (81 H1 trimer pairs).

For visualization, individual VLP were selected from the reconstructed tomogram data. Filtering with Nonlinear Anisotropic Diffusion with Imod package suite (Mastronarde, 1997) was completed. Contours were displayed in Chimera 1.10.2 (Pettersen *et al.*, 2004), and colourized in Photoshop CS4 (Adobe).

2-4.5. Resin-embedded cell monolayer interactions with VLP

Mouse dendritic cells (DCs) were differentiated from mouse bone marrow and cultured in RPMI media containing 10% serum, L-glutamine, pen/strep, BME and 10ng/ml of GM-CSF as previously described (Krawczyk *et al.*, 2008). Cells were plated on Lab-Tek 8-well permanox chamber slides (EMS Inc.) at the concentration of 1 million cells per mL and left to adhere to the plates for 30 min at room temperature (RT). Cells were then washed with serum free media and either incubated with 20µg/mL of H1-VLP at RT for 60 minutes, or incubated with 15µg/mL of H1-VLP at 4°C for 30 minutes before fixation with 2.5% glutaraldehyde. Control cells were mock-treated then fixed. The cells were then post-fixed in 1% osmium tetroxide containing 1% potassium ferrocyanide for 1 hour at 4°C. After washing in distilled water for one hour, the cells were en bloc stained in 2% uranyl acetate for 45 min and dehydrated in ascending concentrations of ethanol (30%, 50%, 70%, 80%, 90%, and 100%) for approximately 10 minutes each followed by three additional washes with 100% ethanol. The cells were progressively embedded with 1:1 ratio of epon: 100% ethanol mixture for 30 min, followed by 3:1 ratio of epon: 100% ethanol mixture for another 30 min. The epon mixture was replaced with pure epon for 1hr at RT. Pure epon was replaced another time and the monolayers polymerized at 57°C for 48hrs. The DC experiments at 4°C were repeated twice and once at RT.

Human monocytoid cells (U-937) (ATCC CRL-1593.2) and maintained in RPMI-1640 Medium, supplemented with 10% fetal bovine serum (FBS), 0.5 IU/mL penicillin, 50 µg/mL streptomycin and 10 mM HEPES (all from Wisent), were plated at a concentration 1 million cells/mL on MatTek glass plates (MatTek Corporation) and allowed to attach for 30 minutes at 37°C. The supernatant was removed and washed with serum free RPMI-1640 media. H5-VLPs in serum free media (15µg/mL based on HA content) were added at 37°C for 45 minutes. PBS

was used as a control. The cells were fixed with 4% paraformaldehyde (PFA). The PFA solution was removed and replaced with 2.5% glutaraldehyde in 0.1M of sodium cacodylate and remained at 4°C overnight. The cells were processed for resin embedding TEM, as above. The U-937 experiment was repeated 7 times.

2-4.6. Quantification of the activation of mouse DCs

Activation of mouse DCs was quantified based on morphological characteristics. We observed 112 control cells and 127 cells incubated with 20µg/mL H1-VLPs at RT for 60 minutes. Cells were considered to be activated if extensive branching/large dendrites were present.

2-5. Results

2-5.1. Majority of VLPs are disc-shaped with HA trimers inserted at the disc-circumference

Negative stain images of H5-VLPs produced using an early purification method initially suggested that the plant-made particles were comprised of a phospholipid membrane variably studded with HA trimers (D'Aoust *et al.*, 2008). In the present study with two clinical-grade preparations, we analyzed the VLPs using cryo-EM, an experimental approach that allows for direct observation of the samples fully-hydrated in the original buffers. Cryo-electron tomography was employed to determine the three-dimensional shape of the VLPs (Fig. 2-1A-C). Unless otherwise mentioned, the cryo-EM findings with H1- and H5-VLP were very similar.

The large majority (65%) of the particles were, flattened oblate spheroid structures (disc-shaped) with loosely packed HA trimeric spikes concentrated at the equatorial region (Fig. 2-1A-D). The H1-VLPs and H5-VLPs were on average 75 ± 25 nm and 60 ± 37 nm in

diameter respectively. The number of HA trimers present on individual VLPs ranged from ~30-50 trimers per particle (Fig. 2-1C). The number of HA trimers per VLP generally increased with the size of the particle. Side orientation images allowed for clearer visualization of the HA trimers inserted into the membrane. These were located almost exclusively at the circumference of the disk, emanating from the membrane at different angles (Fig. 2-1C-D). The H1 trimers were well-separated, with, on average, 176Å and 203Å between tails (distance measured at the membrane) and globular head domains respectively.

The second most abundant class (~30% of the particles) were VLPs with densely packed HA. These particles were 85±20nm in diameter and were spheroid in shape with HA trimers distributed over the entire lipid membrane surface (Fig. 2-1E-G). On these particles, the HA trimers were generally closer to one another, with neighbouring trimers separated by 144Å and 182Å between tails and globular heads respectively. The number of HA trimers/particles was impossible to measure accurately for this class, but was at least three-times higher than the discoid-shaped VLPs and also generally increased with the size of the individual particle.

Other components constituting less than 5% of the vaccine particles were ‘empty’ vesicles (EV: membrane-bound vesicles without any HA trimers, 100±10nm in diameter) and star-shaped particles with ~5-10 protein trimers (Fig. 2-1 H-J). We estimated that no more than 0.1% of the HA trimers assembled as rosettes of 9-20nm in diameter, which indicates that the size-exclusion chromatography included in the preparation of clinical grade material is efficient. Even more rarely seen in the tomograms were cork-screw like structures which could be LPS or endotoxin from *Agrobacteria*.

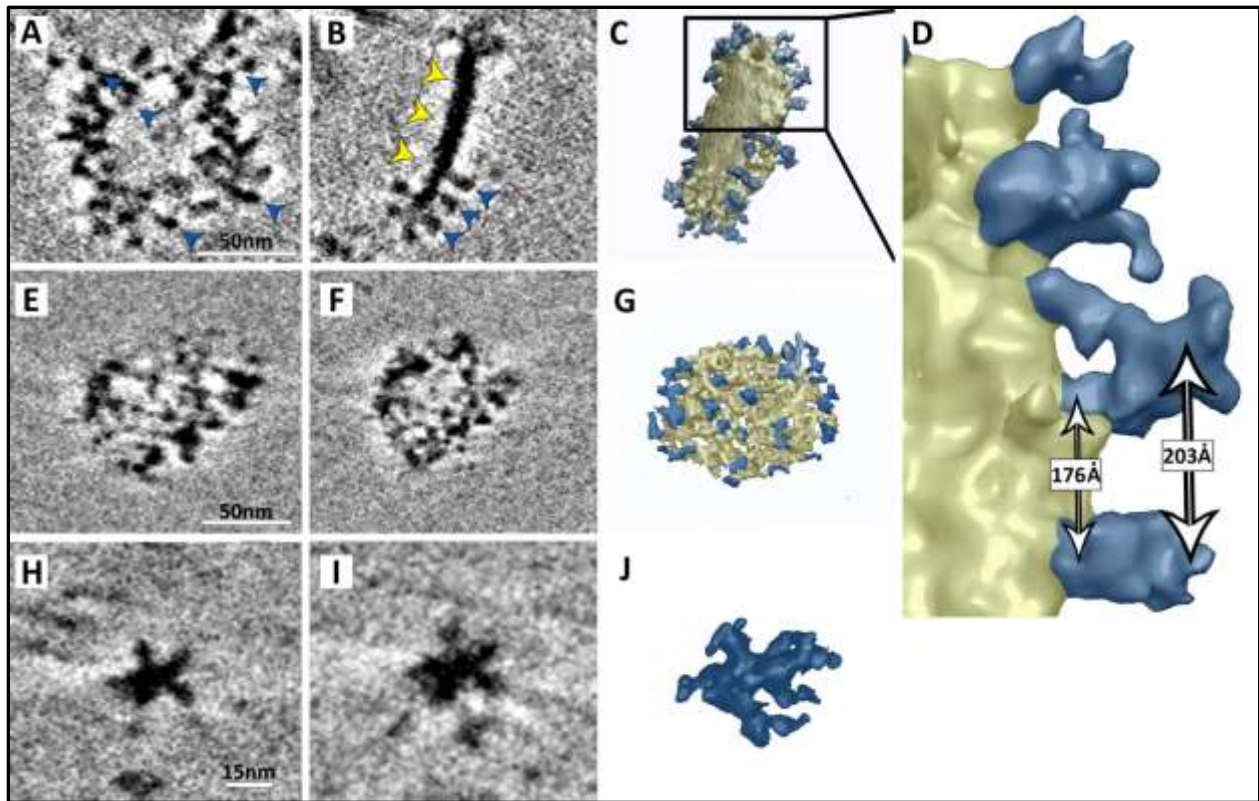


Figure 2-1. 3D-morphological characterization of particles in the H1-VLP and H5-VLP formulations. The most abundant particles were disc-shaped VLPs with loosely packed HA trimers (A-D), followed by spheroid-shaped VLP with more densely packed trimers (E-G). Rosettes composed <0.01% of the HA content (H-J). Tomogram slices show the VLPs in two different orthogonal orientations (A,E,H versus B,F,I). The HA trimers and the membrane are indicated by blue and yellow arrow heads respectively. The isosurface representation (C,D,G,J) of each type of particle have been coloured with the HA trimers in blue and membrane in yellow.

2-5.2. Plant-made VLPs stored at 4°C do not change shape or size over time

On-going quality monitoring of the VLPs using other techniques (e.g: NTA and DLS) suggest that the average particle sizes of the H1- and H5-VLPs are slightly larger than our estimates by cryoEM (data not shown). These differences are likely attributable to the different techniques used and the characteristics of the particles themselves. Our stability data for both the H1- and H5-VLPs are supported by NTA and DLS quality monitoring of these products over time (data not shown).

Using cryo-EM the H1 and H5 formulations were observed every three months. At each time point the morphology and the size of ~1000 particles were determined. The nature and distribution of VLP particles did not change upon storage at 4°C for one year as assessed by One-way Anova (Fig. 2-2).

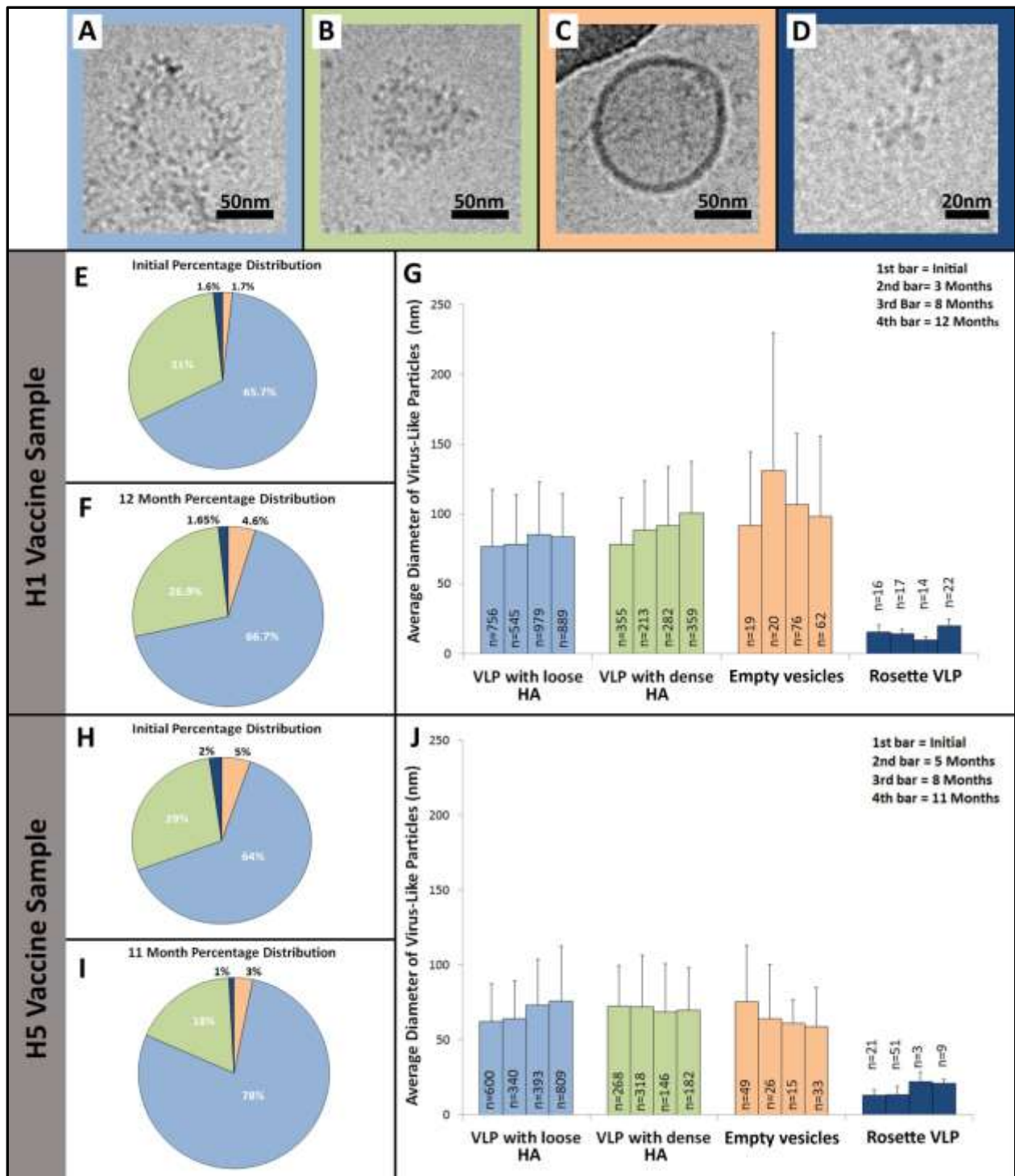


Figure 2-2. Distribution and size of the particles found in the H1-VLP and H5-VLP formulations during storage at 4°C for one year. A-D) 2D cryo-images of the four types of VLPs commonly seen in the sample, discus-shaped VLP with loosely packed HA trimers (A, light blue), spheroid-shaped VLP with densely packed trimers (B, green), empty vesicles (C, pink) and rosettes (D, dark blue). Panels E,F,H and I show the particle distribution using the same colour scheme as above. The average size of the different VLPs (with standard deviation) and the number of particles observed (n) at each time are shown in panels G and J.

By cryo-EM, we observed a degree of settling/clusters of VLPs over time. For both the H1- and H5-VLP preparations, individual VLPs were discernable and had the same morphology within the clusters (Fig. 2-3A), suggesting that the particles were intact. Particles could easily be dissociated with brief vortexing even after 24 months in storage (Fig. 2-3A-B). Particle size measurements by DLS and NTA techniques demonstrate that the size of individual VLPs remains constant (data not shown). We observed a slow increase in the number of clustered VLP by cryo-EM with time (with clusters observed in nearly all images after 8 months for H1 and 11 months for H5, or up to 65% of particles in clusters for H1 and 30% for H5. We cannot exclude to explain the discrepancy that clusters could bind to the grid more so than individual particles.

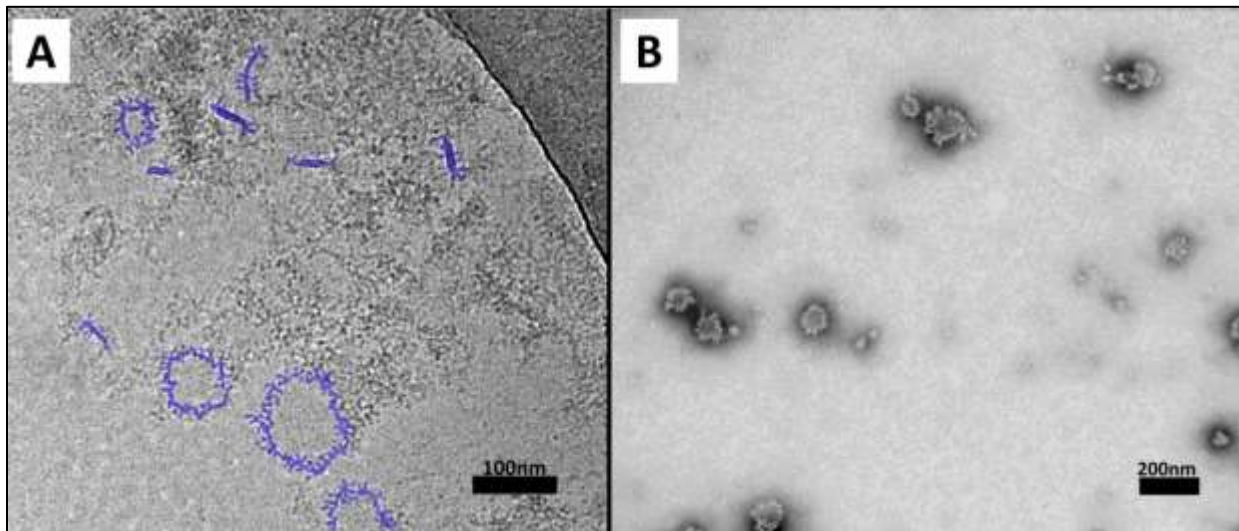


Figure 2-3. Observation by cryo-EM of VLP clustering in the H1 and H5 formulations.

A) Individual VLPs are visible within clusters (eg: some coloured blue). B) Negative stain image of the 24 month old H1 VLP sample after 30s vortexing. Individual VLPs with HA trimers are well separated.

2-5.4. Interaction of H1- and H5-VLPs with antigen presenting cells

When H1-VLPs were incubated with mouse DCs at 4°C to slow the metabolic rate of the cells, VLPs were seen at the plasma membrane (Fig. 2-4A). When DCs were incubated with H1-VLP at RT for 60 minutes, VLPs were observed both at the cell surface and within endosomes (Fig. 2-4C-D). The discus-shaped VLPs were easily recognized in the side view orientation (Fig. 2-4A, C-D). No VLPs were seen at the surface of control cells. Displayed at many of the control cell surface were minimal dendritic branches extended from the plasma membrane surface (Fig. 2-4B). Accumulation of the discus-shape H5-VLPs was also seen at the surface of U-937 blood cells incubated with H5-VLPs at 37°C and within endosomes (Fig. 2-4E) but not in control cells (Fig. 2-4F).

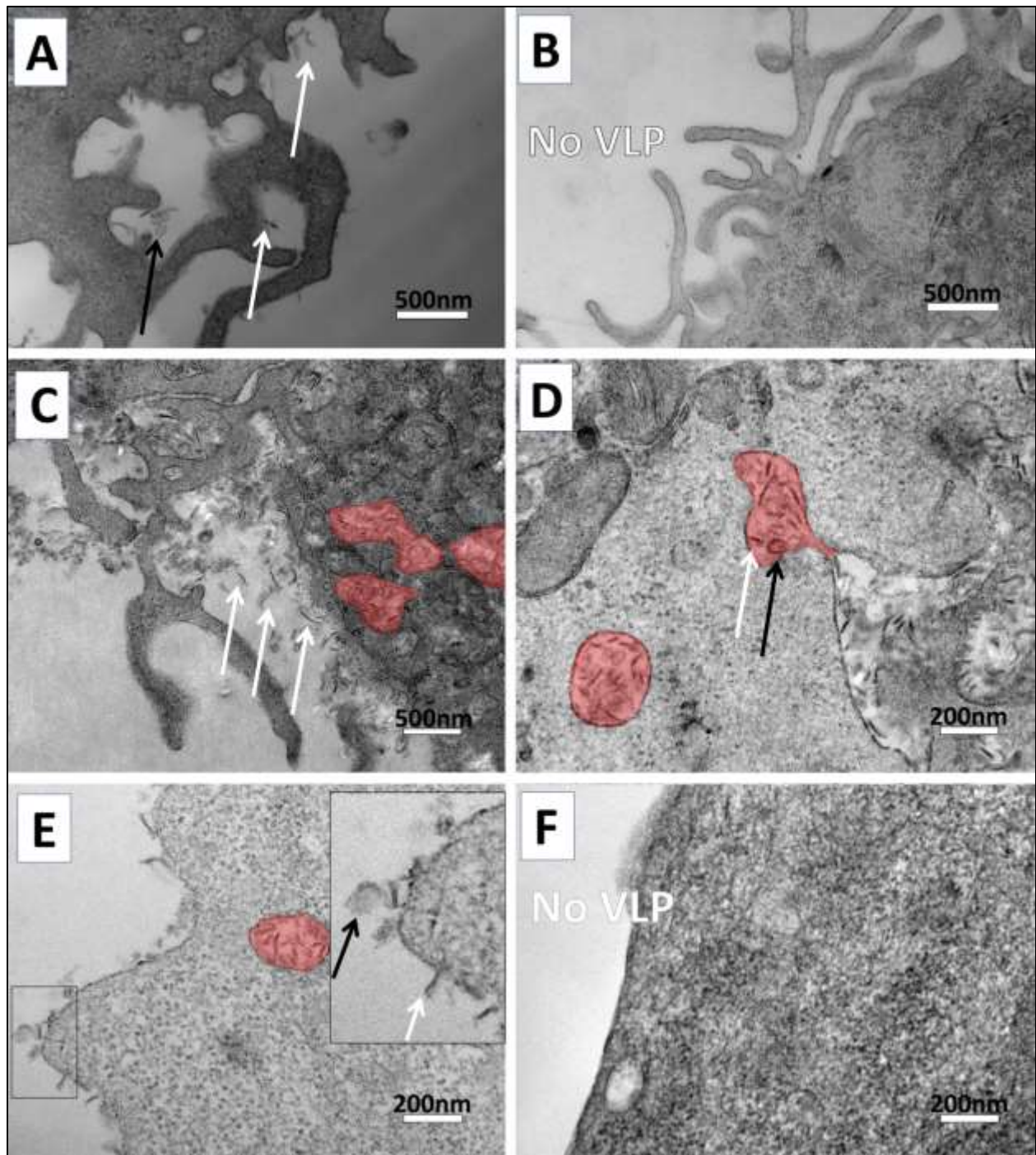


Figure 2-4. Interaction of the discus-shaped H1- and H5-VLPs with murine dendritic cells (DC) and U-937 cells examined by TEM of ultrathin epon resin sections. A) Semi-thin section of mouse DC incubated with H1-VLP at 4°C for 30 minutes. Discus-shaped VLPs observed in side-view orientations (white arrows) and top-views (black arrows) binding to the plasma membrane. B) Control DC not exposed to VLP. C) Mouse DC incubated with H1-VLP at RT for 60 minutes. VLPs observed at the cell membrane and within endosomes (red). D) Higher magnified image of VLPs in endosomes and being internalized within the DCs. E) Section of a

U-937 cell exposed to H5-VLP at 37°C for 45 minutes. Many disc-shaped VLPs were observed along the plasma membrane and within endosomes. D) Control U-937 cell.

Both the murine DCs and the U-937 cells exposed to VLPs at either RT or 37°C had morphologic changes commonly associated with activation, including vacuolization of the cytoplasm and the outgrowth of large dendritic branches. These changes were not seen in control DCs not exposed to VLPs (Fig. 5A-B). Overall, approximately 75% of the murine DCs exposed to the H1-VLP for 60 minutes at RT showed evidence of extensive branching compared to only 21% of the control cells (Fig. 2-6).

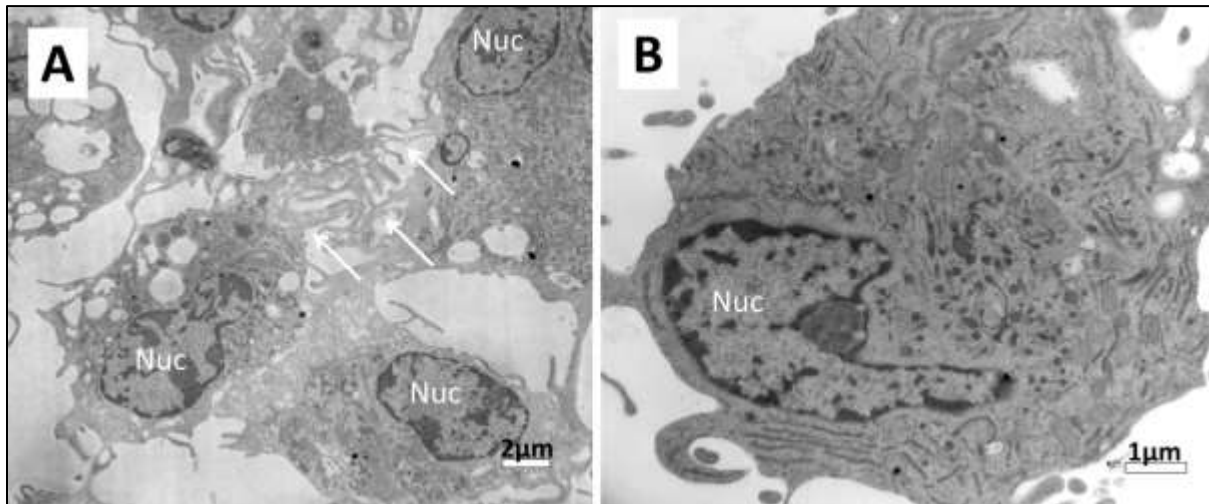


Figure 2-5. Murine DCs activated from incubation with H1-VLP. A) Semi-thin section of DC incubated H1-VLP, cell displaying extensive branching of pseudopodia from the plasma membrane (some examples of branches indicated with white arrows) Nucleus (Nuc). B) Control DC did not display either vacuolization or branching.

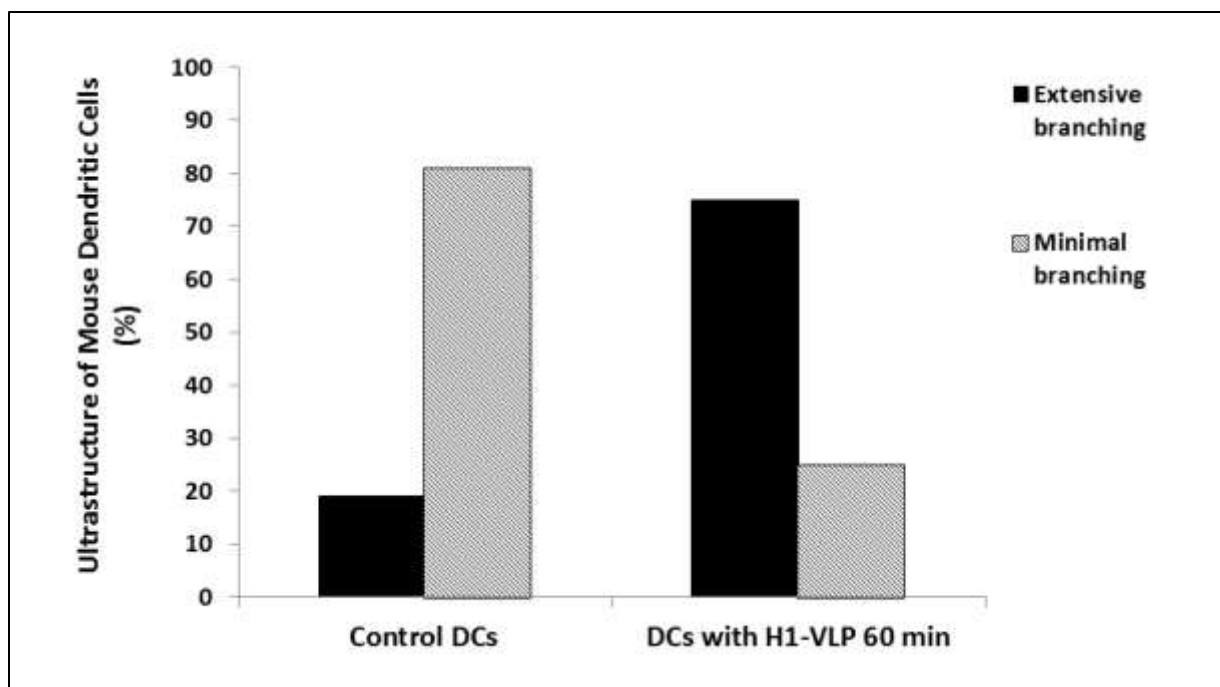


Figure 2-6. Ultrastructural quantification of murine DCs activated from incubation with H1-VLP. Cell activation was quantified by low magnified images of cells. Large branched extensions were compared to non-extended plasma membrane. Control cells had only 25% of cells with extensive branching and treated cells had 75% presence of extensive branching upon exposure to H1-VLP at room temperature for 60 minutes.

2-6. Discussion

Nanoparticles have many attractive features as vaccines that are increasingly being exploited across a number of platforms to target a wide range of pathogens. A relatively new approach is the use of transient *Agrobacterium*-driven transfection to produce VLP vaccines in plants. Although such vaccines have shown considerable promise in eliciting both humoral and cellular responses to influenza antigens (Pillet *et al.*, 2016; Pillet *et al.*, 2015; Landry *et al.*, 2010), very little is currently known about the ultrastructure of these plant-made particles.

In this work, we used cryo-electron tomography to define the 3D shape of both H1- and H5-VLPs, the majority of which (65%) were disc-shaped with HA trimers distributed around the equatorial membrane circumference. This somewhat flattened form is distinct from the

elongated rods or spherical shapes of native influenza particles (Wrigley *et al.*, 1979; Booy *et al.*, 1985; Fujiyoshi *et al.*, 1994; Harris *et al.*, 2006) and may take this form, because the plant-made VLPs carry only the viral HA (D'Aoust *et al.*, 2008; Chen *et al.*, 2007; Le Mauff *et al.*, 2015). In particular, the absence of both the matrix (M1) protein, that interacts with the cytoplasmic tails of the surface glycoproteins (HA and neuraminidase (NA)) in the native virus (Jin *et al.*, 1997; Chen *et al.*, 2007) and genetic material would be likely to influence the general shape of the VLPs. The average size of the plant-made VLPs as determined from 2D cryo-EM images and cryo-electron tomography was 75 ± 25 nm in diameter; slightly smaller than native influenza virions that are 100-200nm in diameter, also analyzed by cryo-EM and cryo-electron tomography (Katz *et al.*, 2014; Harris *et al.*, 2006).

In both the H1- and H5-VLPs, all of the HA molecules appeared to be trimeric in form and these trimers were inserted at relatively low density into the plant-origin membrane. The discoid form had approximately 30-50 trimers per particle comparison to native influenza A virions that have approximately 350 glycoprotein spikes (including both HA trimers and NA tetramers) (Harris *et al.*, 2006) with an average distance of 100 Å between neighbouring HA trimers (Wasilewski *et al.*, 2012). On average the individual HA trimer radius is $\sim 20-40$ Å on the native viral HA (Wilson *et al.*, 1981). This means there is relatively limited access to some HA epitopes (Fleury *et al.*, 1999; Wilson *et al.*, 1981) and particularly to the membrane-proximal stalk region that is well-conserved between strains (Eikert *et al.*, 2009). In comparison the H1-VLPs HA average distance was found to be 176Å from neighbouring stalk regions, and 203Å away from globular head regions. Moreover in the discus-shaped VLPs, most HA trimers had only 2-3 close neighbours and were fully accessible from both sides. The greater average distance between HA trimers on the VLP surface raises the possibility that the immune system

may have greater access to otherwise ‘hidden’ HA epitopes following VLP vaccination than natural infection. Although antibodies appear to be able to squeeze in between the glycoprotein spikes of native influenza virions to target these epitopes (Harris *et al.*, 2013), greater accessibility could certainly facilitate interaction with the membrane-bound B cell receptors in influenza- or specific strain-naïve subjects. Indeed, Schneeman and colleagues used a Flock horse virus-based VLP to make this region of the HA molecule more available to the immune system and elicited cross-reactive stem antibodies in a mouse model (Schneemann *et al.*, 2012). Although the plant-made VLPs have been shown to induce strong antibody responses, it is not yet known if they also preferentially induce anti-stalk antibodies. These studies are currently ongoing. Further structural analysis at even higher resolution is required to determine if the HA 3D structure at the surface of the plant-made VLPs is identical to that found at the surface of native influenza viruses.

Both the morphology and size of the plant-made candidate VLP vaccines were investigated by cryo-EM. Particles proved to be stable over the course of one year, which is consistent with the fact that these formulations maintain their immunogenicity over time (Pillet *et al.*, 2016). The VLP structural stability investigated by cryo-EM data is consistent with data collected using DLS and NTA techniques that are performed at regular intervals within the company’s quality control program (data not shown).

Together, these data suggest that the plant-made VLPs are both morphologically and immunologically stable for at least 12 months at 4°C. Although there was some indication of settling/cluster formation by cryo-EM over time, the apparent clusters were easily disassembled by vortexing, and individual VLPs maintained their integrity. It is noteworthy that electron microscopy studies of native influenza virions have also reported settling/cluster formation over

time (Campbell *et al.*, 2004). Additionally, some adjuvants such as alum are thought to act, at least in part, by clumping antigens into a particulate form, enhancing internalization by APCs (Morefield *et al.*, 2005; Petrovsky & Aguilar, 2004). Taken together, this settling/ clustering of the plant-made VLPs over time are unlikely to have any negative impact on immunogenicity or to result in increased reactive allergic responses.

Finally, we have shown that the plant-made VLPs interact rapidly with the plasma membranes of both murine DCs and human U-937 cells. Like native virions, the VLPs can be seen bound at the surfaces of these APCs, presumably mediated by sialic acid moieties (reviewed in Nayak *et al.*, 2004). At room temperature and 37°C, they appear to be internalized and are readily visualized within endosomes. Although they contain no viral nucleic acid, *in vitro* exposure to the plant-made VLPs appeared to activate murine DCs as evidenced by the presence of extended pseudopodia. The degree of activation could not be attributed to the presence of modest amounts of contaminating *Agrobacterium* endotoxin (data not shown). Although the structure of the plant-made VLPs differs from that of the native virus, these data suggest that at least their initial interactions with APCs may be quite similar: binding of HA to receptors at the APC plasma membrane and cell entry by endocytosis (Steinhauer *et al.*, 2013; Bradley *et al.*, 2011; Neumann *et al.*, 2009., Root *et al.*, 2000., Carroll & Paulson, 1985).

This is the first detailed ultrastructural study of plant-made VLPs bearing two different influenza HA proteins. The H1- and H5-VLPs were very similar overall. The large majority of particles were disc- or ovoid-shaped with HA trimers inserted with relatively wide spacing (~175Å) into the membrane. Using the visualization techniques described in this paper, on average, these VLPs were structurally stable over time. At least in their initial interactions with APCs, the plant-made VLPs appeared to be handled in a manner analogous to native influenza

virions. Morphological changes consistent with striking activation were seen when murine and human APCs upon exposure to either H1- or H5-VLPs. On-going ultrastructural work with these novel vaccine candidates will define HA protein and trimer structure at higher resolution and the use of correlative microscopy will determine the fate of the internalized VLPs. The morphological characteristics of VLPs bearing different HAs will be correlated with immunologic outcomes.

2-7. Acknowledgements

This work was supported by Medicago Inc; Economie, Science et Innovation Quebec; Genome Canada; FEMR McGill University; Alexander McFee Internal Studentship, Faculty of Medicine, McGill University.

Chapter 3. Establishment of a correlative light and electron microscopy method to visualize virus-like particles interacting with immune cells

Authors:

Brianne J. Lindsay¹, Alex Makarkov², Sabrina Chierzi², Nathalie Landry³, Brian Ward², Isabelle Rouiller¹

Affiliation:

1. Department of Anatomy & Cell Biology; Faculty of Medicine; McGill University; Groupe de Recherche Axe sur la Structure des Proteines (Grasp); Groupe d'Etude de Proteines Membranaires (GEPROM), 3640 University Street, Montreal, QC, H3A 2B2, Canada.

2. Research Institute of McGill University Health Centre-Suite EM3-3248, 1001 Decarie Street, Montréal, QC, H4A 3J1, Canada.

3. Medicago Inc. Quebec, QC, Canada.

Corresponding author:

Dr. Isabelle Rouiller
Department of Anatomy & Cell Biology
Faculty of Medicine
McGill University
Tel: 514 398-3244
Email: Isabelle.rouiller@mcgill.ca

3-1. Preface

The influenza virus enters host cells through binding of HA with sialic acid receptors. The binding interaction initiates viral uptake via endocytosis. Plant-generated Virus-like particles (VLPs) produce potent immunogenic responses in animals and humans. In chapter 2, using cryo-electron tomography, we showed that the VLPs are structurally distinct from the native influenza virus. The plant-made VLPs were observed to interact with immune cells similarly to native influenza viral particles by binding to the plasma membrane and discus-shaped VLPs were observed within endosomes of U-937 lymphocytes. As different endocytic pathways eliciting various immune responses, we pursued the study of interactions with different immune cells. To study H1- and H5-VLPs interaction with human macrophages, we utilized fluorescence microscopy and TEM approaches in a correlative fashion (CLEM).

3-2. Abstract

Influenza virus infects the upper respiratory tract and is associated with severe medical complications for individuals with weakened immune systems. Unfortunately, protection is limited with current influenza vaccines. Plant-made influenza VLPs are a promising vaccine alternative for influenza. The plant-made VLPs present some structural differences with the native virus. The VLPs were observed to interact with immune cells by binding to the plasma membrane and were observed within endosomes of U-937 lymphocytes which is a similar mode of interaction for the native virus, however details as to the internalization of the VLPs were left to be understood. The importance of understanding these internalization pathways is vital to comprehend the potential immune cell response triggered within cells. Utilizing fluorescence microscopy, we visualized binding of the DiD-labelled VLPs to human U-937 lymphocytes and human peripheral blood mononuclear cells (PBMCs) plasma membranes. Differential binding characteristics were displayed upon VLPs binding to the plasma membrane of the macrophages. Some of the cells had dispersed binding of VLPs along the membrane, while others had very concentrated binding at one area of the plasma membrane of the cell. By transmission electron microscopy (TEM), the VLPs were found bound to the plasma membrane and within endosomes of the human macrophages. We are developing correlative light and electron microscopy (CLEM) approaches in order to explain the diphasic binding pattern observed by fluorescence microscopy that is diffuse around the cell surface or clustered in a specific region. Here we will summarize progress made by LM, EM and CLEM.

3-3. Introduction

Influenza causes a highly contagious disease most commonly referred to as the ‘flu’. Even though it has been studied for decades, influenza remains a global health threat as the virus undergoes frequent mutations (Carrat & Flahault, 2007; Gabriel *et al.*, 2005). Mutations of the viral surface glycoproteins result in non-recognition of the virus by the immune system. Current vaccines are generated in eggs and rely on prediction strategies. The World Health Organization (WHO) is responsible for tracing mutations within the viral strains. There remain many issues with the current influenza vaccines, including long manufacturing time and occasional poor efficiency when prediction is inaccurate. An alternative vaccine is the generation of Virus-like particles (VLPs) using transient expression of HA gene cloned in *Agrobacterium* as a bacterial vector of the genetic material within a relative of the tobacco plant (*Nicotiana benthamiana*), a technology developed by Medicago Inc.

The influenza virus enters cells mainly via clathrin-mediated endocytosis (Rust *et al.*, 2004) which was first visualized by transmission electron microscopy (TEM) (Patterson *et al.*, 1979). Cryo-EM tomography showed that the majority of the VLPs were on average 75nm in diameter, discus-shaped with HA proteins around their circumference. We found the VLPs bound to the surface of murine dendritic cells, and human U-937 lymphocytes, as well as within endosomes of the human lymphocytes.

The visualization of plant-made VLPs interacting with cells is important to investigate in further detail as different endocytic pathways exhibit various immune responses of either major histocompatibility complex I (MHC I) or MHC II presentation (Duclos *et al.*, 2011; Houde *et al.*, 2003). Plant-made influenza VLPs containing the fusion protein hemagglutinin-enhanced green fluorescent protein (HA-GFP) has been previously generated for *in vivo* studies (Young *et al.*,

2015). We have investigated novel approaches to specifically label HA protein along the VLPs surface to visualize VLPs within endosomes, however immunofluorescence or immunogold (or quantum dot) labelling would interfere with HA's ability to bind to sialic acid receptors on target cell membranes as the antibody would block the receptor binding region of HA.

In the present study, we utilized confocal microscopy in collaboration with TEM techniques to visualize H1 and H5 DiD-labelled VLPs with human U-937 blood lymphocytes and human primary blood mononuclear cells. DiD-labelling is advantageous as it is a lipophilic dye, inserted into the VLP membrane and overall morphology was found to not be modified. We describe the preliminary establishment of CLEM methods to analyze cellular interactions and we suggest further approaches to achieve exact cell monolayer correlation for the visualization of plant-made VLPs interacting with cells.

3-4. METHODS

3-4.1. Virus-like particles (VLPs)

The monovalent VLPs used in the current study were clinical-grade material and were produced by Medicago Inc. (Quebec, QC) as previously described (D'Aoust *et al.*, 2010). The HA sequences targeted were derived from A/California/7/2009 (H1-VLP) or A/Indonesia/5/05 (H5-VLP). VLPs were stained with the fluorescent lipophilic carbocyanine dye DiD (Thermo Fisher Scientific) at concentration 20µg/mL for 30 minutes at room temperature, and then purified from free dye using gel filtration columns (GE Healthcare PD MiniTrap G-25).

3-4.2. Observation of VLPs by cryo-EM

VLP aliquots maintained at 4°C in the dark were prepared as follows: 5µL of the H1-VLPs and 5µL of the DiD-labelled VLPs were placed for 1 minute on a Quantifoil R2/2 copper grid (EMS Inc.) previously glow-discharged for 30 seconds. Excess fluid was removed and the sample was plunged frozen in liquid ethane at -180°C using a Vitrobot (FEI Inc.) The chamber was set to 100% humidity at 4°C. Grids were stored in liquid nitrogen until imaging. The cryo-prepared VLP samples were visualized on a Tecnai F20 microscope (FIE Inc.) Images were recorded at 29,000x magnification and a defocus of 9µm using a Ultrascan 4k x 4k CCD Camera (Gatan Inc.) The micrographs were analyzed using Image J software (Schneider *et al.*, 2012).

3-4.3. U-937 cell preparation

U-937 cells, a human histiocytic lymphoma cell line, were obtained from the American Tissue Culture Collection (ATCC CRL-1593.2) and maintained in RPMI-1640 Medium, supplemented with 10% fetal bovine serum (FBS), 0.5 IU/mL penicillin, 50 µg/mL streptomycin and 10 mM HEPES (all from Wisent).

3-4.4. Human peripheral blood mononuclear cell preparation

Human PBMCs were isolated from whole blood samples donated by healthy volunteers. Written informed consent was obtained from all blood donors. PBMCs were separated by differential density gradient centrifugation. Blood sample was diluted with an equal volume of PBS pH 7.4 (Wisent). 9 mL of diluted blood was layered over 4 mL of the Lymphocyte Separation Medium (Wisent). Gradients were centrifuged at 650 x g for 45 min at room temperature without the brake applied. The PBMCs interface was carefully collected by pipette and washed with PBS by centrifugation at 500 x g for 15 min, and twice at 320 x g for 10 min.

3-4.5. Fluorescence microscope imaging

A total of 7 imaging experiments were conducted on the U-937 cells. Before each round of imaging cells were plated on Ibidi gridded glass plates (Ibidi Inc.) in serum-free RPMI-1640 medium at a density of 1 million cells per mL and left to attach to the glass surface for 30 minutes at 37°C (Fig. 3-1 A-B). The supernatant was removed, and attached cells were washed with serum free RPMI-1640 media. H1 and H5 DiD-labelled VLPs (15µg/mL by HA) were added to the U-937 cells at 37°C for 45 minutes (Fig. 3-1 A-B). PBS and PBS combined with DiD was used as a control. The cells were fixed with 4% paraformaldehyde (PFA).

A total of 4 imaging experiments were conducted with the PBMCs. The cells were re-suspended in serum-free RPMI-1640, plated on Ibidi gridded glass plates and allowed to attach to the glass surface for 30 minutes at 37°C (Fig. 3-1A). The supernatant was removed, and attached cells were washed twice with serum free RPMI-1640 to obtain the PBMCs adherent fraction that was enriched with monocytes (~50% of attached cells, based on assessment of cell and nucleus morphology). H1 DiD-labelled VLPs (15µg/mL by HA) were added to the PBMCs at 37°C for 45 minutes (Fig. 3-1 A-B). PBS and PBS combined with DiD was used as a control. The cells were fixed with 4% paraformaldehyde (PFA).

All LM images were taken using a laser scanning confocal microscope (Zeiss LSM780, RI-MUHC Imaging Core Facility). After fluorescence confocal imaging, the PFA solution was removed and replaced with 2.5% glutaraldehyde in 0.1M of sodium cacodylate and remained at 4°C overnight. For each experiment, VLPs were observed to be present within the fluorescent microscopy analysis.

3-4.6. Resin-embedding cell monolayer preparation for TEM imaging

After the overnight incubation with 2.5% glutaraldehyde in 0.1M of sodium cacodylate the cells were post-fixed in 1% osmium tetroxide containing 1% potassium ferrocyanide for 1 hour at 4°C. After washing in distilled water for one hour, the cells were en bloc stained in 2% uranyl acetate for 45 min and dehydrated in ascending concentrations of ethanol (30%, 50%, 70%, 80%, 90%, and 100%) for approximately 10 minutes each followed by three additional washes with 100% ethanol. The cells were progressively embedded with 1:1 ratio of epon:100% ethanol mixture for 30 min, followed by 3:1 ratio of epon: 100% ethanol mixture for another 30 min. The epon mixture was replaced with pure epon for 1hr at room temperature. Pure epon was replaced another time and the monolayers. Embedding procedures were followed as the method described in (Asakawa *et al.*, 2014) and polymerized at 57°C for 48hrs.

Removal of the epon blocks was conducted as described from Asakawa *et al.*, 2014, however for blocks that had remaining glass on the surface of the gridded map, the epon block was submerged in liquid nitrogen for ~20 seconds and the glass was removed carefully with a razor blade to not destroy the grid embedded pattern within the block. The blocks were trimmed according to the cells of interest confirmed based on the address on the gridded coverslip (Fig 1A). A trapezoid was trimmed around the area of interest (Fig 1B).

Ultra-thin sectioning was completed using a Reichert-Jung Ultracut E microtome (Leica Inc.) and a diamond knife (Diatome Inc.) (~70-80nm thickness). As many serial sections were collected using 200 Hex copper grids (EMS Inc.). The sections were post-stained with 4% uranyl acetate, and lead citrate for 8 and 5 mins and washed with distilled water in between.

Imaging was completed on a Tecnai T12 120Kv transmission electron microscope. Low magnified images were collected to locate the cells of interest from the confocal images. High magnified images were collected of the VLPs interacting with cells. Upon TEM analysis VLPs presence was not always observed, as the exact location was not found within the EM section to match to the LM image due to cell detachment issues. Image Processing was analyzed with Image J software (Schneider *et al.*, 2012) and Photoshop Cs4 (Adobe).

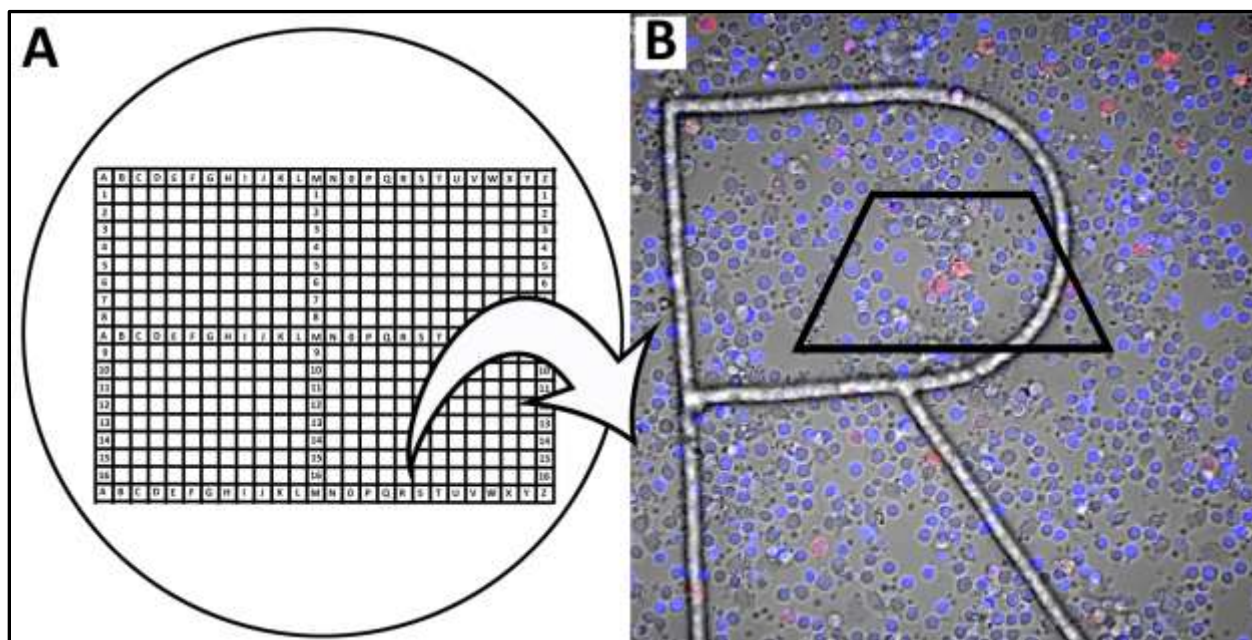


Figure 3-1. Schematic of CLEM experiments with U-937 blood lymphocytes and human PBMCs. A) Schematic of CLEM grid plate coordinate system. B) Fluorescence microscopy image of PBMCs in an area of interest, displaying the letter R. Cell nuclei of PBMCs stained with DAPI, and DiD-VLP labelled in red, a trapezoid is cut around cells of interest and sectioned using a diamond knife.

3-5. Results

3-5.1. DiD lipophilic dye does not interfere with VLPs morphology

A fluorescent lipophilic dye, DiD was treated with the H1 and H5 VLPs and inserted into the lipid membrane. Using cryo-EM, we first verified the VLP's morphology was not modified by the insertion of the dye into the membrane of the VLPs. We observed that the morphology of VLPs remained intact and was not affected by the dye presence (Fig. 3-2A). VLP samples were

imaged without the presence of DiD to compare morphology to the native form (Fig. 3-2B). Morphologically of the two samples were indistinguishable from one another (Fig. 3-2A-B).

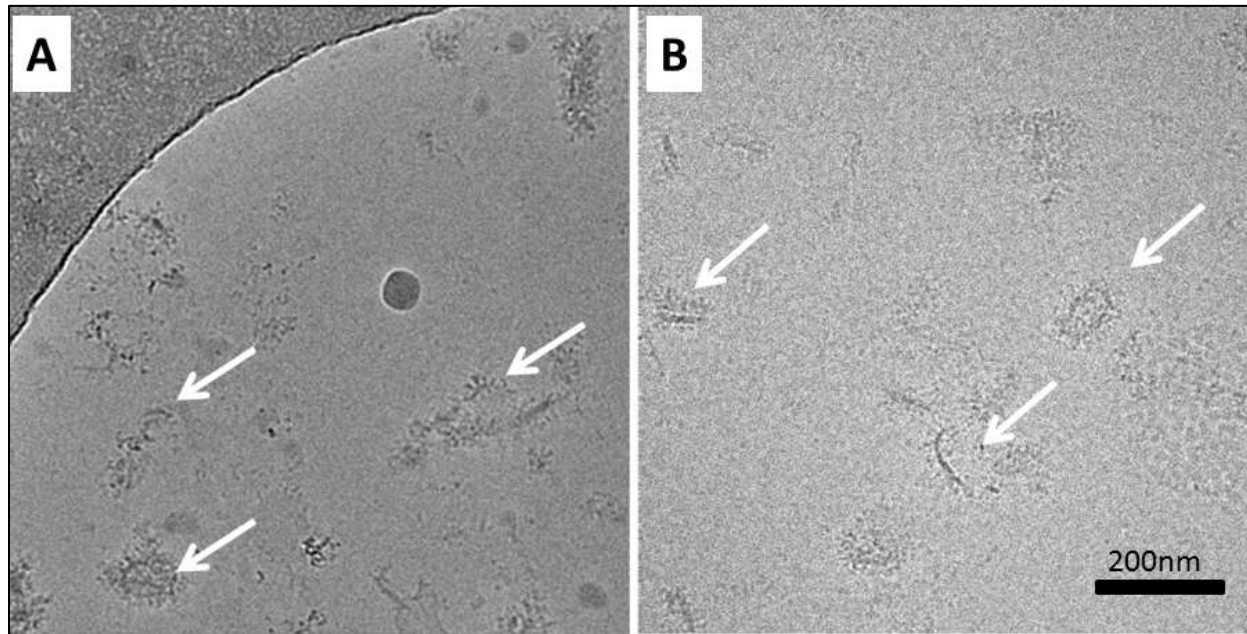


Figure 3-2. Comparison of DiD lipophilically dyed H5 VLPs to non-dyed VLPs by cryo-EM. A) Micrograph of H5 VLPs dyed with DiD, white arrows indicate some examples of VLPs. B) Micrograph of the H5-VLPs preparation not dyed with DiD.

3-5.2. Fluorescence LM studies of the interaction of H1- and H5-VLPs with Human U-937 lymphocytes

When human U-937 blood lymphocytes were incubated with H1 or H5 DiD-labelled VLPs for 45 minutes at 37°C, red stain was observed along the periphery of the cells upon every LM imaging session (Fig. 3-3 A-C). Only a small portion of cells at the LM level had VLPs bound to the plasma membrane (Fig. 3-2 A-C). Differential binding characteristics were observed from the LM images. The cells that had VLPs present had two distinct types of binding; either diffuse binding of VLP around the entire plasma membrane, or only one clustered area of binding at one region of the membrane (Fig. 3-2B) No stain was present in control cells which were incubated with PBS and DiD-dye (Fig 3-3 D).

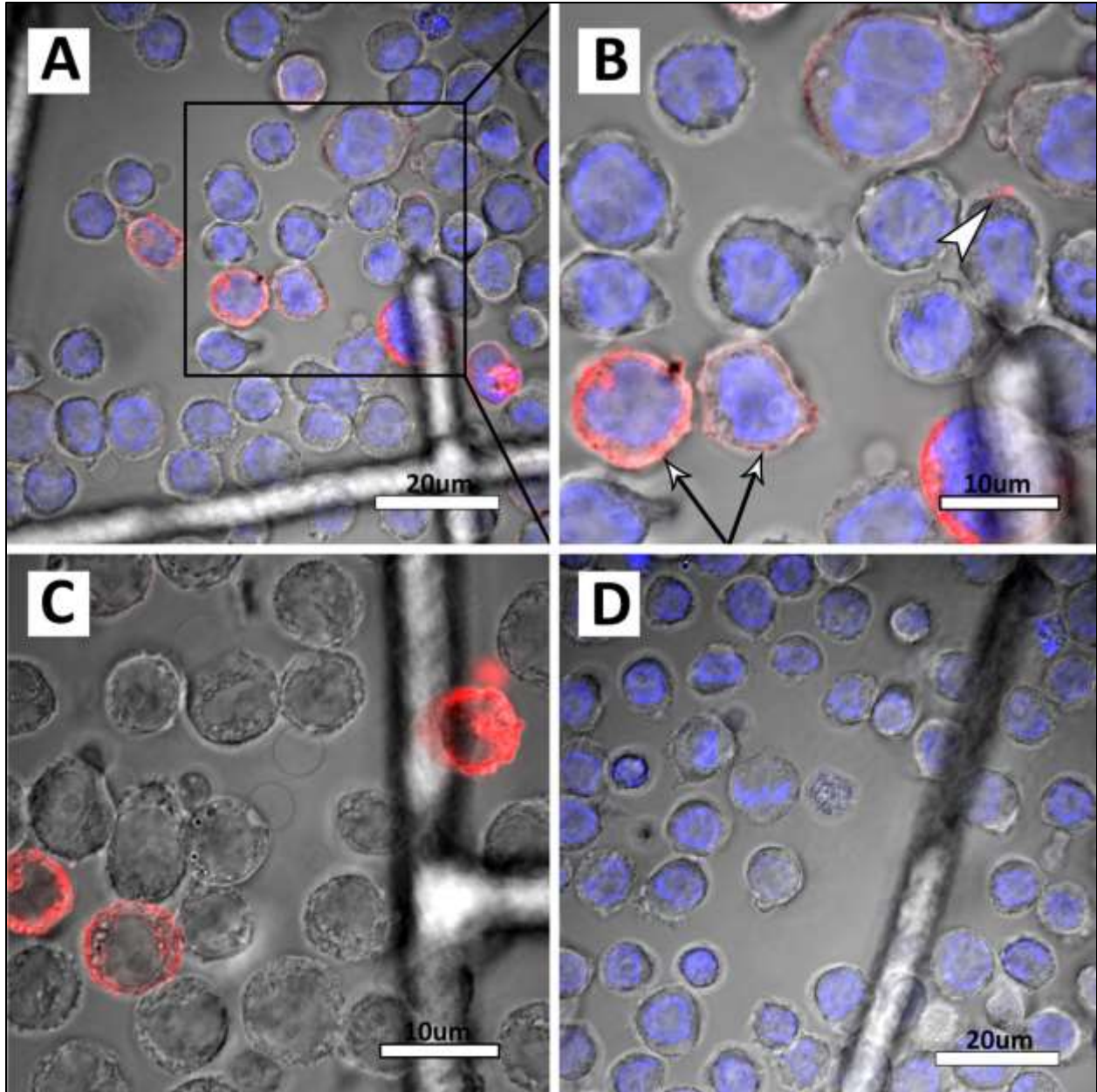


Figure 3-3. U-937 Blood lymphocytes treated with DiD-labelled VLP by confocal microscopy. A) Fluorescence microscope image of H5-DiD VLP, DAPI (blue) B) Higher magnified image of A, white arrows displaying diffuse VLP binding around periphery of plasma membrane, white arrowhead indicating concentrated binding to one area of the plasma membrane. C) Fluorescence microscope image of H1-DiD VLP no DAPI stain incorporated. D) Fluorescence microscope image of control cells not treated with PBS-DiD and DAPI (blue).

3-5.3. Fluorescence LM studies of the interaction of H1- and H5-VLP with Peripheral blood mononuclear cells

Human PBMCs were incubated with H1 or H5 DiD-labelled VLPs. The control cells were treated with PBS and DiD to ensure the fluorescent label was not inducing ultrastructural changes to the cells which would most likely be displayed by cell activation. By confocal microscopy, the H5-DiD labelled VLPs and the H1-DiD labelled VLPs interacted with the cells (Fig. 3-4 A-C). The frequency of binding is currently being quantified from the confocal images by our collaborating laboratory. The PBS-DiD control cells did not have any structural features observed to suspect cell activation from the lipophilic dye (Fig. 3-4D). These interactions were observed consistently throughout the four experiments.

The same observation of concentrated VLPs and diffuse VLP interactions was observed with the human PBMCs by fluorescence microscopy (Fig. 3-4 A-B). It was also interesting to note not all cells imaged by confocal microscopy were positively bound to VLPs similar to the U-937 cells (Fig. 3-4 A-C).

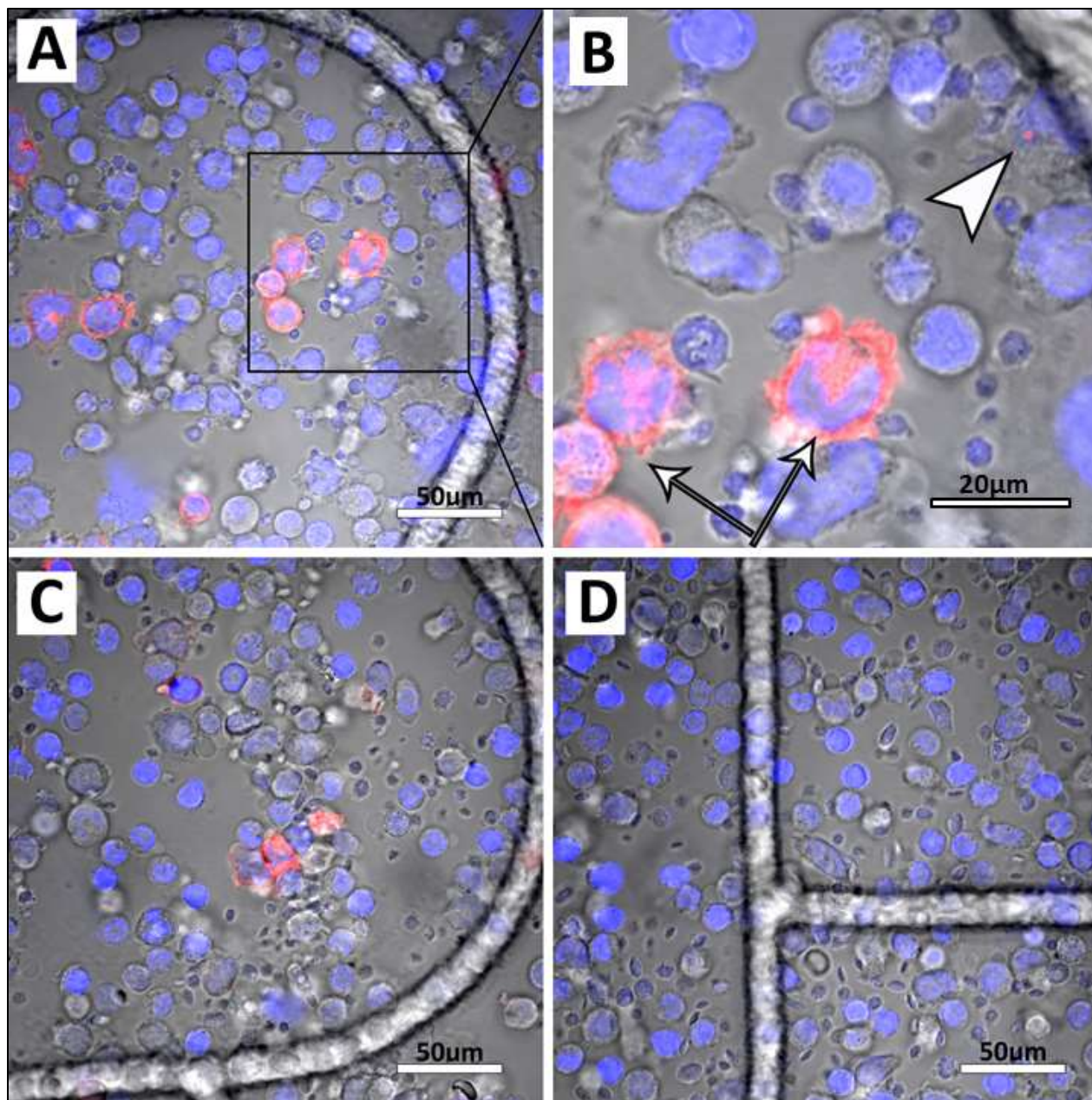


Figure 3-4. Human peripheral blood mononuclear cells (PBMCs) treated with DiD-labelled VLPs. A) Fluorescence micrograph of H1-DiD VLPs, DAPI stain in blue B) Higher magnified image of A, white arrows displaying diffuse VLPs binding around periphery of plasma membrane, white arrowhead indicating concentrated binding to one area of the plasma membrane. C) Fluorescence microscope image of H5-DiD VLPs. D) Fluorescence microscope image of control cells not treated with VLPs, but with PBS-DiD and DAPI.

3-5.4. TEM observations of the interaction of H1- and H5-VLP with human U-937 lymphocytes

By TEM the H1 and H5 DiD-VLPs were observed to be within close proximity and bound to the plasma membrane of the U-937 cells (Fig. 3-5 A-C). H5-VLPs was observed within endosomes, near the border of the plasma membrane by TEM (Fig. 3-5 A-B). H5 DiD-VLPs had increased binding presence on the U-937 cell membrane observed within TEM micrographs (Fig. 3-5 A-B). The TEM ultrastructural findings also demonstrate that the DiD labelled discus-VLPs bind to the plasma membrane and are internalized via endocytosis.

From the TEM micrographs, there was only one experiment out of 7 which demonstrated high frequency of VLPs surrounding the plasma membrane of U-937 cells (Fig. 3-5A-B). For most other experiments the VLP's interaction at the plasma membrane was not as prominent (Fig. 3-5C). We did not observe any structures that could correspond to the clustered stain seen in LM (Fig. 3-5 A-C). There was no presence of VLPs within control cells as expected (Fig. 3-5D).

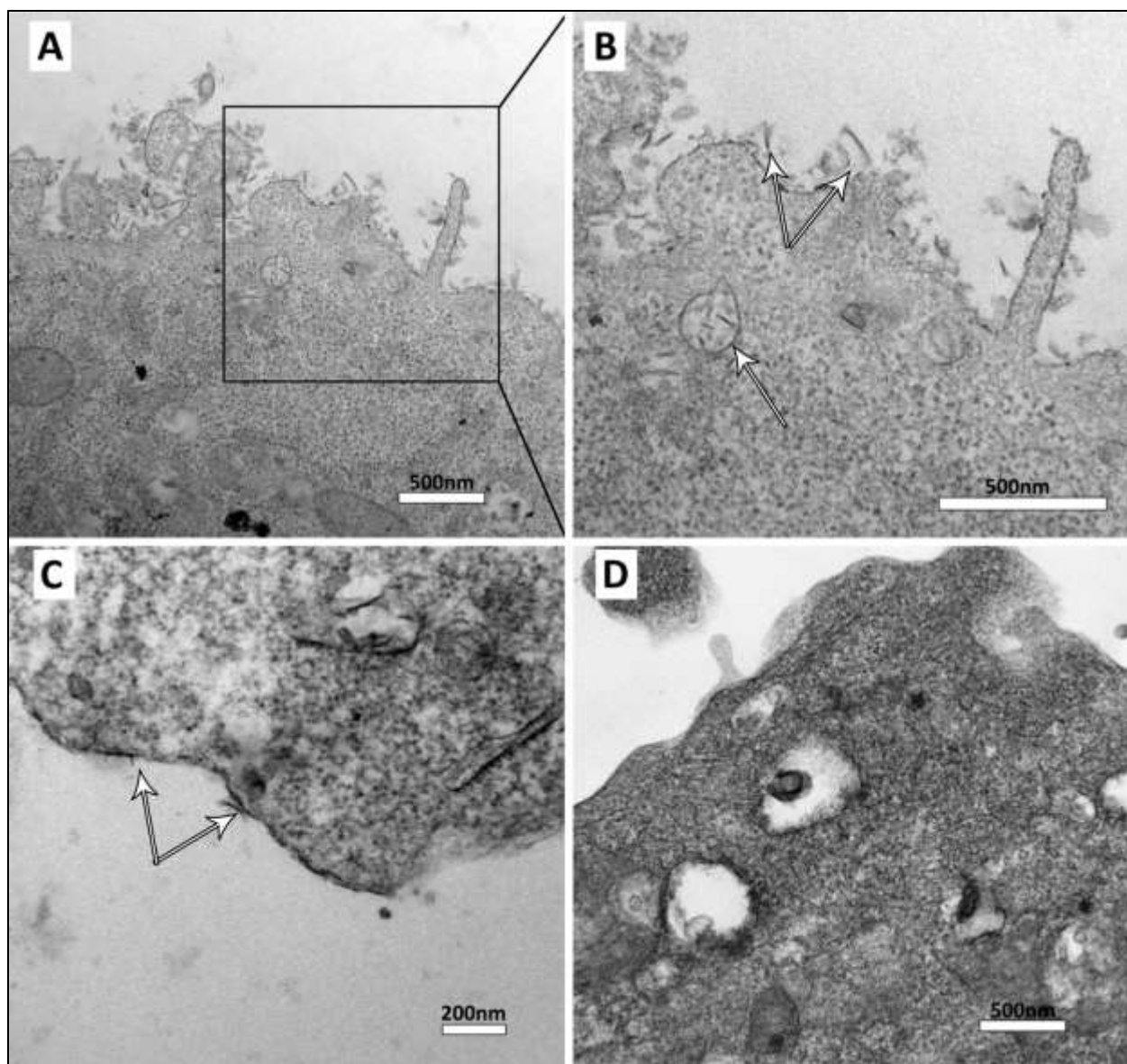


Figure 3-5. TEM micrographs of human U-937 blood lymphocytes treated with DiD-labelled VLPs. A) Semi-thin section of H5-DiD labelled VLPs treated with monolayer U-937 cells. B) Higher magnified image of A, white arrows indicate side orientations of the VLPs disc shape interacting with the plasma membrane of lymphocytes as well within endosomes. C) Semi-thin section of H1 DiD-labelled VLPs, less VLP bound to the plasma membrane. D) Control cell incubated with PBS.

3-5.5. TEM observations of the interaction of H1- and H5-VLP with human PBMCs

H1 DiD-labelled VLPs were observed to be within close proximity of the plasma membrane and bound to the membrane of the human PBMCs observed by TEM (Fig 3-6A-B).

At the EM level, the VLP have been observed to be bound to the plasma membrane throughout the four experiments conducted. H5 DiD-labelled VLPs have also been incubated with human PBMCs however no cellular interaction has been visualized yet. The ultrastructural features of the cells were observed at the TEM level to try and gain insight as to particular structural explanations as to why the VLP bound to cell membranes differentially. Upon TEM observation, the cells were similar to control cells in that the cell morphology appeared healthy.

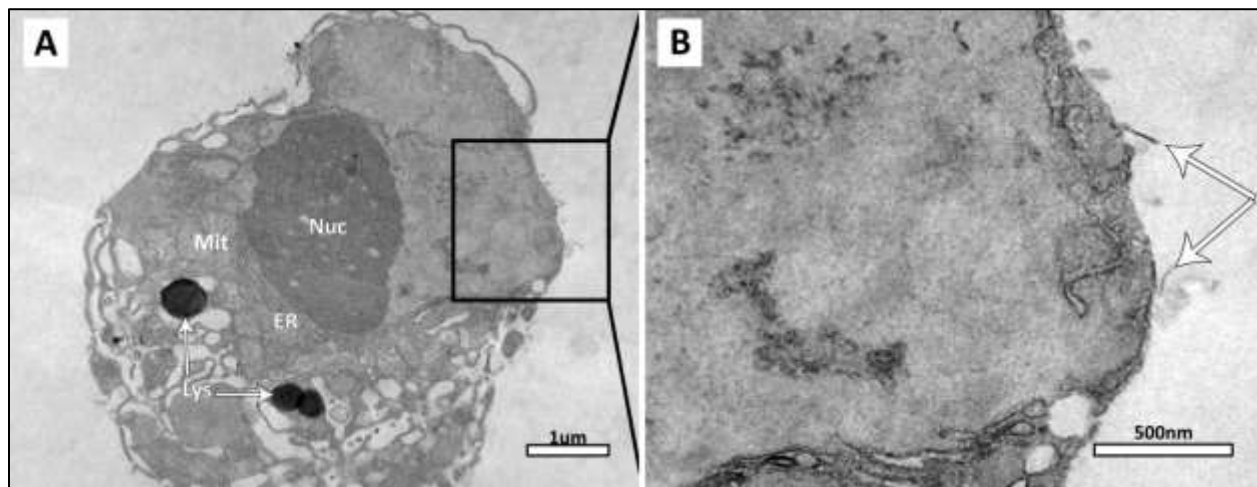


Figure 3-6. TEM micrograph of PBMCs treated with H1-DiD labelled VLPs. A) Semi-thin section of H1-DiD labelled VLP treated with monolayer U-937 cells. Cell nuclei (Nuc), mitochondria (Mit), endoplasmic reticulum (ER), and lysosomes (Lys) all displayed healthy morphology. B) Higher magnified image of A, white arrows indicate side orientations of the VLP discus shape interacting with the plasma membrane of the blood cells.

3-5.6. Methods towards correlative light and electron microscopy (CLEM) with influenza VLP vaccine samples

Correlative microscopy was attempted to analyze at the EM level the differential binding of VLPs to macrophages seen in LM. Using glass slides with a gridded coordinate system we were able to fluorescently image monolayers of human U-937 lymphocytes and human PBMCs (Fig. 3-3 A-C and 3-4 A-C). After resin embedding procedures, EM blocks containing the processed cells had the grid coordinates etched into the block face surface (Fig. 3-1B). The

coordinates were used as a reference location for the cells that were imaged by confocal microscopy (Fig. 3-1A-B). A trapezoid was trimmed around the coordinate, and sectioned for ultrathin sectioning using a diamond knife (Fig. 3-1B).

Upon TEM imaging, the orientations of the sections were scanned to find the optimal trapezoid orientation to match the fluorescent images, and very low magnified images were taken to view clusters and patterns of the cells (Fig 7A-B). The low magnification (480x) images were compared to the confocal microscopy images to identify if the cells of interest were present (Fig 7A-B).

During the CLEM approach, we experienced issues with some cells not remaining attached during EM processing procedures. For some of the semi-thin sections it appeared that some cells had lifted and possibly left plasma membrane observed within the cross-sections. These cross-sections appeared very faint during EM imaging. To investigate whether the cells may be in different planes, rather than in a true monolayer, we prepared EM grids with sections taken from further into the block face. After TEM imaging of those grids, it was demonstrated the cells were not on another plane because the sections did not contain cells. It was concluded that different adherence methods would have to be incorporated for future experiments, such as the addition of poly-lysine before plating the cells. These approaches are being incorporated in current experiments on-going in the two collaborating laboratories at McGill University.

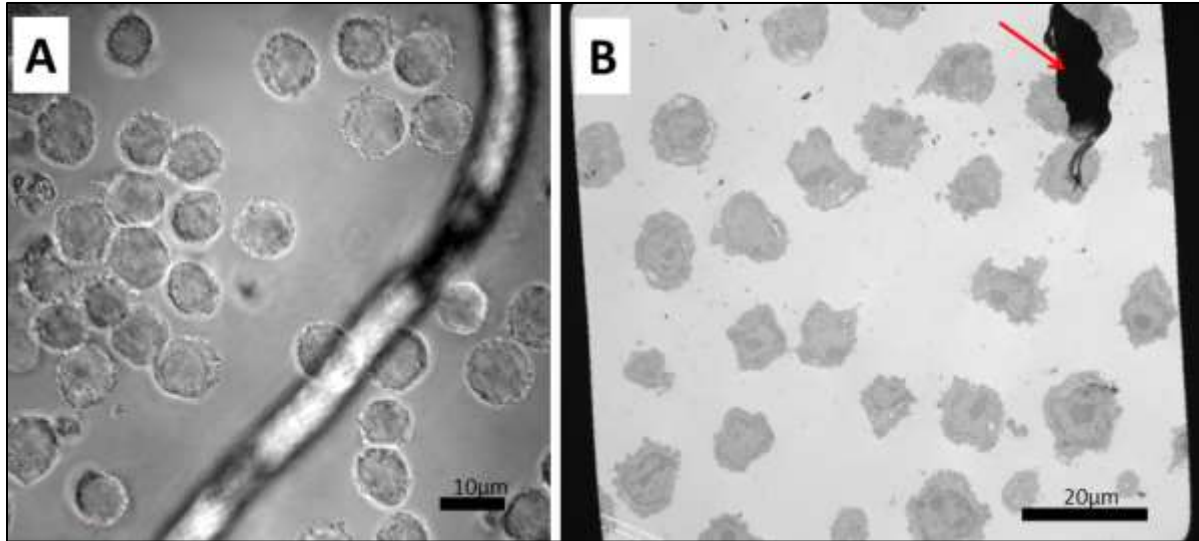


Figure 3-7. CLEM approach to find cells of interest. A) Confocal microscope image of U-937 cells on Ibidi gridded plate B) Semi-thin resin section of U-937 cell monolayer, displaying low magnified strategy to find corresponding cell patterns from fluorescence images. red arrow displaying artifact on the resin section. No matching cell patterns have been observed.

3-6. DISCUSSION

DiD lipophilic dye does not interfere with VLPs morphology

Influenza particle morphology is known to influence the immune cell response (Ruigrok *et al.*, 1985). The presentation of HA to the immune cell surface is essential for binding and endocytosis of the native virus. We demonstrated by cryo-EM, the morphology of the DiD-lipophilic dyed particles was indistinguishable to non-dyed VLPs. Work accomplished in chapter 2 demonstrated there were similar binding patterns observed at the EM level of non-dyed VLPs in comparison to DiD-labelled VLPs. These DiD observations are consistent with many studies as the lipophilic dye has been used to label VLPs and native viral particles before, such as hepatitis C VLPs and influenza viral particles (Lakadamyali *et al.*, 2003; Triyatni *et al.*, 2002). Overall viral fusion is not perturbed by lipophilic dyes (Lakadamyali *et al.*, 2003; Clague *et al.*, 1991; Spruce *et al.*, 1989; Stegmann *et al.*, 1987). Lipophilic dye does not interfere with delays

with membrane fusion either, fusion delays have only been exhibited due to lack of accessibility of HA (Clague *et al.*, 1991).

An experiment done by Lakadamyali *et al.*, 2003 found DiD-labelled influenza viral particles allowed for individual particles to be monitored throughout the entire endocytic pathway using real-time fluorescence microscopy. They found a significant increase in fluorescence intensity when labelled viral particles interacted with the cell membranes (Lakadamyali *et al.*, 2003).

U-937 lymphocytes and Human PBMCs interact with H1 and H5 DiD labelled-VLPs

To determine the interaction between influenza VLPs and immune cells, we used DiD-VLPs to visualize binding at the light microscope level. We observed the DiD-labelled VLPs binding to the blood lymphocytes and the human PBMCs by LM and TEM. However, there were prominent interactions with VLPs as differential binding to the plasma membrane were observed. Some of the cells viewed by fluorescence microscopy had diffuse binding (broad binding around the periphery of the plasma membrane, while others displayed punctate binding (concentrated areas of binding at one area of the plasma membrane) on both the U-937 cells and the PBMCs. Quantification of VLPs binding frequency to cells is ongoing from our collaborating laboratory, this will help to understand experimental reproducibility.

Interestingly Lampe *et al.*, 2007 also observed punctate and diffuse binding of HIV particles upon contact with the membrane of the cell by confocal microscopy. Their findings indicated punctate particles were immobilized and not internalized within the cell, and diffuse bound particles were internalized. The diffuse and punctate binding we observed for the DiD-VLPs are similar to the Lampe *et al.*, 2007 findings. Further studies are required to assess

whether VLPs binding to the cell surface with the diffuse or punctate pattern become internalized.

Another proposed explanation as to diffuse binding of the influenza VLPs, may be due to the expression of sugar-specific receptors on the cell surface, particularly for the U-937 cells. Upon repeated cell culture of the human U-937 cells, we observed variation between experiments for the amount of H1- and H5-VLPs fluorescently bound to the cell surface. This may have been due to the difference in expression of the sugar receptors after repeated cell passages in culture.

We have yet to understand whether the VLP are endocytosed via clathrin-mediated endocytosis, as well as if the VLPs are trafficked toward late endosomal stages for degradation similar to the native virus. For future work it will be enticing to fluorescently label Rab proteins such as Rab 5 and 11 because these proteins are known to be regulate endocytic compartments (Zerial & McBride, 2001) and are essential for influenza viral uptake (Sieczkarski *et al.*, 2003). Specific antibodies are currently being screened for specificity in our collaborating laboratory. Fluorescently labelling endosomes with specific markers will be essential to confirming these structures are indeed endosomes rather than lysosomes. This will also help to clarify that the localization of the VLP within the endosome like structures are not deep invaginations of the cell plasma membrane. The LM localization of Rab positive endosomes with fluorescently labelled VLPs would demonstrate the endosomal stage these particles are present in.

Attempts to achieve correlative light and electron microscopy with VLP vaccine samples

Confocal microscopy allows for the visualization of proteins or structures of interest within living cells, whereas TEM allows for a higher resolution analysis of ultrastructural features of fixed preserved cells. Combination of these two informative techniques would be highly

favorable to understand the dynamic interaction of the plant-made influenza VLPs with human immune cells.

We were successfully able to image cell monolayers of human macrophage cells interacting with plant-made influenza VLPs using glass slides with a gridded coordinate system and embed the cells through EM processing methods. Sectioning and localization of the reference coordinates was completed. However, a few aspects can be considered as to the optimization of the CLEM methodology.

The first methodological hurdle to overcome for future experiments will be to avoid loss of cells during EM processing. This is a common phenomenon during EM processing as the monolayers have to be infiltrated with a number of solutions to facilitate proper fixation and ultrastructural preservation (Asakawa *et al.*, 2014). To avoid this occurrence in the future, we propose the use of ‘cell attachment by enrichment’ methods. This methodology includes multiple washes of the cell monolayer, with either serum free media or PBS before fluorescence confocal microscopy. This ensures all cells that are free floating in the sample are removed before imaging takes place. The second suggestion would be the incorporation of poly-lysine (poly-L) to the glass slides before cell attachment. The addition of poly-L is a standard treatment to facilitate enhanced cell attachment to glass surfaces for imaging procedures.

Another suggestion would be to incorporate serial sectioning of the epon resin block. Serial sectioning through the cell monolayers would help to ascertain all cells present. Imaging software such as Photoshop could be used after micrograph acquisition; each section could be imaged in a sequential manor and the opacity of the images could be decreased to overlay all the successive images. The use of standard 200 hex copper grids has been useful for this preliminary

analysis however the grid bars often are in the field of view. For serial sectioning the use of formvar slotted grids would avoid grid bars covering the sections.

VLPs have been observed to be interacting with immune cells based on recognizable VLPs morphology by resin-embedding TEM, however HA has not been directly visualized interacting with immune cells at higher resolution. The VLP within the cell could be treated with specific immunogold antibody labelling of HA after VLPs have been incubated with immune cells for ~30-45 min. In combination with immunogold antibody labelling the use of lowicryl resins may help to preserve fluorescent signals upon EM processing, LM sections could be imaged and post-labelled with specific HA immunogold antibody.

Conclusion

In conclusion, we have begun to understand the structural interaction of plant-made influenza VLPs upon interaction with human immune cells by confocal and electron microscopy imaging. H1- and H5-VLPs bind to human U-937 blood lymphocytes and human PBMCs with differential binding characteristics and are internalized in U-937 cells by endocytosis. Preliminary correlative light and electron microscopy was attempted to achieve ultrastructural understanding as to reasons for the differential binding of the VLPs. Overall, this preliminary analysis was very informative to help to establish the ultrastructural understanding as to how plant-made VLPs are internalized within human immune cells.

3-7. Acknowledgements

This work was supported by Medicago Inc; Economie, Science et Innovation Quebec; Genome Canada; FEMR McGill University; Alexander McFee Internal Studentship, Faculty of Medicine, McGill University.

Chapter 4. Progress toward determining the 3D structure of HA on the surface of plant-generated virus-like particles

Authors:

Brianne J. Lindsay¹, Zoe Z. Hu¹, Nathalie Landry², Isabelle Rouiller¹

Affiliation:

1. Department of Anatomy & Cell Biology; Faculty of Medicine; McGill University; Groupe de Recherche Axe sur la Structure des Proteines (Grasp); Groupe d'Etude de Proteines Membranaires (GEPROM), 3640 University Street, Montreal, QC, H3A 2B2, Canada.

2. Medicago Inc. Quebec, QC, Canada

Corresponding author:

Dr. Isabelle Rouiller
Department of Anatomy & Cell Biology
Faculty of Medicine
McGill University
Tel: 514 398-3244
Email: Isabelle.rouiller@mcgill.ca

4-1. Preface

From previous chapters, we observed the plant-made virus-like particles (VLPs) by cryo-EM tomography and determined that majority of the particles are discus-shape with hemagglutinin (HA) distributed along the circumference of the particles with broad distances from neighbouring proteins (on average 170Å). We observed the VLPs interacting with immune cells at both the light and electron microscope level, bound to cell plasma membranes and within endosomes. It is known protein glycosylation in plants is different than in mammalian species. Glycosylation affects overall protein folding and consequently protein function. In this chapter, we describe our results using 3D tomograms of the novel VLPs bearing HA proteins on the lipid membrane surface. Using subtomogram averaging approaches methods, we established methods using new imaging technology to gain a preliminary low resolution structure of HA attached to the VLPs. These methods will decipher structural features of the HA expressed within this plant-based system and will help us in determining the structural differences of HA to expressed within mammalian species.

4-2. Abstract

Neutralizing antibody production against hemagglutinin (HA) is the most powerful immunologic tool to aid in the protection against the influenza virus. HA is the most abundant protein on the native viral surface and is essential for inducing infectivity to target cells. Medicago, a biotechnology company, has developed an approach to transiently express HA from specific influenza strains within plants. This approach has allowed the production of Virus-like particles (VLPs) with only HA embedded in lipid vesicles of plant origin. HA is a highly glycosylated protein. Glycosylation does affect virulence and it can affect HA protein folding. We hypothesize slight structural variation for the HA protein expressed in this plant based system due to the glycosylation systems found in plants which differ to those found in animals, structural studies of HA produced in plants are required to determine if folding of HA in plants is similar to that in animals. We will use cryo-electron tomography combined with subtomogram averaging approaches in order to determine the high resolution structure of HA at the surface of the VLPs. Here we summarize the progress made in that direction. Contrast of the VLPs from 3D tomograms was greatly improved when the phase plate was used for data acquisition. The HA proteins were manually selected for subtomogram averaging by viewing the HA side orientations on the VLPs membrane. A preliminary 3D low resolution structure of H1 attached to the membrane was obtained using manually selected model points. A method to automatically select the protein to include top-down views of HA was established. Overall, these studies will allow us to determine if there are any structural differences between plant and mammalian expressed HA. Enticing structural findings implementing new cryo-EM imaging technology has allowed the visualization of the H1 protein along the VLPs surface in the most natural state.

4-3. Introduction

Hemagglutinin (HA) is a glycoprotein that is positioned on the influenza viral surface. Seasonal influenza epidemics occur every year during winter months, due to continuous mutations of the surface glycoproteins, consequently resulting in a variety of HA subtypes (Palese & Shaw, 2007). HA is approximately 200kDa and is a trimeric protein with 3-fold symmetry (Wilson *et al.*, 1981; Skehel & Waterfield, 1975). It is essential for the entrance of infectious replicative material to target respiratory epithelial cells. HA interacts with such cells by binding to sialic acid receptors and this triggers endocytosis of the viral particle (Stegmann *et al.*, 1987).

HA is first synthesized as a single polypeptide, HA0, which then undergoes post-translational cleavage resulting in two polypeptides HA1 and HA2. Each monomer of HA is composed of the two polypeptides which are linked through disulfide bonds (Fig. 1-1 and Fig. 1-2). HA1 consists of the stem domain, and HA2 is the distal globular head region which contains the receptor binding site (Wilson *et al.*, 1981; Palese & Shaw, 2007). At low pH levels, a conformational change occurs causing the fusion peptide at the N-terminal domain of HA2 to become bound to the endosomal membrane (Harrison, 2015). The central helix of HA2 breaks and the portion between the break and the membrane is rearranged; pulling of the fusion peptide, the C-terminal transmembrane anchor, the endosomal membrane and the viral membrane all take place to facilitate the fusion of the viral particle to the cell endosome (Chen *et al.*, 1999).

Glycosylation of surface protein on influenza viruses has been shown to contribute to differences in virulence (Sun *et al.*, 2013). HA undergoes post-translational glycosylation modifications by attaching oligosaccharides to asparagine side chains. The composition of glycans depends on the types of modifying enzymes available in the specific host cell, the variety

of glycans present as well as the level of mannose (Schwarzer *et al.*, 2009; Nakamura *et al.*, 1980). Some glycosylation sites are essential for correct protein folding and removal or disruption of such glycans results in improperly folded HA (Roberts *et al.*, 1993). Other glycosylation sites are important for HA functions such as facilitating correct binding, HA0 cleavage, and ensuring evasion from the host immune system (Klenk *et al.*, 2001).

Although influenza vaccines have been available for the past 60 years they have limitations and novel influenza vaccines have been developed within the last decade. In particular, Medicago, a clinical-stage biotechnology company, has developed an approach to produce plant derived virus-like particles (VLPs), using transient expression of HA genes transferred in a relative of the tobacco plant (*Nicotiana benthamiana*) with *Agrobacterium* as a bacterial vector. The particles are comprised of a lipid layer derived from the plant cell, and HA is inserted along the membrane surface. All the N-glycosylation sites of the extracellular domain of the plant derived HAs carry plant-specific complex-type N-glycans (Le Mauff *et al.*, 2014). Providing further structural information of HA produced within this plant-expression system is important to better characterize the HA-VLP influenza vaccine. In addition, the knowledge of the 3D structure of plant generated HA will provide important clues to understand the immune response generated by the vaccine. The structural findings will be correlated with immunologic data collected from corresponding laboratories investigating the same influenza vaccine.

In the present study, using cryo-EM subtomogram averaging approaches we have manually selected H1-VLPs (attached to the particle surface) to acquire the low resolution 3D structure of H1 expressed in plants. We demonstrate the advantages to using the Volta phase plate (VPP) to improve image contrast, as well as establishing methods toward semi-automatic model selection to increase the number of protein model points for 3D reconstruction. Overall,

this structural analysis will aid in the understanding of H1 composition upon transcription and post-translational modifications that occur within the plant in comparison to mammalian and avian expression. This structural comparison will shed light on protein folding within plants compared to mammalian and avian expression.

4-4. Methods

4-4.1. Observation of VLPs by cryo-EM

The H1 sample (5 μ L) was placed for 1 minute on a Quantifoil R2/2 copper grid (EMS Inc.) previously glow discharged for 30 seconds. Excess fluid was removed and the sample was plunged frozen in liquid ethane at -180°C using a Vitrobot (FEI Company). The chamber was set to 100% humidity at 4°C. The grid was stored in liquid nitrogen until imaging. The cryo-prepared VLP samples were visualized on a Tecnai F20 microscope (FEI Company) to observe the ice thickness.

4-4.2. Cryo-TEM tomography image processing

The frozen hydrated VLPs samples (fiducial-less) were imaged in a FEI Titan Krios 300kV Cryo-STEM equipped with an FEI Volta Phase Plate (VPP) (FEI Company). Images were recorded on a Falcon 2 Direct Detection Device (DDD) (FEI Company) the pixel size at the specimen level was 3.6Å. Tilt series were collected with the FEI tomography software at +/-60° in 2° increments at a magnification of 22,500x and a defocus level of -0.5 μ m. For the tomograms not collected with the VPP, the defocus level was -10 μ m. The images were binned by two for processing. 3D reconstructions were calculated using the Imod Etomo package suite (Mastronarde, 1997).

Simultaneous iterative reconstruction technique (SIRT) was completed with the reconstructed 3D tomograms. SIRT takes an initial reconstruction, which was computed from a flat projection, then that reconstruction is projected with Tilt (A program for reconstructing a 3D object from series of 2D projections). After the original projections get subtracted from the re-projections, the difference between the original and the re-projections is back-projected with a flat filter function to distribute pixel variation. The error between the reconstructions is subtracted from the initial reconstruction. This procedure was performed with 15 iterations.

4-4.3. Manual model point selection

To increase the signal to noise ratio, the selected proteins were aligned and an average calculated. HA protein model points were selected using Imod software package from the VPP acquired tomogram reconstructions (Mastronarde, 1997). VLPs frozen on the side orientation were identified; HA was selected where the protein was first attached to the membrane, followed by a second coordinate selected at the globular head. 571 particles were manually selected following this process from two reconstructed VPP tomograms.

4-4.4. Preliminary 3D reconstruction of manually selected HA using Imod

Manually selected model points were integrated into Imod Peet extension software package 4.8.28 (Mastronarde, 1997). Peet is used to align subvolumes extracted from 3D volumes. It iteratively refines particle alignments against a reference particle; before each new iteration a new reference particle is generated from the previous alignment. For each alignment, angular search ranges are established for each subvolume for 3 rotations in phi, theta and psi (rotations around X, Y, and Z). Peet also has 'missing wedge' compensation; the specified tilt range is integrated before alignment and averaging. Averaging and alignment of particles are

replaced with a weighted average in Fourier space, and only regions of the particle in which its projections are outside of the tomographic missing wedge are used. 571 manually selected subvolumes were integrated from one VPP reconstructed tomogram and underwent two iterative cycles to generate the preliminary H1-VLPs structure.

4-4.5. Semi-automatic particle selection using EMAN2

A few example individual HA particles were picked manually for every 5th 2D tomogram micrograph within EMAN2 software (Ludtke *et al.*, 1999) (Fig. 4-1A). EMAN2 allows users to select identical particles of interest using boxed graphically tools; the program stores the boxed coordinates (x and y). The automation portion of EMAN2 software determines the density and contrast of the pixels that have been manually selected and then automatically selects similarly contrasted pixels. After semi-automatic selection, accuracy of particle selection was assessed per micrograph. Using python command line the coordinate list was assessed to calculate the difference between coordinates in sequential frames of the tomogram 3d volume. ΔX and ΔY coordinates that were <3 pixels were included, coordinates with >3 pixels were excluded. ~1000 particles were selected using this approach (Fig. 4-1B).

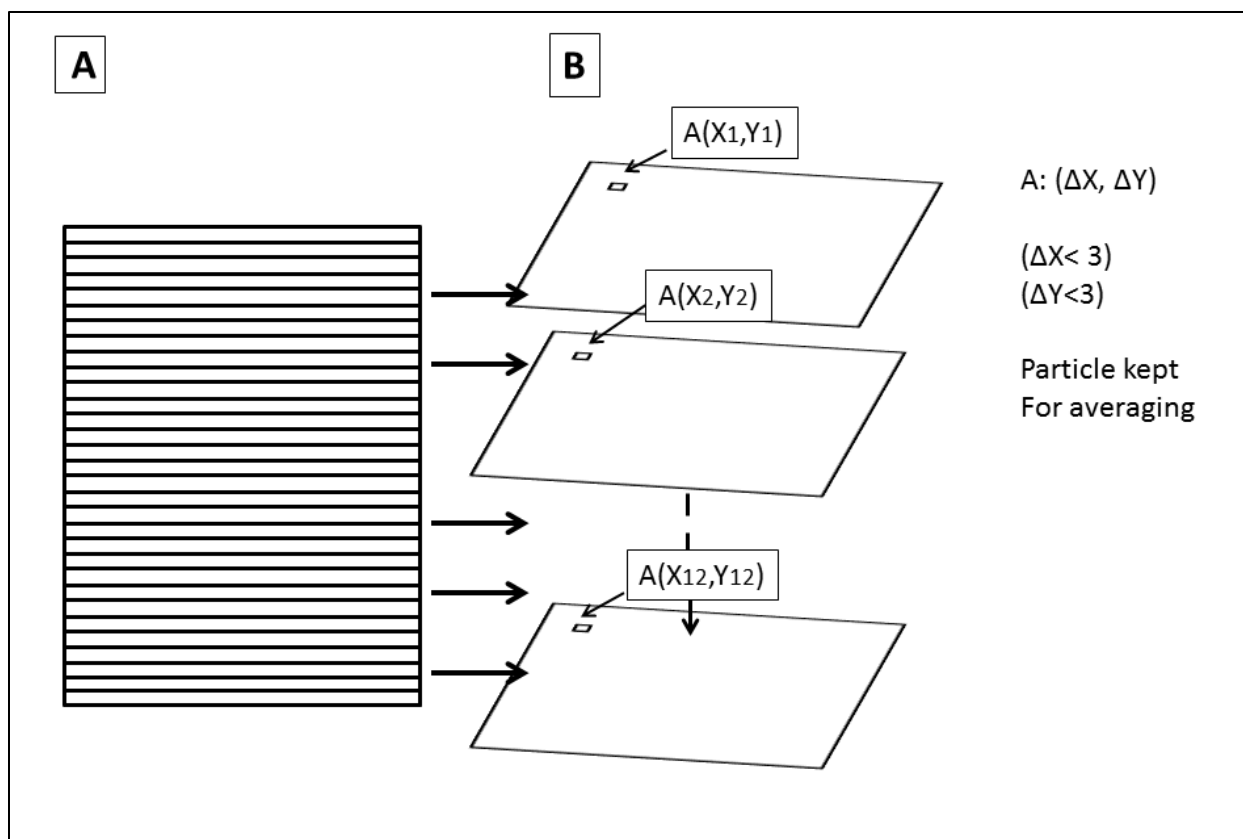


Figure 4-1. Schematic of semi-automatic particle selection. A) Side view of 3D tomogram stack of 2D images. B) Example of every 2D micrograph analyzed for particle selection. Arrow indication coordinate of particle example A. Difference between the x and y coordinates calculated using python script. Particles with more than 3 pixel differences in either x or y were excluded from reconstruction.

4-5. Results

4-5.1. Image contrast improvement employing the VPP for cryo-EM tomography

When the VPP was applied during tomography acquisition of the H1-VLPs sample, the defocus level required for improved contrast was set to $-0.5 \mu\text{m}$. This minor defocus level was enough to clearly identify the VLPs within the amorphous ice. The defocus level for non-phase plate data was set to $-10 \mu\text{m}$. From the 3D reconstructed tomograms, the VPP applied tomograms had sharper and increased contrast in comparison to the highly defocused non-phase plate tomograms (Fig. 4-2A-B).

Within the VPP tomography reconstructions, a distinctive white hollow around the VLPs structure was observed (Fig. 4-2A). This hollow, shown with an accented red bracket, helped distinguish densely contrasted protein and membrane from background noise (Fig. 4-2A). The white hollow was absent from the non-phase plate tomograms (Fig 4-2B).

An important feature observed in the VPP tomogram was the contrast improvement of the stalk region of the protein. Selecting side orientations of HA where the protein was attached to the membrane was clearly evident, in comparison to non-phase plate tomograms (Fig. 4-2A-B). The contrast for the globular head of the HA was observed within the non-phase plate tomograms, but it was difficult to observe the attachment of the protein and the angle at which the protein was extending from the membrane (Fig 4-2B). The lack of clarity was most likely due to background noise (Fig 4-2B).

Data acquisition with the VPP was rather difficult to reproduce consistent results. Often tomograms with the VPP applied went in and out of focus during data acquisition. Those tomograms were not included in the analysis.

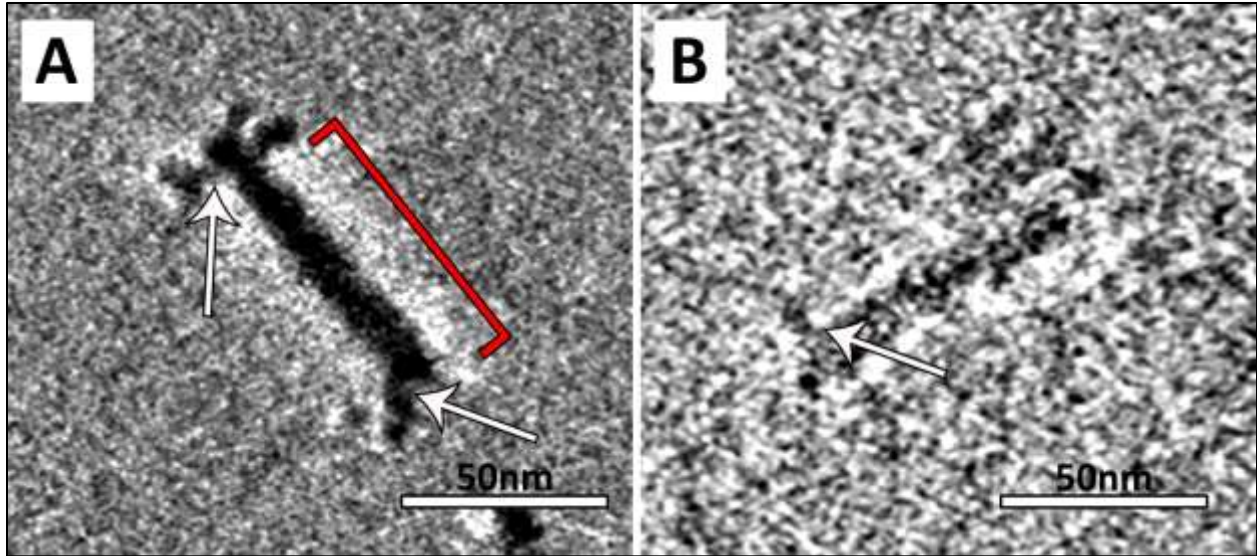


Figure 4-2. Comparison of 3D slices from cryo-EM tomograms of Volta-phase plate applied data to non-phase plate tomograms of H1 HA virus-like particles (VLPs) produced in plants. A) Volta-phase plate acquired tomogram of H1-VLPs sample. White arrows indicate the stalk region of the HA protein attached to the membrane, the red bracket signifies the white hollow observed in phase plate acquired tomograms B) Non-phase plate tomogram of H1-VLPs, white arrow indicating the stalk region of the protein.

4-5.2. Manual model selection of HA protein from the VPP cryo-tomography data

Coordinates within a tomogram z-stack can be extracted using subtomogram averaging methods. From the VPP tomogram reconstructions, the attachment of the HA protein was clearly visible particularly when the individual VLPs were frozen on a side orientation (Fig. 4-2A and 4-3A). From the isosurface view (which displays the entire z-volume reconstruction) it was possible to assess the model points to gain an accurate orientation through the center of the stalk region to the globular head, as the angle of HA from the membrane protruded at various angles (Fig. 4-3B).

The accuracy of manual model selection was displayed in Fig. 4-3B; the first two model points are accurately orientated through the center of the protein, whereas the third is slightly off center. Minor adjustments were made to the off centered model points to ensure high level accuracy. For the VPP collected tomograms precise z-axis coordinates were selected for the

protein due to the improved image contrast (Fig.4-2A and 3A-B). The z-axis coordinate was less accurately determined in the non-phase plate tomograms.

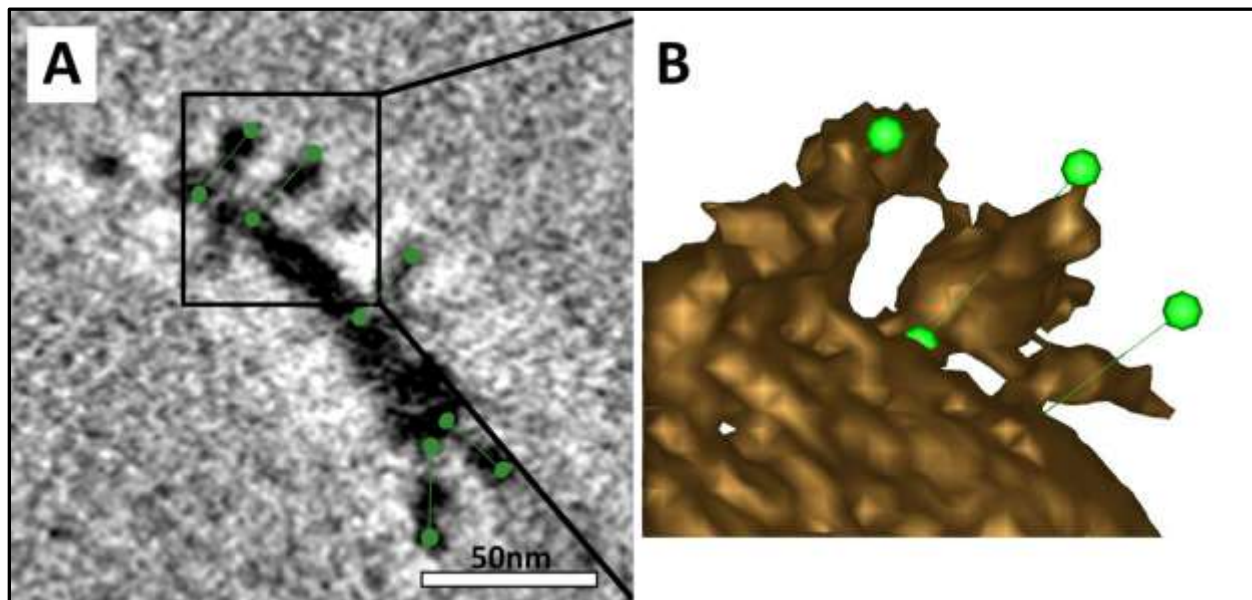


Figure 4-3. Volta phase plate cryo-EM tomogram displaying manual selection of model points. A) Slice through the tomogram displaying HA protein along the VLP membrane, green model points display attachment of HA to the membrane and conjoined model points at the globular head. B) Isosurface 3D view of H1-VLPs displaying model point coordinate accuracy of HA protein in green.

4-5.3. Preliminary 3D reconstruction of H1 attached to the membrane of VLPs by subtomogram averaging

A preliminary low resolution structure of H1 attached to the VLP membrane surface was reconstructed using 571 particles for model point selection side oriented HA from VPP applied tomograms. From the isosurface low resolution structure, the membrane of the VLPs, stalk and head region of the protein were visible (Fig. 4-4A). From the top down view (Fig. 4-4B), the HA transcribed within this plant based system is in the shape of a triangle, indicating it is a trimer.

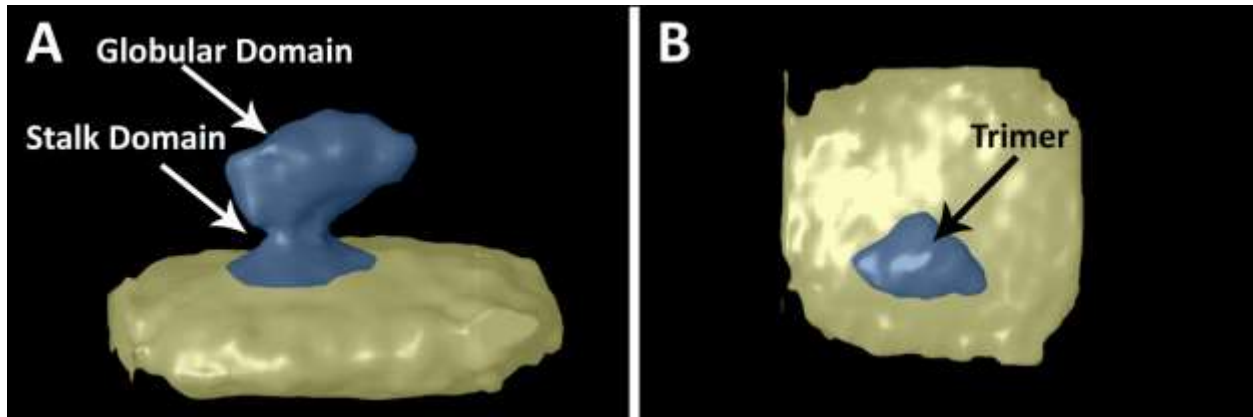


Figure 4-4. Low resolution structure of H1 protein acquired through manual particle selection and subtomogram averaging approaches. A) Side view of HA attached to the lipid membrane, membrane colourized in yellow, HA protein coloured in blue. Stalk and globular domain of HA viewed in this orientation. B) Top-down view of the HA protein, the top of the globular head is in the form of a trimer.

4-5.4. Semi-Automatic approach to HA protein selection

As was mentioned previously, manually selecting the HA structures by viewing the side orientation was clearly distinguishable and accurate (Fig 4-2A and 4-3A-B). However, manual selection was a slow process. Many of the HA proteins were not selected from the tomograms as it was more difficult to distinguish the membrane attachment site from the top-down orientation. A method to semi-automatically select the protein was made possible to include the top-down orientations of HA from the VPP collected tomograms (Fig. 4-5A). Utilizing EMAN2 package software, model coordinates through the entire 3D tomogram volume were followed to track the top-down orientations of the protein (Fig. 4-5B). From the coordinates obtained during particle picking in EMAN2 a python script was used to distinguish the change in X and Y.

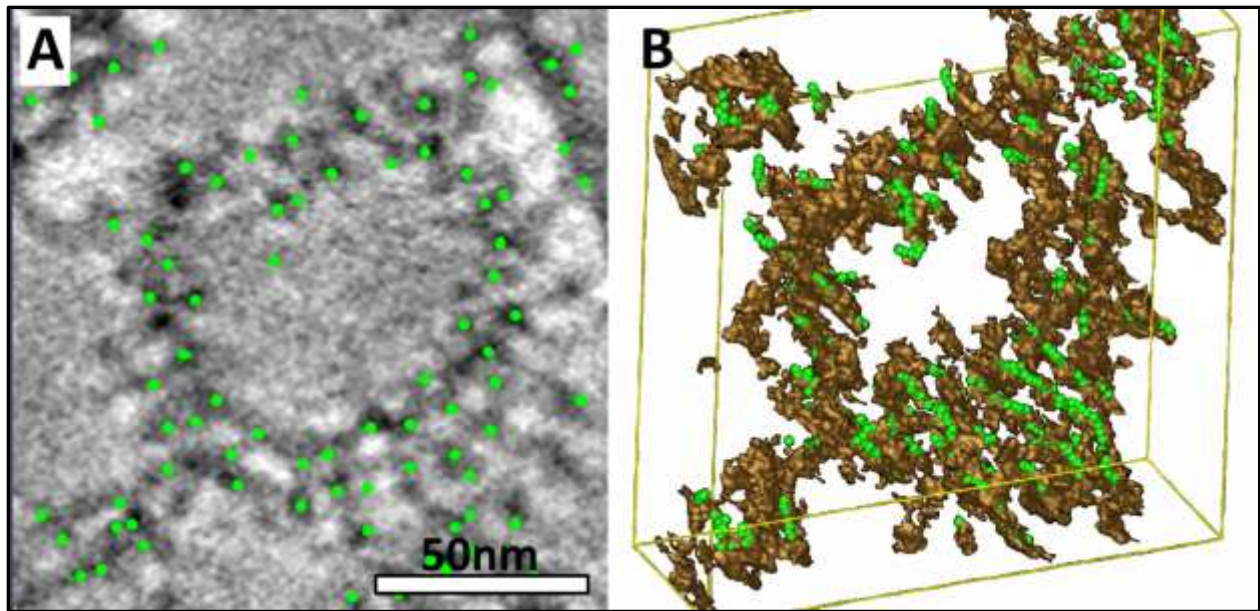


Figure 4-5. Semi-automatic particle selections of H1 attached to the VLPs. A) Slice through a VPP acquired tomogram displaying model point selection of HA protein with green dots. HA proteins orientated in a top down orientation were selected by this approach. B) Isosurface view of the protein selection coordinates followed progressively using the entire 3D volume.

4-6. Discussion

Image contrast improvement employing the VPP for cryo-EM tomography

3D cryo-EM structures can be determined by conventional tomography techniques. However due to large signal-to-noise ratios, low contrasted tomograms contribute to limited structural interpretation. To combat this, researchers typically capture images at increased defocus levels to boost signal to noise ratios. Even though this methodology improves contrast, it causes deformation of the actual structure. Correction of this deformation is possible but remains inaccurate and complex for topographic reconstruction due to the gradient of defocus present in a single tilt image.

Alternatively to defocusing, phase contrast can be improved by electrostatic devices placed in the back-focal plan of the microscope, such as the Volta phase plate technology. The contrast of cryo-prepared H1-VLPs vaccine samples image was improved by applying VPP

technology. The improved contrast within the phase plate acquired tomograms was exhibited by a highly dense HA protein attached to the VLP membrane. A white hollow was observed around the individual VLPs from the VPP acquired tomograms. These hollows helped accent the VLPs from background noise of the tomograms. These hollows were unique to the VPP tomograms and were not observed in the non-phase plate tomograms. Visualizing the HA protein attachment sites to the membrane were clearly discerned from the phase plate tomograms. The globular head of the protein was observed with the non-phase plate acquired tomograms; however the stem region was not as clearly distinguishable. This was most likely due to the increased defocus level and background noise of the tomograms (Fukuda *et al.*, 2015).

The VPP apparatus is an alternative to the defocusing imaging limitations for cryo-EM samples. Recently using a variety of biological samples the VPP has been proven to improve image contrast and to avoid structural deformation (Danev & Baumeister, 2016; Mahamid *et al.*, 2016; Asano *et al.*, 2015; Fukuda *et al.*, 2015; Danev *et al.*, 2014). The VPP can also aid in data collection of samples which are structurally heterogeneous and flexible such as the influenza VLPs.

Fukuda *et al.*, 2015, found largely improved contrast in VPP collected cryo-EM tomograms. A variety of different samples were compared to conventional imaging tomography and the VPP acquired data displayed intracellular and macromolecular features not visible through conventional techniques, there was a significant increase to overall image contrast (Fukuda *et al.*, 2015).

Manual model selection of HA protein from the VPP cryo-tomography data

From the VPP acquired 3D tomography reconstructions, the HA protein was observed to be inserted along the membrane at the equatorial regions of the membrane, at various angles. Model point coordinates for individual HA were collected where the protein attached to the membrane, followed by a second coordinate at the head region. Minor adjustments to inaccurately selected model points were easily corrected by viewing the entire 3D volume isosurface view of the individual VLPs.

A number of proteins have been structurally determined by automatic subtomogram averaging approaches to quite high resolution, such as the native H1 recombinant protein and the HIV-1 capsid, resolved to 8.8Å resolution (Schur *et al.*, 2015; Harris *et al.*, 2013). The manual process we established was done for two essential reasons related to the uniqueness of the VLP vaccine: 1) The HA proteins were identified to be distributed along the membrane with varied distance between neighbours, minimum distance of no less than 43Å but on average ~176Å. 2) The angle at which the HA protein was in reference to the membrane was also variable. Individual HA were not observed to cross over neighbours nor, group together on the membrane.

For subtomogram averaging computational programs such as Peet and Dynamo, the software can be optimized to determine model point coordinates with uniform distance (Castano-Diez *et al.*, 2012; Mastronarde, 1997). If the sample under analysis has a known distance between neighbouring proteins, such as uniform microtubules or HIV viral particles, the software packages can be set to automatically select those areas of interest automatically (Briggs *et al.*, 2015; Castano-Diez *et al.*, 2012).

Preliminary 3D reconstruction of H1 HA using subtomogram averaging approach

A preliminary low resolution 3D structure of the H1 protein attached to the VLP membrane was reconstructed. There is little structurally known about the plant-made HA and to what extent its conformation differs from the mammalian protein. From our preliminary findings we can conclude the protein had similar domains in comparison to mammalian HA, the stalk and globular domains were clearly discernable from the VPP tomogram reconstruction (Wilson *et al.*, 1981). From the 3D reconstructed top-down orientation of H1, it was determined to be a trimeric structure which is similar to the mammalian H1 protein (Wilson *et al.*, 1981).

The identification of binding epitopes for HA proteins has been known for the last two decades. The stem region of the native HA proteins have conserved regions for antibody binding between various subtypes (Okuno *et al.*, 1993). Identification of the epitope binding regions is important for neutralizing antibody generation upon infection. Utilizing cryo-EM approaches other groups have identified 3D maps of the epitope sites on various viruses such as the Polio virus (Bannawarth *et al.*, 2015). In particular, focusing on the mammalian H1 subtype, it has four epitope binding domains found within the stalk region of the protein (Matsuzaki *et al.*, 2014; Carton *et al.*, 1982; Gerhard *et al.*, 1981). Research focused toward ascertaining the structure of antigen binding sites on viral proteins can aid in the generation of improved vaccine development toward robust neutralizing antibody production and binding specificity toward epitope regions (Lilgeroos *et al.*, 2015).

As identified by Le Mauff *et al.*, 2014, there were plant glycans present on the HA protein transiently expressed using the plant based system for VLP influenza vaccine development. As well, HA protein expression confirmed that the HA0 conformation of the protein was the major form present. The H1 and H5 recombinant VLPs were analyzed in their

study and by mass spectroscopy plant specific N-glycans were present at epitope regions (Le Mauff *et al.*, 2014). For future experiments, it will be vital to ascertain a higher resolution structure of the H1-VLPs protein transiently expressed in plants to compare to the already well characterized structure of the mammalian cell-derived protein. A resolution of 10Å will allow the visualization of secondary structures, such as alpha-helices and beta-pleated sheets. We will be able to visualize the stem region of the HA protein and attempt to identify the epitope binding regions. At higher resolution, we will be able to observe the conformation of HA, which will help to establish the folding outcomes of HA transiently expressed within plants. Additionally, there may be an advantage to the N-glycosylation of the HA protein, as plant specific N-glycans have the capacity to facilitate antigen capture by antigen presenting cells through binding to sugar-specific receptors (Saint-Jore-Dupas *et al.*, 2007)

Semi-Automatic approach to HA protein selection

To increase protein selection for tomogram reconstructions we established a method to semi-automatically pick particles to help with selection of protein in top-down orientations. Utilizing EMAN2 software we were successful in adding additional proteins to the data set, which increased from ~500 proteins to ~1000. Not only were proteins selected from their side orientations, but top down views were identified and included in the analysis.

Typically EMAN2 has been used for particle selection during single particle analysis. There has been growing interest for this software to be expanded for use with tomography data as tomography offers an alternative to study conformational heterogeneous macromolecules (Galaz-Montoya *et al.*, 2015; Shahmoradian *et al.*, 2013).

The semi-automated HA subvolumes were incorporated using Peet (an extension of the Imod software package), however preliminary the protein structure of H1 protein have not been successfully reconstructed. Although the protein dataset was increased, merging the two data sets has to be done carefully taking into account the missing information due to the limited tilt images (missing wedge artifact). The aim is to incorporate manually selected subvolumes with the semi-automatic subvolumes to increase particle numbers and orientations. It may be advantageous to incorporate recent algorithms added to EMAN2 software specific for subtomogram averaging as was used for Shahmoradian *et al.*, 2013. They successfully incorporated this software to characterize fibrillary aggregate growth of a huntingtin mutant gene (Shahmoradian *et al.*, 2013).

Conclusion

Using subtomogram averaging methods and technological imaging advancements we have been able to obtain a preliminary low resolution 3D reconstruction of the H1 protein expressed in plants on VLP membrane surface. These established subtomogram approaches will help us to structurally compare protein folding and identify specific binding epitopes on the protein surface to distinguish the outcomes of HA protein expression within this plant-based system.

4-7. Acknowledgements

This work was supported by Medicago Inc; Economie, Science et Innovation Quebec; Genome Canada; FEMR McGill University; Alexander McFee Internal Studentship, Faculty of Medicine, McGill University.

Chapter 5. Conclusion and future perspectives

5-1. Major findings

The work completed in this thesis, chapters 2-4, was an in-depth morphological analysis of Medicago's plant-generated VLP influenza vaccine.

5-1.1. Morphological Characterization of a Plant Made Virus-Like Particle Vaccine Bearing Influenza Virus Hemagglutinins by Electron Microscopy

Analyzing the H1- and H5-VLPs by cryo-EM tomography, we found the majority of the VLPs are composed of discus-shape particles with loosely or densely packed HA trimers. The HA trimers on the VLPs were present at varied angles on the particles circumference. For the discus-shaped VLPs, spacing between neighbouring HA trimers was on average 176Å at the tail region, and 200Å at the head. By cryo-EM imaging the particles were 75 ± 25 nm in diameter (slightly smaller than the native influenza particles), and the low density of HA protein provides excellent accessibility for neutralizing antibody binding. This was important to demonstrate as the influenza shape and size has been shown to be important for eliciting strong immune responses (Ruigrok *et al.*, 1985).

We analyzed the H1- and H5-VLPs vaccines over the course of one year and found there was no variance of the shape characterizations or the size of the particles. These cryo-EM findings indicate that the particles are structurally stable as a consequence of aging. By cryo there was some indication of VLPs clustering together over time, however separation of VLPs was easily completed by brief vortexing of the sample. Thus the VLPs grouping together were lightly interacting and individual VLPs structural integrity was always distinguishable. Overall particle integrity remained after the brief vortexing.

Lastly, from this analysis we were able to observe the discus-shaped H1- and H5-VLPs bind to mouse dendritic cells and are endocytosed within human U-937 lymphocytes. These

findings indicated that even though the plant-made VLPs are slightly structurally distinct from the native viral particles, the influenza VLPs interact in a similar way to the native virus. As well the VLP vaccine initiates cellular activation which was displayed by characteristic morphological changes of the cells.

5-1.2. Establishment of a correlative light and electron microscopy method to visualize virus-like particles interacting with immune cells

We were interested to further analyze cellular interactions with the plant-made VLPs. The observation by cryo-EM DiD-labelled VLPs showed that the lipophilic dye interfered with the overall morphology of the VLPs. There was no morphological difference found between the DiD-labelled VLPs compared to non-dyed VLPs.

Fluorescence light microscopy and TEM analysis to observe the DiD-labelled H1- and H5-VLPs with Human U-937 blood lymphocytes and human peripheral blood mononuclear cells (PBMCs). Upon fluorescence microscopy analysis differential binding characteristics with the H1- and H5-VLPs were observed. Some cells had no VLPs bound to the plasma membrane, whereas some cells exhibited diffuse broad binding. Interestingly some of the cells that had VLPs bound to the membrane showed very concentrated binding at one location. We are interested to determine the ultrastructural reasons why these differential binding characteristics were present and so methods were created to achieve CLEM imaging.

Overall, the established methods for the cell correlation from the LM to EM level still need further improvements. The differential binding of the DiD-labelled VLPs has not been visualized yet at the EM level. Improving cell attachment will facilitate correlation between LM and EM, as well as allow identification of punctate versus diffuse binding.

5-1.3. Progress toward determining the 3D structure of HA on the surface of plant-generated virus-like particles

We demonstrated that applying new phase plate technology, image contrast for the VLPs influenza vaccine was greatly improved in comparison to conventional techniques. Using the phase plate tomograms we were able to create a method to manually select HA protein to incorporate into subtomogram averaging approaches, to obtain an overall 3D structure of the H1 protein attached to the VLP membrane. The 3D coordinate model points were easy to select from VLP orientated on the side within the tomogram.

Using the manually selected model points (~500), a low resolution 3D structure of the H1 protein was reconstructed. Views of the side orientation of the protein display that HA is inserted into the lipid membrane, there was a stem-like domain near the membrane, and a globular head region. The top view of the protein displayed that the globular head region was in the form of a trimer similar to the native virus.

To increase the number of protein included in the data set as well as incorporate top-down orientations of the protein, a method to semi-automatically select model points was developed. This process incorporated Eman2 software and a python algorithm was used to successfully tracked coordinates through the 3D tomogram. A much larger dataset was obtained using this approach as the top-down orientations of the protein were selected as well.

5-2. Future perspectives

The significance of the experimental findings for the structural analysis of the plant-made VLP has been described throughout chapters 2-4 of this thesis. There still remain many experimentally unanswered questions which will be important to pursue in future work to further improve the structural understanding of the VLP influenza vaccine.

5-2.1. Correlative LM and EM experimental improvements

We made progress towards establishing a CLEM approach to understand differential binding of VLPs to human immune cells. Future experiments will have to take into account a few issues with the preliminary methods.

The first factor will have to address the issue of cell detachment during EM processing. We believe that majority of the cells are unable to remain attached to the glass plate during the EM processing procedure. Searching for particular patterns of cells within the area of interest was extremely challenging as the fluorescence images no longer matched the EM sample. We suggest for future experiments poly-L be used to enhance cell attachment to the glass plates. Alternative approaches using lowicryl resins may help to preserve the fluorescent signal upon EM processing, LM sections could be imaged and post-labelled with specific HA immunogold antibody to incorporate into the CLEM methodology.

Once cell attachment has been achieved, the second experimental modification will be to better optimize grid preparation for EM imaging. The collection of serial sections of the semi-thin resin monolayers will aid with the visualizing of cell patterns. Serial sections will be collected on formvar slotted grids and the use of those grids will eliminate the issue of grid bars within the field of view during image acquisition.

Finally when the CLEM methodology is successfully complete, future experiments utilizing these approaches will focus on further characterizing the DiD-VLPs with other immune cells such as human dendritic cells. A complementary tool to incorporate in these studies will be the inclusion of real-time fluorescence microscopy. Lampe *et al.*, 2007, showed there was differential binding displayed by HIV-VLPs due to attachment differences to the membrane

using real-time confocal microscopy. The fluorescently labelled HIV-VLPs light microscope images in their study showed concentrated binding exhibited at one particular area of the plasma membrane (Lampe *et al.*, 2007). Real-time microscopy approaches may help to explain the VLPs mode of interaction and internalization to target immune cells.

Aspects as to VLP endocytic pathways will shed light on the plant-made VLPs internalization within immune cells. The use of specific fluorescent markers for Rab 5 and Rab 11 are known to be essential for influenza viral endocytosis (Sieczkarski *et al.*, 2003). These markers could be used to exemplify that the plant-made VLPs are triggering similar endocytic pathways. Moreover, comparison between endocytosis of VLPs and inactivated whole viruses would be of interest to confirm this assumption. VLPs presence within late endosomes would also clarify whether VLPs are designed for cell recycling or degradation. In dendritic cells, there is evidence that the compartmental degradation and different endocytic pathways exhibit various immune responses of either major histocompatibility complex I (MHC I) or MHC II presentation (Duclos *et al.*, 2011; Houde *et al.*, 2003). VLPs have been observed to be interacting with immune cells based on recognizable VLP morphology by resin-embedding TEM, however HA has not been directly visualized interacting with immune cells at higher resolution. VLP within the cell could be treated with specific immunogold antibody labelling of HA after VLPs have been incubated with immune cells for ~30-45 min for TEM immunogold imaging.

The group we have collaborated with during the CLEM experiments, at McGill University, have used fluorescently engineered GFP-VLPs construct in the past, and have visualized VLPs within draining lymph nodes of mice (Young *et al.*, 2015). Reproducibility of the GFP-VLPs remains problematic, however currently constructs of m-cherry labelled VLPs are under investigation. Understanding the ultrastructure of VLPs induction at the tissue level will be

highly enlightening at higher resolution as to gaining a better understanding of the VLPs interaction and degradation within the lymphatic system.

5-2.2. Higher resolution of H1 and H5 subtomogram structures

To further compare the structure of HA transcribed within this plant based system, a higher resolution structure will have to be determined for the H1 and H5 protein, using the subtomogram averaging approaches we have developed. Other groups have been able to break the limits of subtomogram resolution. Such proteins include the H1 native protein, and the HIV-1 capsid protein achieving 8.8Å resolution (Schur *et al.*, 2015; Harris *et al.*, 2013). At such levels, detailed structures such as alpha helices and beta sheets are discernable. We would be able to structurally identify antibody binding domains and interpret how the N-glycosylation in plants affects the overall structure of the protein.

Le Mauff *et al.*, 2014, demonstrated that transiently expressed HA in plants is mainly composed of uncleaved full-length HA0 conformation for both the H1- and H5-VLPs as detected from SDS-PAGE and immunoblot analyses. We have not confirmed this full-length HA0 conformation of HA attached to the VLP surface at high resolution.

To achieve higher resolution we propose future work should incorporate a GIF and DDD camera system, The next round of imaging should incorporate tomograms with higher magnification and increased electron dose per frame and reduce the number of frames collected (frames collected every 3 degrees rather than 2). Gold fiducials shall be incorporated to promote better image alignment as well.

The method of manual selection was an accurate approach for the H1-VLPs, however as described earlier, it was time consuming and a limited number of proteins were selected resulting

in a low resolution structure. We propose the new tomography data set should be analyzed with the incorporation of semi-automatically selected HA to maximize the number of proteins selected as well as incorporate as many orientations of the protein possible. Incorporation of subvolumes from the semi-automatic approach using EMAN2 subtomogram averaging algorithms may be better suited in comparison to the Peet software package. Merging the two data sets has to be done carefully to account for the missing information due to the limited tilt images, also known as missing wedge artifact.

Other programs such as Dynamo should also be tested and compared to Peet, and EMAN2 we used in the present methods discussed in Chapter 4. Other software packages may be better suited for the uniqueness of particle selection of the influenza VLPs.

5-3. Concluding statement

In this thesis, we describe an integrative structural analysis of plant-made VLPs that are an alternative, approach for influenza vaccine production. The alternative vaccine is for the protection of vulnerable populations from seasonal and pandemic flu strains. Utilizing TEM methods we have proposed the VLPs are structurally stable, interact with immune cells similarly to the native virus, and HA is structurally similar compared to the native protein. We describe methods to achieve CLEM approaches to better comprehend the VLPs interacting with cells, and subtomogram averaging methods to gain a high resolution structure of the HA protein on the VLPs surface. Overall these findings help to understand the structure and elucidate information as to the function of the plant-based VLPs influenza vaccine.

5-4. References

Air.G.M., Compans.R.W.(1983). Influenza B and Influenza C viruses. *Genetics of Influenza Viruses* (Palese,P., and Kingsbury,D.W.,eds) 280-304, Springer, New York.

Allison.A.B., Ballard.J.R., Tesh.R.B., Brown.J.D., Ruder.M.G., Keel.M.K., Munk.B.A., Mickley.B.A., Gibbs.S.E., Travassos da Rosa.A.P., Ellis.J.C., Ip.H.S., Shearn-Bochsler.V.I., Rogers.M.B., Ghedin.E., Holmes.E.C., Parrish.C.R., Dwyer.C.(2015). Cyclic avian mass mortality in the northeastern United States is associated with a novel orthomyxovirus. *Journal of Virology*. 89(2):1389-403.

Andre.F.E., Booy.R., Bock.H.L., Clemens.J., Datta.S.K., John.T.J., Lee.B.W., Lolekha.S., Pettola.H., Ruff.T.A., Santosham.M., Schmitt.H.J.(2008). Vaccination greatly reduces disease, disability, death and inequity worldwide. *Bulletin of the World Health Organization*. 86(2):81-160.

Asano.S., Fukuda.Y., Beek.F., Aufderheide.A., Forster.F., Danev.R., Baumeister.W.(2015). A molecular census of 26S proteasome in intact neurons. *Science*. 347:439-42.

Asakawa.H., Hiraoka.Y., Haraguchi.T. (2014). A method of correlative light and electron microscopy for yeast cells. *Micron*. 53-61.

Bachmayer.H., Liehl.E., Schmidt.G.(1976). Preparation and properties of a novel influenza :subunit vaccine. *Postgraduate Medical Journal*. 52(608):360-7.

Bannwarth.L., Girerd-Chambaz.Y., Arteni.A.A., Guigner.J.M., Lemains.J., Ronzon.F., Manin.C., Venian-Bryan.C.(2015). Structural studies of virus-antibody immune complexes (poliovirus type 1): Characterization of the epitopes in 3D. *Molecular Immunology*. 63(2):279-86.

Bouvier.N.M., Palese.P. (2008). The biology of influenza viruses. *Vaccine*. 26(4):49-53.
Carrat.F., Flahault.A. (2007). Influenza vaccine: The challenge of antigenic drift. *Vaccine*. 25: 6852-62.

Briggs.J.A.(2013). Structural Biology in situ- the potential for subtomogram averaging. *Current Opinion in Structural Biology*. 23(2):261-7.

Bright.R.A., Carter.D.M., Daniluk.S., Toapanta.F.R., Ahmad.A., Gavrilov.V., Massare.M., Pushko.P., Mytle.N., Rowe.T., Smith.G., Ross.T.M.(2007). Influenza virus-like particles elicit broader immune responses than whole virion inactivated influenza virus or recombinant hemagglutinin. *Vaccine*. 25(19): 3871-8.

Carton.A.J., Brownlev.G.G., Yewdell.J.W., Gerhard.W.(1982). The antigenic structure of the influenza virus A/PR/8/34 hemagglutinin (H1 subtype). *Cell*. 31(2):417-27.

Castano-Diez.D., Kudryashev.M., Arbeit.M., Stahlberg.H.(2012). Dynamo: a flexible, user-friendly development tool for subtomogram averaging of cryo-EM data in high-performance computing environments. *Journal of Structural Biology*. 178:139-151.

Centers of Disease Control and Prevention Morbidity and Mortality Weekly Report. (2016). Prevention and control of seasonal influenza with vaccines recommendations of the advisory committee on immunization practices-United States, 2016-17 Influenza season. *Center for Surveillance, Epidemiology, and Laboratory Services, Centers of Disease Control and Prevention*. 65(5): 1-52.

Centers for Disease Control and Prevention (2009). The 2009 H1N1 Pandemic: Summary Highlights, April 2009-2010. Retrieved from <http://www.cdc.gov/h1n1flu/cdcresponse.html>.

Chemali.M., Radtke.K., Desjardins.M., English.L.(2011). Alternative pathways for MHC class I presentation: a new function for autophagy. *Cellular and Molecular Life Sciences*. 68(9):1533-41.

Chen.B.J., Leser.G.P., Morita.E., Lamb.R.A.(2007). Influenza virus hemagglutinin and neuraminidase, but not the matrix protein, are required for assembly and budding of plasmid-derived virus-like particles. *Journal of Virology*. 81(13):7111-23.

Chen.J., Skehel.J.J., Wiley.D.C.(1999). N-and C-terminal residues combine in the fusion-pH influenza hemagglutinin HA(2) subunit to form an N cap that terminates the triple-stranded coiled coil. *PNAS USA*. 96:8967-72.

Chen.W., Calvo.P.A., Malide.D., Gibbs.J., Schubert.U., Bacik.I., Basta.S., O'Neill.R., Schickli.J., Palese.P., Henklein.P., Bennink.J.R., Yewdell.J.W.(2001). Novel influenza A virus mitochondrial protein that induces cell death. *Nature Medicine*. 7:1306-12.

Clague.M.J., Schoch.C., Blumenthal.R.(1991). Delay time for influenza virus hemagglutinin-induced membrane fusion depends on hemagglutinin surface density. *Journal of Virology*. 65(5):2402-07.

Corti.D., Voss.J., Gamblin.S.J., Codoni.G., Macagno.A., Jarrossay.D., Vachieri.S.G., Pinna.D., Minola.A., Vanzetta.F., Silacci.C., Fernandes-Rodriguez.B.C., Agatic.G., Bianchi.S., Giacchetto-Sasselli.I., Calder.L., Sallusto.F., Collins.P., Haire.L.F., Temperton.N., Langedijk.J.P., Skehel.J.J., Lanzavecchia.A.(2011). A neutralizing antibody selected from plasma cells that binds to group 1 and group 2 influenza A hemagglutinins. *Science*. 333(6044):850-6.

Cox.R.J., Brokstad.K.A., Orga.P.(2004). Influenza virus: Immunity and vaccination strategies. Comparison of the immune response to inactivated and live, attenuated influenza vaccines. *Scandinavian Journal of Immunology*. 59(1):1-15.

Cox.N.J., Subbarao.K.(2000). Global epidemiology of influenza: past and present. *Annual Review of Medicine*. 51:407-21.

Crowther.R.A., DeRosier.D.J., Klug.A.(1970). The reconstruction of a three-dimensional structure from projections and its application to electron microscopy. *Proceedings of the Royal Society of London*. 317(1530):319-40.

Danev.R., Baumeister.W.(2016). Cryo-EM single particle analysis with the Volta Phase Plate. *Nature Methods*. 13: 395. doi:10.1038/nmeth.3842.

Danev.R., Buijsse.B., Khoshouei.M., Plitzko.J.M., Baumeister.W.(2014). Volta potential phase plate for in-focus phase contrast transmission electron microscopy. *PNAS*. 111(44):15635-40.

D'Aoust.M.A., Lavoie.P.O., Couture.M.M., Trepanier.S., Guay.J.M., Dargis.M., Mongrand.S., Landry.N., Ward.B.J., Vezina.L.P.(2010).The production of hemagglutinin-based virus-like particles in plants: a rapid, efficient and safe response to pandemic influenza. *Journal of Plant Biotechnology*. 8(5):607-19.

D'Aoust.M.A., Lavoie.P.O., Couture.M.M., Trepanier.S., Guay.J.M., Dargis.M.,Mongrand.S., Landry.N., Ward.B.J., Vezina.L.P. (2008). Influenza virus-like particles produced by transient expression in *Nicotiana benthamiana* induce a protective immune response against a lethal viral challenge in mice. *Journal of Plant Biotechnology*. 6(9): 930-40.

Dawood.F., Luliano.D., Reed.C., Meltzer.M.I., Shay.D.K., Cheng.P., Bandaranayake.D., Breiman.R.F., Brooks.A., Buchy.P., Feikin.D.R., Fowler.K.B., Gordon.A., Tran Hien.N., Horby.P., Sue Huang. Q., Katz.M.A., Krishnan.A., Lal.R., Montgomery.J.M., Molback.K., Pebody.R., Presanis.A.M., Razuri.H., Steens.A., O Tinoco.Y., Wallinga.J., Yu. H., Vong.S.,

Bresee.J., Widdowson.M.A.(2012). Estimated global mortality associated with the first 12 months of 209 pandemic influenza A H1N1 virus circulation: a modelling study. *The Lancet Infectious Disease*. 12(9):687-95.

Douce.G., Turcotte.C., Cropley.I., Roberts.M., Pizza.M., Domenghini.M., Rappuoli.R., Dougan.G.(1995). Mutants of Escherichia coli heat-labile toxin lacking ADP-ribosyltransferase activity act as nontoxic, mucosal adjuvants. *PNAS USA*. 92(5):1644-8.

Dreyfus.C., Ekiert.D.C., Wilson.I.A.(2013). Structure of a classical broadly neutralizing stem antibody in complex with a pandemic H2 influenza virus hemagglutinin. *Journal of Virology*. 87(12):7149-54.

Duclos.S., Clavarino.G., Rousserie.G., Goyette.G., Boulais.J., Camossetto.V., Gatti.E., LaBoissiere.S., Pierre.P., Desjardins.M.(2011). The endosomal proteome of macrophage and dendritic cells. *Proteomics*. 11(5):854-64.

Duxbury.A.E., Hampson.A.W., Sievers.J.G.(1968). Antibody response in humans to deoxycholate treated influenza virus vaccine. *Journal of Immunology*. 10(1):62-7.

Ehret.J.,(2003). The global value of vaccination. *Vaccine*. 21(7-8): 596-600.

Faruqi.A.R., Subramaniam.S.(2000). CCD detectors in high-resolution biological electron microscopy. *Quarterly Reviews of Biophysics*. 33(1):1-27.

Fukuda.Y., Lauguks.U., Lucic.V., Baumeister.W., Danev.R (2015). Electron cryotomography of vitrified cells with a volta phase plate. *Journal of Structural Biology*. 190:143-54.

Gabriel.G., Dauber.B., Wolff.T., Planz.O., Klenk.D.H., Stech.J.(2005). The viral polymerase mediates adaptation of an avian influenza virus to a mammalian host. *Proceedings of the National Academy of Sciences of the USA*. 102(51):18590-95.

Galaz-Montoya.J.G., Flanagan.J., Schmid.M.F., Ludtke.S.J.(2015). Single particle tomography in EMAN 2. *Journal of Structural Biology*. 190(3):279-90.

Gerhard.W., Yewdell.J., Frankel.M.E., Webster.R.(1981). Antigenic structure of influenza virus haemagglutinin defined by hybridoma antibodies. *Nature*. 290:713-17.

Giocondi.M.C., Ronzon.F., Nicolai.M.C., Dosset.P., Milhiet.P.E., Chevalier.M., Le-Grimellec.C. (2010). Organization of influenza A virus envelope at neutral and low pH. *Journal of General Virology*. 91: 329-338.

Haq.K., McElhaney.J.E. 2014. Immunosenescence: influenza vaccination and the elderly. *Current Opinion in Immunology*. 29: 38-42.

Harper.D.M., Franco.E.L., Wheeler.C., Ferris.D.G., Jenkins.D., Schuind.A., Zahaf.T., Innis.B., Naud.P., De Carvalho.N.S., Roteli-Martins.C.M., Teixeira.J., Blatter.M.M., Korn.A.P., Quint.W., Dubin.G.(2004). Efficacy of a bivalent L1 virus-like particle vaccine in prevention of infection with human papillomavirus types 16 and 18 in young women: a randomised controlled trial. *The Lancet*. 364(9447):1757-65.

Harris.A.K., Meyerson.J.R., Matsuoka.Y., Kuybeda.O., Moran.A., Bliss.D., Das.S.R., Yewdell.J.W., Sapiro.G., Subbarao.K., Subramaniam.S.(2013). Structure and accessibility of HA trimers on intact 2009 H1N1 pandemic influenza virus to stem region-specific neutralizing antibodies. *Proceedings of the National Academy of Sciences of the USA*. 110(12):4592-97.

Harris.A., Cardone.G., Winkler.D.C., Heymann. B.J., Brecher.M., White.J.M., Steven.A.C. (2006). Influenza virus pleiomorphy characterized by cryoelectron tomography. *PNAS*. 103(50): 19123-27.

Harrison.S.C.(2015). Viral membrane fusion. *Virology*. 479-80:498-507.

- Hoppe.W., Gabmann.J., Hunsmann.N., Schramm.H.J., Sturm.M.(1974). Three-dimensional reconstruction of individual negatively stained yeast fatty-acid synthetase molecules form tilt series in the electron microscopy. *Hoppe Seyler's Z. Physiological Chemistry*. 355:1483-87.
- Houde.M., Bertholet.S., Gagnon.E., Brunet.S., Goyette.G., Laplante.A., Princiotta.M.F., Thibault.P., Sacks.D., Desjardins.M.(2003). Phagosomes are competent organelles for antigen cross-presentation. *Nature*. 425(6956):402-6.
- Jenner.B.E.(1798): The three original publications on vaccination against smallpox. *Harv.Class.* 1909-1914.
- Kang.S.M., Song.J.M., Quan.F.S., Compans.R.W.(2009). Influenza vaccines based on virus-like particles. *Virus Research*. 143(2): 140-6.
- Katz.G., Benkarram.Y., Wei.H., Rice.W.J., Bucher.D., Alimova.A., Katz.A., Klukowska.J., Herman.G.T., Gottlieb.P. (2014). Morphology of Influenza B/Lee/40 Determined by Cryo-Electron Microscopy. *PLoS-One*. DOI:10.1371/journal.pone.0088288.
- Knappek.E., Dubochet.J.(1980). Beam damage to organic material is considerably reduced in cryo-electron microscopy. *Journal of Molecular Biology*. 141(2):147-61.
- Kibenge.F.S., Munir.K., Kibenge.M.J., Joseph.T., Moneke.E.(2004). Infectious salmon anemia virus: causative agent, pathogenesis and immunity. *Animal Health Research Reviews*.5(1):65-78.
- Klenk.H.D., Wagner.R., Heuer.D., Wolff.T. (2001). Importance of hemagglutinin glycosylation for the biological functions of influenza virus. *Virus Research*. 82(1-2):73-5.
- Krammer.F., Palese.P.(2014). Universal influenza virus vaccines: need for clinical trials. *Nature Immunology*. 15(1):3-5.
- Krawczyk.C.M., Sun. J., Pearce.E.J. (2008). Th2 differentiation is unaffected by Jagged 2 expression on dendritic cells. *Journal of Immunology*. 180:7931-37.
- Kuhlbrandt.W.(2014). The resolution revolution. *Science*. 343:1443-4.
- Lamb.R.A(1983). The influenza virus RNA segments and their encoded protein. *In Genetics of Influenza Viruses* (Palese, P., and Kingsbury, D.W., eds)22-69, Springer, New York.
- Lakadamyali.M., Rust.M.J., Babcock.H.P., Zhuang.X.(2003). Visualizing infection of individual influenza viruses. *Proceedings of the National Academy of Sciences of the USA*. 100(16):9280-85.
- Lakadamyali.M., Rust.M.J., Zhuang.X.(2004). Endocytosis of influenza viruses. *Microbes and Infection*. 6(10):929-36.
- Lakhani.S.(1992). Early Clinical Pathologists: Edward Jenner. *Journal of Clinical Pathology*. 45(9):756-8.
- Landry.N., Ward.B.J., Trepanier.S., Montomoli.E., Dargis.M., Lapini.G., Vezina.L.P.(2010). Preclinical and clinical development of plant-made virus-like particle vaccine against Avian H5N1 influenza. *PLOS one*. 5(12): 1-12.
- Lamb.R.A., Zebedee.S.L., Richardson.C.D.(1985). Influenza virus M2 protein is an integral membrane protein expressed on the infected-cell surface. *Cell*. 40(3):627-33.
- Lampe.M., Briggs.J.A.G., Endress.T., Glass.B., Rigelsberger.S., Krausslich.H.G., Lamb.D.C., Brauchle.C., Muller.B.(2007). Double-labelled HIV-1 particles for study of virus-cell interaction. *Virology*. 360(1):92-104.
- Leahy.M.B., Dessens.J.T., Weber.F., Kochs.G., Nuttall.P.A.(1997). The fourth genus in the Orthomyxoviridae: sequence analyses of two Thogoto virus polymerase proteins and comparison with influenza viruses. *Virus Research*. 50(2):215-24.

- Le Mauff.F., Mercier.G., Chan.P., Burel.C., Vaudry.D., Bardor.M., Vezina.L.P., Couture.M., Lerouge.P., Landry.N.(2014). Biochemical composition of hemagglutinin-based influenza virus-like particle vaccine produced by transient expression in tobacco plants. *Plant Biotechnology Journal*. 13(5):717-25.
- Lerouge.P., Cabanes-Macheteau.M., Rayon.C., Fischette-Laine.A.C., Gomond.V., Faye.L.(1998). N-glycoprotein biosynthesis in plants: recent developments and future trends. *Plant Molecular Biology*. 38(1-2):31-48.
- Li.J., Arevalo.M.T., Zeng.M.(2013). Engineering influenza viral vectors. *Bioengineered*. 4(1):9-14.
- Li.X., Mooney.P., Zhen.S., Booth.C.R., Braunfeld.M.B., Gubbens.S., Agard.D.A., Cheng.Y.(2013). Electron counting and beam-induced motion correction enable near-atomic-resolution single particle cryo-EM. *Nature Methods*.10. 584-90.
- Liljeroos.L., Malito.E., Ferlenghi.I., Bottomly M.J.(2015). Structural and Computational Biology in the Design of Immunogenic Vaccine Antigens. *Journal of Immunology Research*. 2015:1-17.
- Lin.S.C., Huang.M.H., Tsou.P.C., Huang.L.M., Chong.P., Wu.S.C.(2011). Recombinant trimeric HA protein immunogenicity of H5N1 Avian influenza viruses and their combined use with inactivated or adenovirus vaccines. *PLOS One*. 6(5): doi:10.1371/journal.pone.0020052.
- Liu.G., Song.L., Reiserova.L., Trivedi.U., Li.X., Noah.D., Hou.F., Weaver.B., Tussey.L.(2012). Flagellin-HA vaccines protect ferrets and mice against H5N1 highly pathogenic avian influenza virus (HPAIV) infections. *Vaccine*. 30(48): 6833-8.
- Ludtke.S.J., Baldwin.P.R., Chiu.W.(1999). EMAN: Semiautomated software for high-resolution single particle reconstructions. *Journal of Structural Biology*. 128(1):82-97.
- Mahamid.J., Pfeffer.S., Schaffer.M., Villa.E., Danev.R., Kuhn Cuellar.L., Forster.F., Hyman A.A., Plitzko.J.M., Baumeister.W. (2016). Visualizing the molecular sociology at the HeLa cell nuclear periphery. *Science*. 351:969-72.
- Matlin.K.S., Reggio.H., Helenius.A., Simons.K.(1981). Infectious entry pathway of influenza virus in a canine kidney-cell line. *Journal of Cell Biology*. 91:601-13.
- Matsuzaki.Y., Sugarwara.K., Nakauchi.M., Takahashi.Y., Onedera.T., Tsunetsugu-Yokota.Y., Matsumura.T., Ato.M., Kobayashi.K., Shimotai.Y., Mizuta.K., Hongo.S., Tashiro.M., Nobusawa.E.(2014). Epitope mapping of the hemagglutinin molecule of A/(H1N1)pdm09 Influenza virus by using monoclonal antibody escape mutants. *Journal of Virology*. 88(21): 12364-73.
- Milazzo.A-C., Chen.A., Moeller.A., Lyumkis.D., Jacovetty.E., Polukas.J., Ellisman.M.H., Xuong.N-H., Carragher.B., Potter.C.S.(2011). Initial evaluation of a direct detection device detector for single particle cryo-electron microscopy. *Journal of Structural Biology*. 176(3):404-8.
- Minor.P.D.(2015). Live attenuated vaccines: Historical successes and current challenges. *Virology*. (479-480):379-92.
- Morens.D.M., Taubenberger.J.K., Fauci.A.S. (2008). Predominant Role of Bacterial Pneumonia as a Cause of Death in Pandemic Influenza: Implication for Pandemic Influenza Preparedness. *The Journal of Infectious Diseases*. 198(7):962-70.

- Morens.D.M., Fauci.A.S.(2007). The 1918 influenza pandemic: insights for the 21st century. *Journal of Infectious Disease*. 195(7):1018-28.
- Mould.J.A., Li.H.C., Dudlak.C.S., Lear.J.D., Pekosz.A., Lamb.R.A., Pinto.L.H.(2000). Mechanism for proton conduction of the M(2) ion channel of influenza A virus. *Journal of Biological Chemistry*. 12:8592-9.
- Nakamura.K., Bhowan.A.S., Compans.R.W.(1980). Glycosylation sites of influenza viral glycoproteins Tryptic glycopeptides form the A/WSN(H0N1) hemagglutinin glycoprotein. *Virology*. 107(1):208-21.
- Nayak.D.P., Hui Kai-Wai.E., Barman.S.(2004). Assembly and budding of influenza virus. *Virus Research*. 106(2):147-65.
- Noda.T., (2011). Native Morphology of Influenza Virions. *Frontiers in Microbiology*. 2(269):1-5.
- Okuno.Y., Isegawa.Y., Sasao.F., Ueda.S (1993). A common neutralizing epitope conserved between the hemagglutinins of influenza A virus H1 and H2 strains. *Journal of Virology*. 67(5):2552-8.
- Oxford.J.S.(2000). Influenza A pandemics of the 20th century with special reference to 1918: virology, pathology and epidemiology. *Reviews in Medical Virology*. 2:119-33.
- Palese.P. Shaw.M. (2007). Orthomyxoviridae: The Viruses and Their Replication. In Knipe D.M., P, editors. *Fields Virology*, 5th Edition. Philadelphia: Lippincott Williams & Wilkins. pp. 1647-89.
- Patterson.S., Oxford.J.S., Dourmashkin.R.R.(1979). Studies on the mechanism of influenza-virus entry into cells. *Journal of General Virology*. 43: 223-9.
- Patriarca.P.A., Kendal.A.P., Zakowski.P.C., Cox.N.J., Trautman.M.S., Cherry.J.D., Averbach.D.M., McCusker.J., Belliveau.R.R., Kappus.K.D.(1984). Lack of significant person-to person spread of swine influenza-like virus following fatal infection in an immunocomprised child. *Americal Journal of Epidemiology*. 119:152-58.
- Petrovsky.N., Aguilar.J.C.(2004). Vaccine adjuvants: current state and future trends. *Immunology and Cell Biology*. 84: 488-96.
- Pettersen.E.F., Goddard.T.D., Huang.C.C., Couch.G.S., Greenblatt.D.M., Meng.E.C., Ferrin.T.E.(2004). UCSF Chimera-A visualization system for exploratory research and analysis. *Journal of Computational Chemistry*. 25(13). 1605-12.
- Pfeiffer.R.F.J., 1892. From the Institute for Infectious Diseases. II. Provisional communication on the cause of influenza. *Deutsche medicinische Wochenschrift*. 18:28.
- Pillet.S., Aubin.E., Trepanier.S., Bussiere.D., Dargis.M., Poulin.J.F., Yssine-Diab.B., Ward.B.J., Landry.N.(2016). A plant-derived quadrivalent virus like particle influenza vaccine induces cross-reactive antibody and T cell response in healthy adults. *Clinical Immunology*. 168:72-87.
- Pillet.S., Racine.T., Nfon.C., Di Lenardo.T.Z., Babiuk.S., Ward.B.J., Kobinger.G.P., Landry.N.(2015). Plant-derived H7 VLP vaccine elicits protective immune response against H7N9 influenza virus in mice and ferrets. *Vaccine*. 33(46):6282-9.
- Plotkin.S.A.(2009). Vaccines: the fourth century. *Clinical Vaccine Immunology*. 16(12):1709-19.
- Plotkin.S.L., Plotkin.S.A.(2008). A short history of vaccination. *Vaccines*. Philadelphia, PA: Saunders Elsevier (5th ed). 1-16.
- Reis.C. (2016, October 11). *FDA Approves Flublok Quadrivalent Influenza Vaccine*. Retrieved from <http://www.proteinsciences.com/PDF/pscp2.pdf>.

- Riedel.S.(2005). Edward Jenner and the history of small pox and vaccination. *Baylor University of Medical Centre Proceedings*. 18(1): 21-25.
- Roberts.P.C., Garten.W., Klenk.H.D.(1993). Role of conserved glycosylation sites in maturation and transport of influenza A virus hemagglutinin. *Journal of Virology*. 67(6):3048-60.
- Roldao.A., Mellado.M.C., Castilho.L.R., Carrondo.M.J., Alves.P.M.(2010): Virus-like particles in vaccine development. *Expert Review of Vaccines*. 9(10):1149-76.
- Root.C.N., Wills.E.G., McNair.L.L., Whittaker.G.R.(2000). Entry of influenza viruses into cells is inhibited by a highly specific protein kinase C inhibitor. *Journal of General Virology*. 81: 2697-705.
- Rosendahl-Huber., S.K., Camps.M.G.M., Jacobi.R.H.J., Mouthaan.J., Van Dijken.H., Van Beek.J., Ossendrop.F., de Jonge.J. (2015). Synthetic long peptide influenza vaccine containing conserved T and B cell epitopes reduces viral load in lungs of mice and ferrets. *PLOS one*. 10(6). E0127969.
- Roy.A.M., Parker.J.S., Parrish.C.R., Whittaker.G.R.(2000). Early stages of influenza virus entry in MV-1 lung cells: involvement by dynamin. *Virology*. 267(1):17-28.
- Ruigrok.R.W., Wrigley.N.G., Calder.L.J., Cusack.S., Wharton.S.A., Brown.E.B., Skehel.J.J.(1986). Electron microscopy of the low pH structure of influenza virus hemagglutinin. *European Molecular Biology Organization*. 5(1):41-49.
- Ruigrok.R.W.H., Krijgsman.P.C.J., de Ronde-Verloop.F.M., de Jong.J.C.(1985). Natural heterogeneity of shape, infectivity and protein composition in an influenza A (H3N2) virus preparation. *Virus Research*.3:69-76.
- Rust.M.J., Lakadyami.M., Zhang.F., Zhuang.X.(2004). Assembly of endocytic machinery around individual influenza viruses during viral entry. *Nature Structural & Molecular Biology*. 44:567-73.
- Saint-Jore-Dupas.C., Faye.L., Gomord.V. (2007). From planta to pharma with glycosylation in the toolbox. *Trends in Biotechnology*. 25(7):317-23.
- Scallan.C.D., Tingley.D.W., Lindbloom.J.D., Toorney.J.S., Tucker.S.N.(2013). An adenovirus-based vaccine with a double-stranded RNA adjuvant protects mice and ferrets against H5N1 avian influenza in oral delivery models. *Clinical and Vaccine Immunology*. 20(1): 85-94.
- Schur.F.K.M., Hagen.W.J.H., Rumlova.M., Ruml.T., Muller.B., Krausslich.H.G., Briggs.J.A.G.(2015). Structure of the immature HIV-1 capsid in intact virus particles at 8.8Å resolution. *Nature*. 517(7535):505-510
- Schur.F.K.M., Hagen.W.J.H., Marco.A., Briggs.J.A.G. (2013). Determination of protein structure at 8.5 resolution using cryo-electron tomography and sub-tomogram averaging. *Journal of Structural Biology*. 184(3):394-400.
- Schwarzer.J., Rapp.E., Hennig.R., Genzel.Y., Jordan.I., Sandig.V., Reichl.U.(2009). Glycan analysis in cell culture-based influenza vaccine production: Influence of host cell line and virus strain on the glycosylation pattern of viral hemagglutinin. *Vaccine*. 27(32):4325-36.
- Seveno.M., Bardor.M., Paccalet.T., Gomord.V., Lerouge.P., Faye.L.(2004). Glycoprotein sialylation in plants? *Nature Biotechnology*. 22(11):1351-2.
- Shahmoradian.S.H., Galaz-Montoya.J.G., Schmid.M.F., Cong.Y., Ma.B., Speiss.C., Frydman.J., Ludtke.S.J., Chiu.W.(2013). TRiC's tricks inhibit huntingtin aggregation. *ELife*. 2: e00710.
- Sheifele.D.W., Duval.B., Russell.M.L., Warrington.R., DeSerres.G., Skowronski.D.M., Dionne.M., Kellner.J., Davies.D., MacDonald.J.(2003). Ocular and respiratory symptoms

attributable to inactivated split influenza vaccine: evidence from a controlled trial involving adults. *Clinical Infectious Diseases*. 36(7):850-7.

Shope.R.E.(1931). Swine Influenza-III. Infiltration Experiments and Etiology. *Journal of Experimental Medicine*.54(3):373-85.

Sieczkarski.S.B., Whittaker.G.R.(2003). Differential requirements of Rab5 and Rab7 for endocytosis of influenza and other enveloped viruses. *Traffic*. 4:333-43.

Sieczkarski.S.B., Whittaker.G.R.(2002). Influenza virus can enter and infect cells in the absence of clathrin-mediated endocytosis. *Journal of Virology*. 76:10455-65.

Skehel.J.J., Bizebard.T., Bullough.P.A., Hughson.F.M., Knossow.M., Steinhauer.D.A., Wharton.S.A., Wiley.D.C.(1995). Membrane fusion by influenza hemagglutinin. *Cold Spring Harbour Symposia on Quantitative Biology*. 60:573-80.

Skehel.J.J., Bayley.P.M., Brown.E.B., Martin.S.R., Waterfield.M.D., White.J.M., Wilson.I.A., Wiley.D.C.(1982). Changes in the conformation of influenza virus hemagglutinin at the pH optimum of virus-mediated membrane fusion. *Proceedings of the National Academy of Sciences of the USA*.79: 968-72.

Skehel., J.J., Waterfield.M.D.(1975). Studies on the primary structure of the influenza virus hemagglutinin. *Proceedings of the National Academy of Sciences of the USA*.72(1):93-7.

Smith.F.I., Palese.P. (1989). Variation in influenza virus genes: Epidemiological, pathogenic, and evolutionary consequences. *The Influenza Viruses* (Krug, R.M., ed) 1: 319-59, Plenum Press, New York

Spruce.A.,E., Iwata.A., White.J.M., Almers.W.(1989). Patch clamp studies of single cell-fusion events mediated by a viral fusion protein. *Nature*. 342: 555-8. doi:10.1038/342555a0.

Stephenson.I., Nicholson.K., Wood.J., Zambon.M., Katz.J.(2004). Confronting the avian influenza threat: Vaccine development for potential pandemic. *The Lancet Infectious Disease*. 4:499-509.

Subbarao.K., Joseph.T.(2007). Scientific barriers to developing vaccines against avian influenza viruses. *Nature Reviews Immunology*. 7(4):267-78.

Subramaniam.S., Milne.J.L.S.(2004). Three-dimensional electron microscopy at molecular resolution. *Annual Review of Biophysics and Biomolecular Structure*. 33:141-55.

Sui.J., Hwang.W.C., Perez.S., Wei.G., Aird.D., Chen.L.M., Santelli.E., Stec.B., Cadwell.G., Ali.M., Wan.H., Muakami.A., Yammanuru.A., Han.T., Cox.N.J., Bankston.L.A., Donis.R.O., Liddington.R.C., Marasco.W.A.(2009). Structural and functional bases for broad-spectrum neutralization of avian and human influenza A viruses. *Nature Structural & Molecular Biology*. 16(3):265-73.

Sun.X., Jayaraman.A., Maniprasad.P., Raman.R., Houser.K.V., Pappas.C., Zeng.H., Sasisekharan.R., Katz.J.M., Tumpey.T.M.(2013). N-linked glycosylation of the hemagglutinin protein influences virulence and antigenicity of the 1918 pandemic and seasonal H1N1 influenza A viruses. *Journal of Virology*. 87(15):8756-66.

Takeuchi.M., Takabe.K., Mineyuki.Y(2010). Immunoelectron microscopy of cryofixed and freeze substituted plant tissues. *Methods Molecular Biology*. 657.155-65.

Tang.G., Peng.L., Baldwin.P.R., Mann.D.S., Jiang.W., Rees.I., Ludtke.S.J.(2007). EMAN2: an extensible image processing suite for electron microscopy. *Journal of Structural Biology*. 157(1):38-46.

Throsby.M., Van den Brink.E., Jongeneelen.M., Poon.L.L.M., Alard.P., Cornelissen.L., Bakker.A., Cox.F., Van Deventer.E., Guan.Y., Cinatl.J., Ter Meulen.J., Lasters.I., Carsetti.R., Peiris.M., De Kruif.J., Goudsmit.J.(2008). Heterosubtypic neutralizing monoclonal antibodies

cross-protective against H5N1 and H1N1 recovered from human IgM+ memory B cells. *PLoS ONE*.3(12):e3942-

-Triyatni.M., Saunier.B., Maruvada.P., Davis.A.R., Ulianich.L., Heller.T., Patel.A., Kohn.L.D., Liang.T.J.(2002). Interaction of hepatitis C virus-like particles and cells: a model system for studying viral binding and entry. *Journal of Virology*. 76(18):9335-44.

Thach.R.E., Thach.S.S. (1971). Damage to biological samples caused by the electron beam during electron microscopy. *Biophysical Journal*. 11(2): 204-10.

Vanderlinden.E., Naesens.L.(2013). Emerging antiviral strategies to interfere with influenza virus entry. *Medicinal Research Reviews*. 34(2):301-39.

Varghese.J.N., Colman.P.M. (1991). Three dimensional structure of the neuraminidase of influenza virus A/Tokyo/3/67 at 2.2Å resolution. *Journal of Molecular Biology*. 221:473-486.

Varghese.J.N., Laver.W.G., Colman.P.M.(1983). Structure of the influenza virus glycoprotein antigen neuraminidase at 2.9Å resolution. *Nature*. 303:35-40.

Vezina.L.P., Faye.L., Lerouge.P., D'Aoust.M.A., Marquet-Blouin.E., Burel.C., Lavoie.P.O., Bardor.M., Gomord.V(2009). Transient co-expression for fast and high-yield production of antibodies with human-like N-glycans in plants. *Plant Biotechnology Journal*. 7:442-55.

Viboud.C., Grais.R.F., Lafont.B.A., Miller.M.A., Simonsen.L.(2005). Multinational impact of the 1968 Hong Kong influenza pandemic:evidence for a smoldering pandemic. *Journal of Infectious Disease*. 192(2):233-48.

Wacheck.V., Egorov.A., Groiss.F., Pfeiffer.A., Fuereder.T., Hoeflmayer.D., Kundi.M., Popow-Kraupp.T., Redlberge-Fritz.M., Mueller.C.A., Cinatl.J., Michaelis.M., Geiler.J., Bergmann.M., Romanova.J., Roethl.E., Morokutti.A., Wolschek.M., Ferko.B., Seipelt.J., Dick-Gudenus.R., Muster.T.(2010). *Journal of Infectious Disease*. 201(3):354-62.

Ward.B.J., Landry.N., Trépanier.S., Mercier.G., Dargis.M., Couture.M., D'Aoust.M.A., Vézina.L.P.(2014). Human antibody response to N-glycans present on plant-made influenza virus-like particle (VLP) vaccines. *Vaccine*. 32(46):6098-106.

Wasilewski.S., Calder.L.J., Grant.T., Rosenthal.P.B. (2012). Distribution of surface glycoproteins on influenza A virus determined by electron cryotomography. *Vaccine*. 30(5):7368-73.

White.J., Kartenbeck.J., Helenius.A.(1982). Membrane fusion activity of influenza virus. *European Molecular Biology Organization*. 1:217-222.

Wilson.S.M., Bacic.A. (2012). Preparation of plant cells for transmission electron microscopy to optimize immunogold labeling of carbohydrate and protein epitopes. *Nature Protocols*. 7(9): 1716-27.

Wilson.,I.A., Skehel.J.J., Wiley.D.C.(1981). Structure of the haemagglutinin membrane glycoprotein of influenza virus at 3Å resolution. *Nature*. 289: 366-73.

Wilney.M., Meehl.J.B., O'Toole.E.T., Giddings Jr.T.H.(2014). Conventional transmission electron microscopy. *Molecular Biology of the Cell*. 25(3):319-23.

Wise.H.M., Foeglein.A., Sun.J., Dalton.R.M., Sheetal.P., Howard.W., Anderson.E.C., Barclay.W.S., Digard.P.(2009). A complicated message: Identification of a novel PB1-related protein translated form influenza A virus segment 2 mRNA. *Journal of Virology*. 83(16):8021-31.

Wong.S., Webby.R.(2013). Traditional and new influenza vaccines. *Clinical Microbiology Review*. 26:476-92.

World Health Organization. (1980). The global eradication of smallpox: Final report of the global commission for the certification of smallpox eradication. Geneva: World Health Organization. Global Commission for Certification of Smallpox Eradication.

Wright.P.F., Neumann.G., Kawaoka.Y. (2007). Orthomyxoviruses. In: Knipe.D.M., Howley.P.M, editors. *Fields Virology*. 5th Philadelphia: Lippincott Williams & Wilkins. 1697-740.

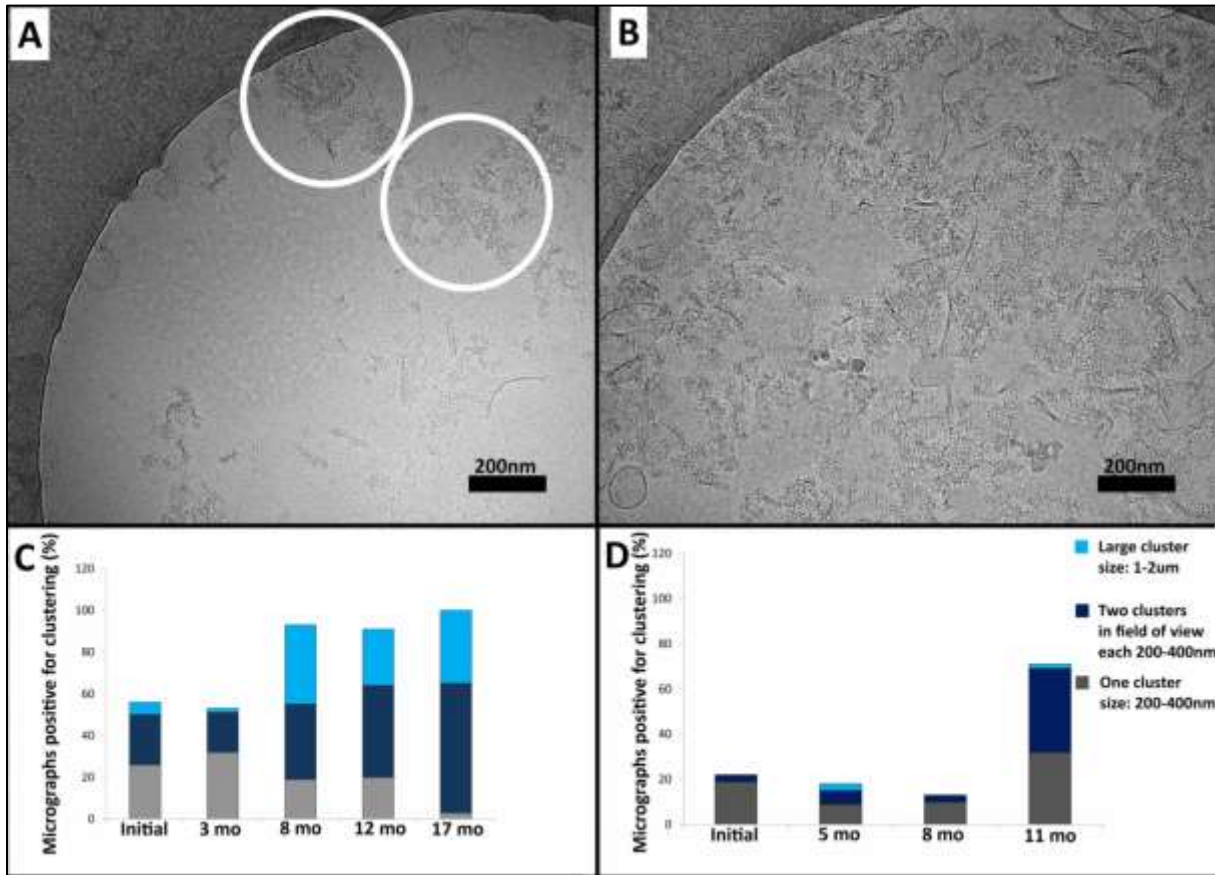
Wright.P.F., Webster.R.G. (2001). Orthomyxoviruses. In Knipe.D.M., Howley.P.M., Griffin.D.E., Lamb.R.A., Martin.M.A., Roizman.B., Straus.S.E. editors. *Fields Virology*. 4th Philadelphia: Lippincott Williams & Wilkins.1533-79.

Young.K.R., Arthus-Cartier.G., Yam.K.K. Lavoie.P.O., Landry.N., D'Aoust.M.A., Vezina.L.P., Couture.M.M., Ward.B.J.(2015). Generation and characterization of a trackable plant-made influenza H5 virus-like particle (VLP) containing enhanced green fluorescent protein (eGFP). *FASEB Journal*. 29(9): 3817-27.

Zebedee.S.L., Lamb.R.A.(1988). Influenza A virus M2 protein: monoclonal antibody restriction of virus growth and detection of M2 in virions. *Journal of Virology*. 62:2762-72.

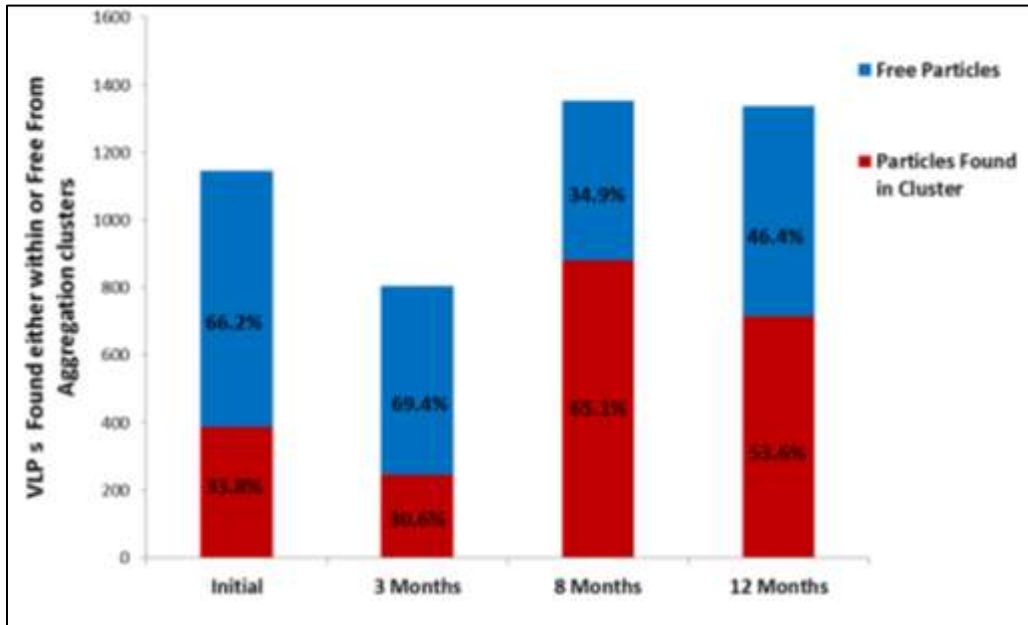
Zerial.M., McBride.H.(2001). Rab proteins as membrane organizers. *Nature Review Molecular & Cell Biology*. 2:107-17.

Appendix A: Quantification of VLP clustering over time visualized by cryo-EM

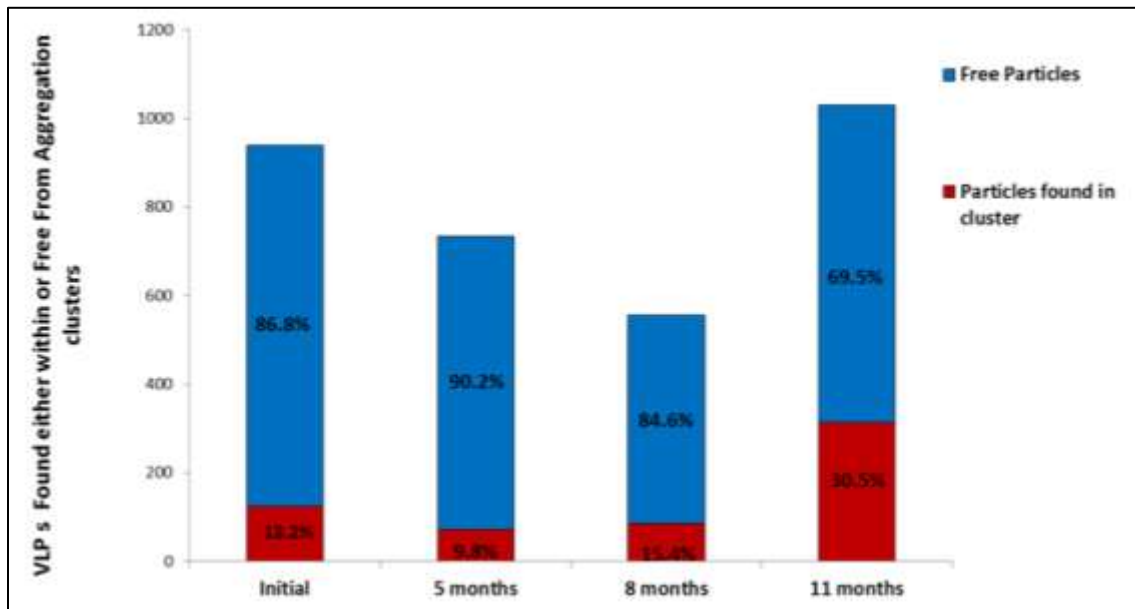


Quantification of VLP clustering in the H1 and H5 formulations over one year. A-B) Cryo-EM micrographs of small (white circles and large clusters respectively). C-D) Micrographs positive for presence of clustering, (gray-one small cluster per micrograph, dark blue- two small clusters per field of view, light blue-large cluster in field of view).

Appendix B: Quantification of cluster bound VLPs versus free VLPs by cryo-EM



Quantification of VLPs found within clusters or free from clusters in the H1-VLP formulations over one year.



Quantification of VLPs found within clusters or free from clusters in the H5-VLP formulations over one year.